FORSCHUNGSBERICHT AGRARTECHNIK
des Fachausschusses Forschung und Lehre der
Max-Eyth-Gesellschaft Agrartechnik im VDI (VDI-MEG) **567**

Joseph Kudadam Korese

Experimental and modeling studies of forced convection storage and drying systems for sweet potatoes

Dissertation Witzenhausen 2016

Universität Kassel

Fachbereich Ökologische Agrarwissenschaften

Fachgebiet Agrartechnik

Prof. Dr. sc. agr. Oliver Hensel

Experimental and modeling studies of forced convection storage and drying systems for sweet potatoes

Dissertation zur Erlangung des akademischen Grades Doktor der Agrarwissenschaften (Dr. agr.)

von

M.Sc. Joseph Kudadam Korese

aus Langbensi, Ghana

2016

Die vorliegende Arbeit wurde vom Fachbereich für Ökologische Agrarwissenschaften, Fachgebiet Agrartechnik der Universität Kassel als Dissertation zur Erlangung des akademischen „Grades Doktor der Agrarwissenschaften“ angenommen.

Tag der mündlichen Prüfung: 09.12.2016

Erster Gutachter:	Prof. Dr. Oliver Hensel
Zweiter Gutachter:	Prof. Dr.-Ing Werner Hofacker
Mündliche Prüfung:	Prof. Dr. Oliver Hensel
	Prof. Dr.-Ing Werner Hofacker
	Prof. Dr. Gunter Backes
	Prof. Dr. Jürgen Heß

Gedruckt mit Unterstützung des Deutschen Akademischen Austauschdienstes.

Im Selbstverlag: Joseph Kudadam Korese

Bezugsquelle: Universität Kassel, FB Ökologische Agrarwissenschaften
Fachgebiet Agrartechnik
Nordbahnhofstr. 1a
37213 Witzenhausen

Dedication

To my beloved mother, Faustina Atanditiga

My loving wife, Brenda

My wonderful children, Pearl and John Baptist

&

those children yet to come

Affidavit

I herewith give assurance that I completed this dissertation independently without prohibited assistance of third parties or aids other than those identified in this dissertation. All passages that are drawn from published or un-published writings, either word-for-word or in paraphrase, have been clearly identified as such. Third parties were not involved in the drafting of the material content of this dissertation; most specifically I did not employ the assistance of a dissertation advisor. No part of this thesis has been used in another doctoral or tenure process.

Erklärung

Hiermit versichere ich, dass ich die vorliegende Dissertation selbständig, ohne unerlaubte Hilfe Dritter angefertigt und andere als die in der Dissertation angegebenen Hilfsmittel nicht benutzt habe. Alle Stellen, die wörtlich oder sinngemäß aus veröffentlichten oder unveröffentlichten Schriften entnommen sind, habe ich als solche kenntlich gemacht. Dritte waren an der inhaltlichen Erstellung der Dissertation nicht beteiligt; insbesondere habe ich nicht die Hilfe eines kommerziellen Promotionsberaters in Anspruch genommen. Kein Teil dieser Arbeit ist in einem anderen Promotions- oder Habilitationsverfahren durch mich verwendet worden.

Witzenhausen, den 5.10.2016 Joseph Kudadam Korese

Acknowledgements

The journey of my PhD study at the University of Kassel (Witzenhausen campus), Germany started from May 23rd, 2013. During the almost four years' of research stay in Germany, I have learnt not only academic knowledge, but also on how to become a responsible and independent scientist. I am very grateful that I have worked with and have met many people who have been very helpful and have guided me all the way long. I have now the opportunity to express my appreciation to all of them.

I am highly indebted to my academic supervisor, Prof. Dr. Oliver Hensel, Department of Agricultural Engineering, University of Kassel, Witzenhausen, Germany, for his unreserved advice, support and guidance throughout this study. I enjoyed the freedom to explore all options during the various stages of my research. I sincerely honour his vision towards doctoral studies, his philosophy of supervision and his big heart. Even with his busy schedules, he always has time for me whenever I approach his office, or even when we meet outside. His diligence in meeting deadlines has provided me with the impetus to complete this work. Prof. Hensel has also inspired me in many other aspects of my life; his devotion to work, accomplishments, academic and research excellence, commitment and simplicity are emulative. Without his critical comments and useful suggestions, commitment and rapid feedback, this work would not have been accomplished. I would also like to thank Prof. Dr.-Ing. Werner Hofacker, Institute of Applied Thermo- and Fluid Dynamics, HTWG Konstanz, Germany for agreeing to assess this thesis, and Prof. Dr. Gunter Backes and Prof. Dr. Jürgen Heß for their participation as oral examiners.

I am grateful to Dr. Uwe Richter, Dr. Franz Román and Dr. Babara Sturm for all the suggestions and the never ending support throughout the study period. Further, I will like to thank the anonymous reviewers for their helpful suggestions on the articles presented in this thesis. Without the family-like atmosphere created by the employees of the Agricultural Engineering Department, this work would not be possible. I am particularly thankful to Christian Schellert, Heiko Tostmann, Karin Link, Michael Hesse, Christian Höing, Daniela Schwarz, Stefanie Retz, Gardis von Gersdorff and Sascha Kirchner for their helpful assistance, friendship and hospitality. My sincere appreciation to staff of the University of Kassel Tropical Greenhouse (Witzenhausen), especially Rainer Braukmann for taking care of my sweet potato plants which

enabled year round multiplication and subsequent planting.

I gratefully acknowledge the German Academic Exchange Service (DAAD) for their financial support of my residence in Germany. The PhD research was partly financed by the Global Food Supply (GlobE) project RELOAD (FKZ 031A247 A), funded by the German Federal Ministry of Education and Research (BMBF). I appreciate the financial support for my experiments. Protocol is incomplete if I ignore the role played by my employer; the University for Development Studies, Ghana, for granting me study leave to Germany. Such positive decision cannot pass without profound acknowledgement and gratitude.

It was not easy to live a life in a foreign country for such a long time. I thank my Ghanaian sister Dora Neina, my Kenyan friends Guyo Malicha Roba, Ivan Solomon Adolwa and Jackline Ogolla, my Ethopian friend Chemeda Abedeta Garbaba, my Nepali friend Luna Shrestha and my Indian friend Aditya Parmar for been part of my life during this journey and being such good friends.

I am thankful to family back home for the constant support and encouragement. Most importantly, to my dearest wife Brenda for supporting me throughout, being patient and tolerant and accepting to take a dual responsibility of being a mum and dad to our children, and in particular John Baptist Awedoba who was born in my absence. Thank you very much. To my daughter Pearl Wepia and son John Baptist Awedoba – my absence from home for such a long time will all make sense in due time.

For those who contributed in diverse ways but are denied mention here by my poor memory, and for who did not get the opportunity to contribute, I am still very grateful. To the Almighty Father; I THANK THEE.

Preliminary remarks

This thesis is based on manuscripts either published, accepted or prepared for publication in peer-reviewed journals and are referred to in the text by their chapter Arabic numbers as shown below. Throughout the thesis, the word, fan and ventilator is used interchangeably. They refer to the system used to move air and should be treated to mean same in the context of this thesis.

Chapter 3: **Korese, J. K.,** & Hensel, O. (2016). Resistance to airflow through sweet potato aerial vine components. Applied Engineering in Agriculture, 32(4), 483-491. doi:10.13031/aea.32.11359.

Chapter 4: **Korese, J. K.,** Richter, U., & Hensel, O. (2016). Airflow resistance through bulk sweet potato roots. Transactions of the ASABE, 59(4), 961-968. doi:10.13031/trans.59.11283.

Chapter 5 **Korese, J. K.,** Sturm, B., Román, F., & Hensel, O. (2017). Simulation of transient heat transfer during cooling and heating of whole sweet potato (*Ipomoea batatas* (L.) Lam.) roots under forced-air conditions. Applied Thermal Engineering, 111, 1171-1178. doi.org/10.1016/j.applthermaleng.2016.09.137.

Chapter 6: **Korese, J. K.,** & Hensel, O. (2016). Experimental evaluation of bulk charcoal pad configuration on evaporative cooling effectiveness. Agricultural Engineering International: CIGR Journal (Accepted).

Chapter 7[*]: **Korese, J. K.,** Román, F., & Hensel, O. Application of computational fluid dynamics in the simulation of airflow in a low-cost ventilated mud storehouse for storage of sweet potato roots.

Chapter 8: **Korese, J. K.,** Román, F., & Hensel, O. Development and performance evaluation of an autonomous photovoltaic ventilated mud storehouse for storage of sweet potato roots under tropical conditions (Draft manuscript to be submitted).

[*] Parts of this chapter has been presented in the Tropentag 2015 annual conference as a poster and published in the book of abstracts (page 643). Online. http://www.tropentag.de/2015/abstracts/links/Korese_CGW4aOSv.php.

Table of contents

List of figures

List of tables

Nomenclature

Symbol	Units	Description
a, b, c, d	-	regression coefficients/empirical constants
A, B, A_1, B_1	-	parameters of the model which depends upon the properties of the sweet potato roots
A_f	-	ideality factor
A_B	-	constant, dimensionless
A_{PV}	m^2	PV panel effective area
A_{mfr}	m^2	wetted-medium frontal area
Bi	-	Biot number, dimensionless
C	m^{-1}	Forchheimer drag constant
C_B	-	constant, dimensionless
C_a	J kg^{-1} $°C^{-1}$	specific heat at T_a
C_{sp}	J kg^{-1} $°C^{-1}$	heat capacity of sweet potato root
C_w	Kg h^{-1} m^{-2} $°C^{-1}$	specific water consumption
d_{eff}, D_{sp}	m	effective diameter of sweet potato root
e, E	%	error or relative error, respectively
emf	V	electromotive force
E_i	Pa m^{-1}	experimental pressure drop per unit depth
E_g	eV	band gap energy
Fo	-	Fourier number, dimensionless
Ga	W m^{-2}	solar irradiance
G_{as}	W m^{-2}	standard solar irradiance
h	W m^{-2} $°C^{-1}$	heat transfer coefficient
H_a	%	ambient relative humidity
$H_{1...7}$	%	relative humidity inside the mud storehouse
I	A	PV cell output current
I_A	A	starting current
I_d	A	diode current
I_{mot}	A	motor current
I_{max}	A	peak power current

I_o	A	no load current
I_r	A	reverse saturation current
$I_{r(TS)}$	A	reverse saturation current on standard test condition
I_{ph}	A	photo current
$I_{sc(TS)}$	A	short circuit current on standard test condition
J_0 ( ), J_1 ( )	-	Bessel function of first kind, dimensionless
k	(1.381×10^{-23} J K^{-1})	Bolzmann's constant
k_a	W m^{-1} °C^{-1}	thermal conductivity of air
k_i	-	temperature coefficient on short circuit current
K_m	Nm A^{-1}	torque constant
K_n	V (1000 rpm)$^{-1}$	speed constant
k_{sp}	W m^{-1} °C^{-1}	thermal conductivity of sweet potato root
K	m^2	Darcy permeability of the porous matrix
K_{sp}	$m^{-1/2}$	characteristic constant for a particular sweet potato root size
L	m	bulk depth
L_{mot}	mH	terminal inductance, motor
L_{sp}	m	characteristic length of a particular sweet potato root size
m_a	kg h^{-1}	air mass flow rate
m_e	kg h^{-1}	water evaporation rate
m_{sp}	kg	mass of sweet potato root
m_{v1}, m_{v2}	kg h^{-1}	inlet and outlet water vapor flow rate, respectively
M_H	Nm	stall torque
M_L	Nm	impeller torque
M_{mot}	Nm	motor torque
M_R	Nm	friction torque
MC	%	moisture content
n	rpm	speed
n_o	rpm	no load speed
n_p	-	number of PV panels on parallel in an array

n_s	-	number of cells in series in a PV panel
$\Delta n/\Delta M_{mot}$	$N^{-1}cm^{-1}min^{-1}$	speed/torque gradient
NOCT	°C	PV normal operating cell temperature
Nu	-	Nusselt number, dimensionless
P_i	Pa m^{-1}	predicted pressure drop per unit depth
P_{pv}	W	PV panel output power
P_{max}	W	peak power
P_T	Pa	total pressure
Pr	-	Prandtl number, dimensionless
ΔP	Pa m^{-1}	pressure drop per unit depth
P (%)		mean relative deviation modulus
q	1.602 x 10^{-19} (Coulomb)	charge of the electron
Q_a	m^3 h^{-1}	volumetric airflow rate
r	m	characteristic radius of a particular sweet potato root size
r^2	-	coefficient of determination
Re	-	Reynolds number, dimensionless
RH	%	relative humidity
R_p	Ω	PV cell parallel resistance
R_s	Ω	PV cell series resistance
R_{mot}	Ω	terminal resistance, motor
t	s	time for sweet potato roots in a given medium T_a to reach target T
T	°C	target (centreline) temperature of cooled or heated sweet potato root
T_1, T_2	°C	inlet and outlet dry-bulb temperature
T_a	°C or K	temperature of the medium (environment) or ambient temperature
T_i	°C	initial uniform temperature of sweet potato root
T_j	K	operating temperature of the PV cell
T_r	K	standard temperature

T_{wb}	°C	thermodynamic wet-bulb temperature of the inlet air
$T_{1...7}$	°C	air temperature inside the mud storehouse
V	V	PV output voltage
v, v_a	m s^{-1} or m^3 s^{-1} m^{-2}	air velocity or volumetric airflow rate
V_d	V	voltage across the diode
$V_{oc(TS)}$	V	PV panel open circuit voltage on standard test condition
V_{ind}	V	induced voltage
V_{mot}	V	motor voltage
V_{max}	V	peak power voltage
V_N	V	nominal voltage of motor
V_S	V	voltage across shunt resistor
V_{sp}	m^3	characteristic volume of sweet potato root
W_1, W_2	kg_w kg_a^{-1}	Inlet and outlet humidity ratio, respectively
x_a	-	mass fraction of ith component
x_i	-	mass fraction of air

Greek symbols

ε	-	bed porosity
θ_0	°C	target temperature difference ($T-T_a$)
θ_i	°C	target temperature difference (T_i-T_a)
ρ_a, ρ	kg m^{-3}	density of air (fluid)
ρ_b	kg m^{-3}	bulk density
ρ_{sp},	kg m^{-3}	density of sweet potato root
$\rho_{apparent}$	kg m^{-3}	apparent density
ρ_{true}	kg m^{-3}	true density
ρ_i	kg m^{-3}	density of the ith constituent
μ_a, μ	kg m^{-1} s^{-1}	viscosity of air (fluid)
α_{sp}	m^2 s^{-1}	thermal diffusivity of sweet potato root
α_r	-	roughness factor of sweet potato roots
λ	-	shape factor of sweet potato roots or constant for calculating PV cell temperature

η_{cool}	%	cooling efficiency
η_{mot}	%	motor efficiency
$\eta_{imp.}$	%	impeller efficiency
η_{PV}	%	efficiency of PV panel
η_T	%	total efficiency

Subscript

exp	-	experimental
sim	-	simulated
sp	-	sweet potato root (*Ipomoea batatas* (L.))

Acronyms

ANSI/ASHRAE	American National Standards Institute/ American Society of Heating, Refrigerating, and Air-conditioning Engineers
ASAE	American Society of Agricultural Engineers
ASABE	American Society of Agricultural and Biological Engineers
ANOVA	Analysis of Variance
CFD	Computational Fluid Dynamics
CRD	Completely Randomized Design
LSD	Least Significant Difference
RMSE	Root Mean Square Error
SPSS	Statistical Package for the Social Sciences
SSA	Sub-Saharan Africa
USDA	United States Department of Agriculture
VDI/VDE	Verein Deutscher Ingenieure/Verband der Elektrotechnik Elektronik Informationstechnik

1 General introduction

Sweet potato (*Ipomoea batatas* (L.) Lam) is an important strategic agricultural crop in the world and is cultivated in all tropical and subtropical regions, particularly Asia, Africa and the Pacific. The crop is counted among root crops that represent the second most important staple foods in developing countries, closely following cereal crops (Bovell-Benjamin, 2007; Woolfe, 1992). In tropical developing countries, sweet potato is valued as an important food security crop because of the relatively high yield, adaptability to a wide range of climatic and soil conditions and the promising health benefits that may be derived from its consumption (Bovell-Benjamin, 2007). The roots of orange-fleshed sweet potato varieties in particular, which have been found to be rich in ß-carotene, is being promoted in most agricultural and nutritional programmes in developing countries as a dietary therapy to combat vitamin A deficiency in children (Amoah, 2014; Hagenimana et al., 1998). Awareness of the abundance of other beneficial food ingredients in sweet potato roots has also enhanced its export to international markets (Loebenstein and Thottappilly, 2009). The nutritional attributes of the aerial portions of sweet potato have also been recognized as a better understanding emerges in the relationship between diet and human health as well as their potential for use as a feed supplement in the poultry industry. Sweet potato, apart from its value as wholesome food, has also been considered a substrate for alcohol fermentation (El Sheikha and Ray, 2015).

In spite of the desirable traits listed above, harvested sweet potato (roots and aerial vine components) has limited shelf-life and is easily susceptible to post-harvest losses, especially in many parts of tropical and subtropical countries (Jeng et al., 2015; Woolfe, 1992). Currently, the shelf-life of fresh sweet potato roots within the marketing chain in East Africa for example, is considered to be no longer than one week (van Qirschot et al., 2003). Delay harvesting (in-ground storage) of roots is often not possible due to infestation by sweet potato weevil while the use of traditional storage structures results in severe losses due to decay, shrinkage, sprouting as well as insect pests attack (Rees et al., 1998; Woolfe, 1992). Hall and Devereau (2000) contend that losses of sweet potato roots vary between 15-70% if stored for a period of one to four months in these storage systems. Generally, these losses arise because the existing traditional storage systems can hardly generate the ideal environment required for storage of fresh sweet potato roots. Unlike the roots, harvested sweet potato aerial vine components are considered as a waste, because animals cannot consume all of the huge

amounts produced in the short time available. Previous studies have indicated that these aerial vine components easily decay within two to three days after harvest due to their high moisture content (Sugiura, 2012; Giang et al., 2004). The lack of appropriate post-harvest handling (storage and preservation) systems among sweet potato farmers in developing countries is a disincentive to large-scale investment into its production. Therefore, viable post-harvest storage and preservation systems that can be adapted by farmers in these regions are urgently required. Experts have agreed that any effort to extend the shelf-life of sweet potato (roots and aerial vine components), particularly in tropical developing countries, would make marketing over a longer period of time feasible, thus improving food security and farmers' incomes (Woolfe, 1992).

It is well-known that temperature, relative humidity (RH) and airflow are the key factors for the establishment and maintenance of proper environmental conditions for storage and preservation of perishable agricultural products. Earlier studies have indicated that fresh sweet potato roots in developed countries can be held in a marketable condition for up to a year under optimum storage temperature of 13 to 15 °C and RH of 85 to 95% (Boyette, 2009; Stewart et al., 2000; Woolfe, 1992; Picha, 1986). For short-term handling for marketing, optimum RH range of 70 to 90% is recommended (Cantwell and Suslow, 2001). While these conditions are attainable in developed countries, farmers in tropical developing countries are restrained by lack of temperature and RH controlled storage infrastructure. Nevertheless, evaporative cooling systems which are low-cost can be used to extend the shelf-life of fruits, vegetables and roots and tubers (Kitinoja and Kader, 2002). Ventilation during storage of roots is crucial to remove the respiratory heat produced in storage buildings (Boyette, 2009). For the fresh aerial vine components, these factors (temperature, RH and airflow) play a key role during preservation (drying) in reducing moisture content, thereby inhibiting enzymatic degradation as well as limiting microbial growth (Sugiura, 2012). The facts highlighted above as well as data presented by Garzon (2013) on sweet potato roots shelf-life underlined the importance of controlling the environment conditions during storage and drying of sweet potato roots and aerial vine components, respectively.

Although post-harvest losses of both sweet potato roots and aerial vine components is significant, there is little information in the literature that will support the design and development of appropriate storage and drying systems, especially in tropical developing

countries. In this context, the present study was initiated toward improving scientific knowledge of sweet potato post-harvest handling. A central theme of the thesis is that it is important to fully understand the key design parameters before appropriate post-harvest handling systems can be design to support the sweet potato industry. Aside this, mud as a construction material have been described as having a beneficial effect in maintaining and regulating environmental conditions inside structures (Bengtsson and Whitaker, 1988). By keeping this fact in view, the study also intended to develop a forced convection mud storehouse system in order to establish adequate environmental conditions (temperature, RH and airflow) for storage of sweet potato roots under tropical conditions.

1.1 Objectives of the research

Overall, two approaches have been be taken in the present study to remediate the problems associated with the current sweet potato post-harvest handling. First, improve scientific knowledge about sweet potato post-harvest handling, through experimental and modeling studies of design parameters in order to support decision-making in the design and optimization of forced convection storage and drying systems and the development of new processes. Applying mathematical modeling in the design of such storage and drying facilities can aid in the development of control strategy and reduce energy requirement of the system. Secondly, utilize locally available material such mud which is thermic and has good humidity balancing behaviour to construct a simple storage structure, explore the possibility for integrating evaporative cooling media as well as renewable energy sources, such as photovoltaic (PV) panels as energy sources for decentralized applications in tropical countries. Generally, uniform exposure of perishable agricultural products to air in bulk storage systems is crucial to maintain quality. Hence, Computational Fluid Dynamics (CFD) technique was used to provide an in-depth understanding of flow distribution during the development of the storage structure. Specific objectives of the study include:

1. To investigate airflow resistance of sweet potato components (**Chapter 3 & 4**).
2. To simulate heat transfer of whole sweet potato root under forced convection conditions and multiple air temperatures (**Chapter 5**).

3. To experimentally study the performance of low-cost wetted media and operation related issues for the development of forced-air evaporative cooling systems for sweet potato roots storage under tropical climates (**Chapter 6**).
4. To apply CFD in the simulation of airflow in a low-cost ventilated mud storehouse system (**Chapter 7**).
5. To utilize part of the experimentally generated data in order to develop a directly coupled PV ventilated mud storehouse system for storage of sweet potato roots under tropical conditions (C**hapter 8**).

1.2 Thesis structure

The previous section introduces the thesis and gives background to the entire research as well as the research objectives addressed. Following this, current state of the art that relates to the research is presented. To address the specific objectives listed above (Section 1.1), the research work was divided into two parts: laboratory experiments and field work. Chapter 3 deals with airflow resistance through sweet potato aboveground parts. Experimental results are presented and predictive models developed which allow for broader application of research results. In Chapter 4, the resistance of bulk unwashed and clean sweet potato roots to airflow is presented and discussed. The physical properties of the roots are explicitly incorporated into a physically meaningful mathematical model in order to predict pressure drop realistically. In Chapter 5, a reliable simulation model which is based on the fundamental solution for heat transfer equations is extended for estimating the cooling and heating times of individual sweet potato roots under forced convection conditions and multiple air temperatures. Experimental results validated the simulation model and also provide detail understanding of temperature variations in the roots during forced-air cooling and heating treatments. Chapter 6 gives test results of low-cost evaporative cooling media configuration in terms of pressure drop, cooling efficiency and water consumption rate which are discussed in detail. The experimental results are a foundation for recommending suitable pad configuration for use in the development of low-cost evaporative cooling systems. Chapter 7 presents assessment of airflow distribution through CFD simulation and experimental measurements in a low-cost mud storehouse. Results of the CFD simulation served as an aid in the design of an optimal air inlet and plenum chamber size as well as the air outlet size and its placement. Using the results of the laboratory experiments as well as the CFD simulations

(Chapter 4, 6 & 7), an autonomous PV powered ventilated mud storehouse is developed (Chapter 8). In this chapter, detailed description of the constructed mud store is presented, followed by theoretical presentation of PV driven fan development process as well as the procedure for matching the developed fan with a PV panel. Accordingly, results of technical performance in terms of airflow, total pressure drop, patterns of temperature and RH inside the developed mud storehouse is described. Finally, key results of all research papers are discussed in Chapter 9 with recommendations for further research.

1.3 References

Amoah, R.S. (2014). The effect of ethylene on sweetpotato storage. PhD thesis, Cranfield University.

Boyette, M. D. (2009). The investigation of negative horizontal ventilation for long-term storage of sweetpotatoes. Applied Engineering in Agriculture, 25(5), 701-708.

Bovell-Benjamin, A. C. (2007). Sweet potato: A review of its past, present, and future role in human nutrition. Advances in Food and Nutrition Research, 52, 1-59.

Bengtsson, L.P., & Whitaker, J.H. (1988). Farm structures in tropical climates. Rome, Italy: United Nations FAO, SIDA Rural Structures Program.

Cantwell, M., & Suslow, T. (2001). Sweetpotato. Recommendations for maintaining postharvest quality.Online.http://postharvest.ucdavis.edu/Commodity_Resources/Fact_Sheets/Datastores/Vegetables_English/?uid=34&ds=799 (accessed on 23.08.2016).

El Sheikha, A.F., & Ray, R.C. (2015). Potential impacts of bio-processing of sweet potato: Review. Critical Reviews in Food Science and Nutrition. Online. doi:10.1080/10408398.2014.960909.

Loebenstein, G., & Thottappilly, G. (2009). The sweetpotato. Springer Science and Business Media B.V.

Garzon, J. G. (2013). Analysis by applying Near-Infrared-Refractography and statistical modeling of sweetpotato weight loss, density and quality change due to long-term storage, temperature and water stress. PhD thesis, North Carolina State University, p. 131.

Giang, H.H., Ly, L.V., & Ogle, B. (2004). Evaluation of ensiling methods to preserve sweet potato roots and vines as pig feed. Livestock Research for Rural Development, 16, Article 45.

Hall, A. J., & Devereau, A. D. (2000). Low-cost storage of fresh sweet potatoes in Uganda: lessons from participatory and on-station approaches to technology choice and adaptive

testing. Outlook on Agriculture, 29(4), 275-282.

Hagenimana, V., Carey, E.E., Gichuki, S.T., Oyunga, M.A., & Imungi, J.K. (1998). Carotenoid contents in fresh, dried and processed sweet potato products. Ecology of Food and Nutrition, 37 (5), 455-473.

Jeng, T. L., Lai, C.C., Liao, T. C., Lin, S. Y., & Sung, J. M. (2015). Effects of drying on caffeoylquinic acid derivative content and antioxidant capacity of sweet potato leaves. Journal of Food and Drug Analysis, 23(4), 701-708.

Katinoja, L., & Kader, A.A. (2002). Small-scale post-harvest handling practices: A manual for horticultural crops (4th edition). Post-harvest Horticulture Series, No. 8E.

Picha, D.H. (1986). Weight loss in sweet potatoes during curing and storage. Contribution of transpiration and respirations. Journal of the American Society for Horticultural Science, 111 (6), 889-892.

Rees, D., Kapinga, R., Rwiza, E., Mohammed, R., van Qirchot, Q. E. A., Carey, E., & Westby, A. (1998). The potential for extending shelf-life of sweet potato in east Africa through cultivar selection. Tropical Agriculture (Trinidad), 75(2), 208-211.

Sugiura, R. (2012). Production of dried sweet potato leaves and stems with high polyphenol content using airflow drying and steam blanching. Transactions of the ASABE, 55(5), 1887-1892.

Stewart, H.E., Farkas, B.E., Blankenship, S.M., & Boyette, M.D. (2000). Physical and thermal properties of three sweetpotato cultivars (*Ipomoea batatas* L.). International Journal of Food Properties, 3(3), 433-446.

van Qirschot, Q. E. A., Rees, D., & Aked, J. (2003). Sensory characteristics of five sweet potato cultivars and their changes during storage under tropical conditions. Food Quality and Preference, 14(8), 673-680.

Woolfe, J. A. (1992). Sweet potato: An untapped food resource. Cambridge, UK: Cambridge University Press.

2 State of the art

The current study was conducted to improve knowledge on post-harvest handling of sweet potato, through experimental and modeling studies of design parameters and also to develop an autonomous PV ventilated mud storehouse for storage of sweet potato roots under tropical conditions. This chapter presents the review of related literature to the sweet potato plant, post-harvest handling strategies and associated constraints, relevance of design parameters for forced convection systems design and evaporative cooling. It further presents information on the essentials of mud as a construction material, computer application in post-harvest systems design and finished off with energy use during force convection post-harvest storage and preservation operations with special emphasis on PV energy.

2.1 Sweet potato: botany, production, nutritional efficacy and uses

Sweet potato (*Ipomoea batatas* (L.) Lam) is a dicotyledonous plant, which belongs to the family Convolvulaceae. Plants in this family are characterized by having woody, herbaceous or often climbing stems. Amongst the approximately 50 genera and more than 1000 species of the family, only the *I. batatas* is of economic importance (Woolfe, 1992). Unlike yams (*Dioscorea* spp.), *I. batatas* does not produce tubers which correspond to subterranean stems or part of a stem that thicken and contain stored reserves. Sweet potato produces storage roots which present a cellular arrangement identical to a primary root with a radial vascular bundle (Lebot, 2009). Because of human intervention by domestication selection, as well as spontaneous mutations and natural hybridization, there are currently large number of sweet potato cultivars in existence, differing in the colour of the root skin and flesh, in the size and shape of the roots and leaves, in the depth of rooting, in the time of maturity and resistance to diseases (Aina et al., 2009; Woolfe, 1992).

Ranking seventh from the view point of total production, sweet potato is cultivated in over 100 countries, and serves as an important monetary source in many parts of the world (Woolfe, 1992).According to FAOSTAT (2014), an estimated of over 104 million tonnes (MT) of sweet potato roots were produced globally. Asia is the world's largest producer with 78.6 MT, while Sub-Sahara Africa (SSA) produce roughly 21.1 MT, representing 20.2% of the world's production (FAOSTAT, 2014). Specifically, China is the dominant producer of sweet potatoes, cultivating roughly 68% of the global crop, while Nigeria, Tanzania and Ethiopia produce

roughly 9% of the global crop and rank 2nd, 3rd and 4th, respectively. In the United States, sweet potatoes are considered a specialty crop and the nation currently ranks 9th in terms of total global production and crop value (FAOSTAT, 2014).

As a crop, sweet potato combines a number of advantages (El Sheikha and Ray, 2015; Brinley et al., 2008; Islam, 2006; Islam et al., 2003; Woolfe, 1992), which gives it an exciting potential in combating the food shortages and malnutrition that may increasingly occur as a result of population growth and pressure on land utilization. The Japanese used it when typhoons demolished their rice fields. Further, it kept millions from starvation in famine-plagued China in early 1960's and came to the rescue in Uganda in the 1990's, when a virus ravaged cassava crops (CIP, 2010). Generally, the crop can provide an important part of dietary carbohydrates of the population, particularly in developing countries (CIP, 2010). According to USDA (2016) and Lareo et al. (2013), besides carbohydrates, they are also rich in dietary fiber and have high water content and also provide 359 kj energy low lipids content, which is only about 0.05 g $(100g)^{-1}$. In addition, sweet potato roots also are high in minerals such as potassium, calcium, magnesium, sodium, phosphorus, and iron (USDA, 2016). Research by CIP (2010) have indicated that, just 125 g of fresh sweet potato roots from most orange-fleshed varieties contain enough ß-carotene to provide the daily pro-vitamin A needs of a preschooler.

The sweet potato crop produces a lush foliage in addition to the commercially valuable roots. Claessens et al. (2009) reported that the aboveground portion of dual-purpose sweet potato plant yields approximately 14.6 tonnes per hectare, which is very high compared with the yield of other green vegetables and natural pasture. Hue et al. (2012) and Ishida et al. (2000) have indicated that the aboveground part of sweet potato is about 1.56-folds of the roots, but 95 to 98% are discarded during the harvesting period, while the remaining 2 to 5% are used as human and animal food. This practice results in the underutilization of a potentially high nutritional and functional valuable components of the aerial vines (Johnson and Pace, 2010; Islam et al., 2006; Almazan et al., 1997). Recent studies suggest that animals fed on high protein sweet potato vines produce less methane gas than with other feed, potentially contributing to an important reduction in harmful global emissions (CIP, 2010).

2.2 Sweet potato post-harvest handling strategies and associated constraints

As previously mentioned, the components of sweet potato are subject to post-harvest losses and different handling strategies have been used in the past to extend the shelf-life. In mainland USA, reliable and year round storage of sweet potato roots has been achieved with the advent of negative horizontal ventilation storage facilities (Boyette, 2009). The design employed for these facilities is very similar to the ‘‘letterbox’’ method commonly used for storage of potato in Europe except for one major difference – the air is sucked from the operational space of the storage room. Successful application of chemicals as a means for the control of fungal pathogens as well as insect pests has also been documented (Johnson and Gurr, 2016; Ray and Nedunchezhiyan, 2012; Edmunds and Holmes, 2009). Nevertheless, the use of chemicals in recent times is limited by health concerns associated with chemical residues and environmental effect.

Marginal farmers in developing countries store sweet potato roots using various traditional methods. Storage of sweet potato roots in structures such as pit storage (Tortoe et al., 2008; Hall and Davereau, 2000); evaporative cooling barns (Abano et al., 2011); clamps (heaps), bamboo baskets and jute sacks (Gautam, 1991) and *Machan* (raised platform made of bamboo slices) and *Dhol* (made of bamboo thatched *chatai*) (Ali et al., 1991) are common practices. Roots of sweet potato have also been stored in different media: rice or millet husk (Gautam, 1991); dry sand (Samarasinghe, 1991); earth or sawdust (Mukhopadhyay et al., 1991) and in alternate layers of sand and roots (Chattopadhyay et al., 2006). The success of these traditional storage methods, however has been variable, with huge losses occurring as a result of accumulation of carbon dioxide, lack of protection against pests, insects and rodents among others.

Similar to other leafy vegetables or medicinal plants, fresh sweet potato aerial vine components has to be processed to extend their shelf-life for commercial-scale processing (Jeng et al., 2015; Sugiura, 2012). The most common and fundamental method for post-harvest preservation of agricultural products is drying. There are well reviewed papers that sum up the important results of individual studies (Öztekin and Martinov, 2013; Sagar and Suresh, 2010; Müller, 2007). Drying of the aerial vine components is not a common occurrence, although it is practiced to some extent in some parts of the world, where these

aboveground components are dried in the sun (Woolfe, 1992). Sun drying method is however reported to affect the quality of agricultural products (Öztekin and Martinov, 2013), hence various drying techniques have been developed for drying agricultural plants (Lewicki, 2006). Among these techniques, forced hot air drying is frequently used to dry plant materials because of its lower cost and less drying time (Vashisth et al., 2011). Several factors are reported in the literature to affect the performance of forced hot air drying systems (Müller and Heindl, 2006; Wilhelm et al., 2004; Henderson and Miller Jr, 1972). As energy requirements of forced hot air drying is often considerable, these factors represent a major expense in the air drying procedures (Müller and Heindl, 2006) which need to be considered when designing these systems.

2.3 Relevance of design parameters information for forced convection systems design

Previous researchers have asserted that, good ventilation in storage and in drying systems is necessary to supply air for control of air temperature and RH, deliver this air where it is required, and to circulate the air within a storage or drying system to assure uniform conditions (Amjad et al., 2015; Román et al., 2012; Boyette, 2009; Brooker et al., 1992). The resistance of agricultural products to airflow is an important parameter in the design of forced ventilation systems. The growth of the practice of forced ventilation or drying of perishable agricultural products made airflow resistance characteristics of these biological products important because ventilation and drying systems design involves a prediction of pressure drop across the bed of products to be ventilated or dried (ASABE standard D272.3, 2011). Optimal control of crop ventilation or drying also requires an accurate knowledge of the crop property values. Many properties of sweet potato crop remain to be determined, especially at various moisture contents and bulk depths, sizes as well as roughness and shape factors for both the roots and the aerial vine components. Moreover, without reliable values of the influencing parameters of agricultural crops, forced-air post-harvest systems simulations are of questionable value (Bakker-Arkema, 1984).

Research efforts on cooling and heat treatment of perishable agricultural products has also been increasing steadily in recent years, with successful laboratory investigations and some scale-up development of the use of hot air, hot water, radio frequencies and microwaves in disinfestation, chilling injury control and the slowing down of breakdown and ripening process

in various fresh horticultural crops. Several aspects of the mechanisms of cooling or heat treatments in terms of heat transfer have been thoroughly evaluated (da Silva et al., 2010; Wang et al., 2001). The influence of air velocity, temperature and product size on the duration of the entire process are the most important factors that should be taken into account during cooling and heat treatment process development. Information on these influencing parameters is essential for designing and optimizing forced-air treatment equipment's (Defraeye et al., 2014; Kumar et al., 2008; Wang et al., 2001).

Furthermore, earlier studies have established the need for maintaining lower air temperatures and high RH during storage of fresh sweet potato roots to ensure maximum storage life (Boyette, 2009; Woolfe, 1992; Picha, 1986). For high RH, there are different types of equipment that can be used successfully for adding moisture to the air in storage facilities, including centrifugal humidifiers, high pressure water spray nozzles, air assisted spray nozzles and wetted surface air washers (Brook et al., 1995; Reisinger et al., 1987). Due to the cost associated with the current humidification systems, low-cost evaporative cooling pads that promote sustainable engineering is required for resource-constrained regions. Choosing a suitable pad and configuration for a specific application however requires knowledge of different working parameters (Franco et al., 2010). Amongst them, the medium performance is crucially important.

2.4 Evaporative cooling: basic working principle, benefits, opportunities and limitations

Evaporative cooling is a physical phenomenon in which evaporation of a liquid, typically into the surrounding air, cools an object or a liquid in contact with it. The conversion of sensible heat to latent heat causes a decrease in the ambient temperature as water is evaporated providing useful cooling. The wet-bulb temperature, as compared to the air dry-bulb temperature is the measure of the potential for evaporative cooling when considering water evaporating into the air. Therefore, the greater the difference between the two temperatures, the greater the evaporative cooling effect (Basediya et al., 2013). Evaporative cooler works on the principle of cooling resulting from evaporation of water from the surface of the structure. Generally, most evaporative coolers are made of a porous material that is fed with water. The cooling achieved by this device also results in high relative humidity of the air in a cooling chamber from which the evaporation takes place relative to ambient air. The atmosphere in

the chamber therefore becomes more conducive for fruit and vegetable storage (Dadhich et al., 2008) and is therefore helpful to small farmers in rural areas. The benefits of evaporative cooling has been recognized by the World Bank (Bom et al., 1999), including substantial energy and cost savings, no chlorofluorocarbons, reduced CO_2 and power plant emissions, improved indoor air quality, life-cycle cost effectiveness, greater regional energy independence, etc. Evaporative cooling is used in tropical savanna climates such as in the northeast of Brazil, the Sahel region of Africa, the southwest Dominican Republic, for some cooling applications such as greenhouses and poultry houses (Bom et al., 1999). They are also widely used in the Middle East, Australia, the Indian subcontinent, Eastern African, northern Mexico, and the southwestern United States. Nevertheless, the major limitations for the application of evaporative cooling however centers on ambient humidity levels, and water availability. Evaporative cooling as a principle does not work in areas with high levels of humidity, since the air is already saturated with moisture and thus not much evaporation will occur. Evaporative cooling may not also be feasible in locations with limited access to water, although the water use does not need to be potable as long as food stored using evaporative coolers is protected from contamination.

2.5 Application of CFD technique in post-harvest systems design

In the last years, there has been considerable growth in the application of CFD technique for the simulation and optimization of post-harvest systems. CFD is a numerical method that solves fluid flow and heat transfers as well as other relevant physical and biochemical processes. Because of the high cost of experiments at commercial scale, this computer-based simulation and evaluation have become an attractive alternative for engineers. CFD tools allow engineers to, in an early stage of the design cycle, test different concepts up to, in the later stage, optimize a complete process and system. The enhancement of computing power and efficiency coupled with the reduced cost of CFD software packages has advanced it as a viable technique to provide effective and efficient design solutions (Norton and Sun, 2006). Recent reviewed papers that sum up important studies related to the application area are reported by Ambaw et al. (2013). This section of the state of the art, however, deals mainly with the simulation of airflow distribution in post-harvest forced-air systems. Mathioulakis et al. (1998) applied CFD to simulate airflow distribution in a tray dryer. Such flow simulations allow air distribution in the dryer to be visualized, thus facilitating the identification of

possibilities for design changes. CFD technique have also been used in the design and improvement of forced-air handling systems such as a diagonal batch type dryer (Amjad et al., 2015); fixed-bed dryer (Román et al., 2012); cabinet dryer (Amanlou and Zomorodian, 2010); cold store (Delele et al., 2009; Hoang et al., 2000) and a refrigerated vehicle (Moureh et al., 2009). Nevertheless, simulation results should still be validated by experiments because CFD uses many approximate models as well as few assumptions (Xia and Sun, 2002).

2.6 Crop storage structures: the essentials of mud as a construction material

A crop storage structure refers to a container which is originally designed and constructed or an existing structure that is remodeled for the primary purpose of safe keeping of agricultural crops from the harsh conditions of the ambient environment (Bengtsson and Whitaker, 1988). Throughout the storage period, a good storage structure is expected to protect stored produce and maintain their quality. Even though several materials have been used in the construction of storage structures among which are concrete, steel, wood; these are faced with certain limitations which hampered their widespread use for crop storage, especially in tropical regions of SSA. For instance, concrete and steel even though strong, are very expensive while wood is easily biodegradable. Mud is one of the low-cost material commonly used for the construction of both dwellings and storage structures, particularly in most rural areas of developing countries. Traditional mud silos which were promoted in some districts of northern Ghana for grain storage (World Bank, 2011) are examples of such rural storage structures. Mud material is readily available at most construction sites, fire resistant and easy to work using simple tools and skills (Bengtsson and Whitaker, 1988). The thermal storage properties and humidity balancing effect of mud provide the advantages to keep the inside of mud structures cool when the outside is hot and vice versa (Minke, 2006). Thus, mud construction act as a RH flywheel, equalizing the RH of the external environment with that of pores with the walls (Allinson and Hall, 2010). The application of mud as wall material was investigated to control room air temperature for buildings by Duffin and Knowles (1981).Chel and Tiwari (2009) reported that the thermal properties of mud such as low thermal conductivity and high heat capacity are responsible for keeping the inside room air temperature value nearly constant.

2.7 Energy use during forced convection post-harvest operations with focus on PV energy

In recent years, energy demand for post-harvest operations such as cool storage and drying of agricultural products have risen significantly. An analysis of the present situation worldwide shows a completely contrasting situation between industrialized and developing countries. This disparity has greatly influenced the possibilities of utilizing solar energy in crop post-harvest operations such as cool storage and drying. At present, the energy supply in developed countries is still sufficient. Electricity and fossil fuels are available at relatively low prices and almost all post-harvest operations are connected to national grid. As a result, solar technologies that can be used independently of the weather conditions have to compete with highly efficient and reliable conventional technologies (Mühlbauer and Esper, 1999). In developing countries however, the possibility of utilizing solar energy are economically feasible compared with its use in developed countries. High solar irradiance, decentralized use and low energy demand favour its use especially in rural areas.

No discussion of rural electricity needs for cool storage and drying can ignore the potential of PV panels. The special attraction of PVs compared with that of other power generation technologies lies in the fact that solar radiation is converted directly into electric power by an electronic solid-state process (Esper et al., 1999). An important advantage of a PV system is its modularity, permitting flexible system sizing for decentralized applications down to small demands. These characteristics are of particular benefit for applications in post-harvest operations in rural areas, for which features such as reliability, simple installation, and simple operation are important (Esper, 1995; Roger, 1979). For example, powering electric fans used in crop storage and drying systems is an important application of PV energy. Through comprehensive optimization concept of PV panels, propellers and direct current (DC) motors, a PV ventilated solar tunnel was developed (Esper, 1995) and successfully introduced in more than 60 countries worldwide (INNOTECH Ingenieursgesellschaft GmbH, 2016). The concept has since been successfully applied in the design of solar greenhouse dryers (Janjai et al., 2009; Barnwal and Tiwari, 2008; Janjai et al., 2007). The use of PV energy in vapour compression cooling systems for potatoes (*Solanum tuberosum* (L.)) is also well documented in the literature (Eltawil, 2003).

2.8 References

Amjad, W., Munir, A., Esper, A., & Hensel, O. (2015). Spatial homogeneity of drying in a batch type food dryer with diagonal air flow design. Journal of Food Engineering, 144, 148-155.

Ambaw, A., Delele, M.A., Defraeye, T., Ho, Q.T., Opara, L.U., Nicolaï, B.M., & Verboven, P. (2013). The use of CFD to characterize and design post-harvest storage facilities: Past, present and future. Computers and Electronics in Agriculture, 93, 184-194.

ASABE Standards. (2011). D272.3: Resistance to airflow of grains, seeds, other agricultural products and perforated metal sheets. St. Joseph, MI: ASABE.

Abano, E.E., Teye, E., Amoah, R.S., & Tetteh, J.P. (2011). Design, construction and testing of an evaporative cooling barn for storing sweetpotaotes in the tropics. Asia Journal of Agricultural Research, 5(2), 115-126.

Allinson, D., & Hall, M. (2010). Hygrothermal analysis of a stabilised rammed earth test building in the UK. Energy and Building, 42(6), 845-852.

Amanlou, Y., & Zomorodian, A. (2010). Applying CFD for designing a new fruit cabinet dryer. Journal of Food Engineering, 101, 8-15.

Aina, A., Falade, K.O., Akingbala, J. O., & Titus, P. (2009). Physicochemical properties of twenty-one Caribbean sweet potato cultivars. International Journal of Food Science and Technology, 44, 1696-1704.

Almazan, A.M., Begum, F., & Johnson, C. (1997). Nutritional quality of sweetpotato greens from greenhouse plants. Journal of Food Composition and Analysis, 10, 246-253.

Ali, M.S., Bhuiyan, M.K.R., Mannan, M.A., & Rashid, M.M. (1991). Post-harvest handling and utilization of sweet potato in Bangladesh. In Dayal, T.R., Scott, G.J., Kurup, G.T., Balagopalan, C. (Eds.), sweet potato in South Asia: post-harvest handling, storage, processing and use. Proceedings of a workshop held at CICRI, Trivandrum, 9-13 September, pp. 13-22.

Basediya, A.L., Samuel, D.V.K., & Beera, V. (2013). Evaporative cooling system for storage of fruits and vegetables. A review. Journal of Food Science and Technology, 50(3), 429-442.

Boyette, M. D. (2009). The investigation of negative horizontal ventilation for long-term storage of sweetpotatoes. Applied Engineering in Agriculture, 25(5), 701-708.

Brinley, T.A., Truong, V.D., Coronel, P., Simunovic, J., & Sandeep, K.P. (2008). Dielectric properties of sweet potato purees at 915 MHZ as affected by temperature and chemical

composition. International Journal of Food Properties, 11, 158-172.

Barnwal, P., & Tiwari, G.N. (2008). Grape drying using hybrid photovoltaic-thermal greenhouse dryer: An experimental study. Solar Energy, 82(12), 1131-1144.

Bom, G.J., Foster, R., Dijkstra, E., & Tummers, M. (1999). Evaporative air-conditioning: Applications for environmentally friendly cooling. Washington, D.C. World Bank.

Brook, R.C., Fick, R.J., & Forbush, T.D. (1995). Potato storage design and management. American Potato Journal, 72(8), 463-480.

Brooker, D.B., Bakker-Arkema, F.W., & Hall, C.W. (1992). Drying and storage of grains and oilseeds. New York: Van Nostrand Reinhold.

Bengtsson, L.P., & Whitaker, J.H. (1988). Farm structures in tropical climates. Rome, Italy: United Nations FAO, SIDA Rural Structures Program.

Bakker-Arkema, F.W. (1984). Selected aspects of crop processing and storage: A review. Journal of Agricultural Engineering Research, 30, 1-22.

Chel, A., & Tiwari, G.N. (2009). Thermal performance and embodied energy analysis of a passive house – Case study of vault roof mud-house in India. Applied Energy, 86(10), 1956-1969.

Claessens, L., Stoorvogel, J.J., & Antle, J.M. (2009). Ex *ante* assessment of dual-purpose sweet potato in the crop-livestock system of western Kenya: A minimum-data approach. Agricultural Systems, 99, 13-22.

Chattopadhyay, A., Chkraborty, I., Kumar, P. R., Nanda, M. K., & Sen, H. (2006). Uncontrolled storage behaviour of sweetpotato (*Ipomoea batatas* L. Lam). Journal of Food Science and Technology, 43, 41-45.

Defraeye, T., Lambrecht, R., Delele, M.A., Ambaw, A.T., Opara, U. L., Cronjé, P., Verboven, P., & Nocolaï, B. (2014). Forced-convection cooling of citrus fruit: Cooling conditions and energy consumption in relation to package design. Journal of Food Engineering, 121, 118-127.

da Silva, W.P., e Silva, C.M.D.P.S., Farias, W.S.O., & e Silva D.D.P.S. (2010). Calculation of convection heat transfer and cooling kinetics of an individual fig fruit. Heat and Mass Transfer, 46 (3), 371-380.

Delele, M.A., Schenk, A., Ramon, H., Nicolaï, B.M., & Verboven, P. (2009). Evaluation of a chicory root cold store humidification system using computational fluid dynamics. Journal of Food Engineering, 94(1), 110-121.

Dadhich, S. M., Dadhich, H., & Verma, R.C. (2008). Comparative study on storage of fruits and vegetables in evaporative cool chamber and in ambient. International Journal of Food Engineering, 4(1),1-11.

Duffin, R. J., & Knowles, G. (1981).Temperature control of buildings by adobe wall design. Solar Energy, 27(3),241-249.

El Sheikha, A.F., & Ray, R.C. (2015). Potential impacts of bio-processing of sweet potato: Review. Critical Reviews in Food Science and Nutrition. Online. http://dx.doi.org/doi:10.1080/10408398.2014.960909.

Edmunds, B.A., & Holmes, G.J. (2009). Evaluation of alternative decay control products for control of postharvest *Rhizopus* soft rot of sweetpotatoes. Online. Plant Health Progress. Online. http://dx.doi.org/doi:10.1094/PHP-2009-0206-01-RS.

Eltawil, M.A.M.A. (2003). Solar photovoltaic powered cooling system for potato storage. PhD thesis, Agricultural Engineering, IARI, New Delhi.

Esper, A., Schumm, G., & Mühlbauer (1999). Solar energy – Utilization as power. CIGR - Handbook Vol. V: Energy and Biomass Engineering, St. Joseph, Mich.: ASAE. pp. 66-91.

Esper, A. (1995). Solarer Tunneltrockner mit photovoltaischen Antriebssystem. Forschungsbericht Agrartechnik 264 des Arbeitskreises Forschung und Lehre der Max-Eyth Gesellschaft Agrartechnik. VDI (VDI-MEG).

FAOSTAT (2014). Production for sweet potato. Online. http://faostat3.fao.org/browse/Q/QC/E (accessed on 30.06.2016).

Franco, A., Valera, D. L., Madueño, A., & Peña, A. (2010). Influence of water and air flow on the performance of cellulose evaporative cooling pads used in Mediterranean Greenhouses. Transactions of the ASABE, 53 (2), 565-576.

Gautam, D.M. (1991). Production, post-harvest handling and utilization of sweet potato in Nepal. In Dayal, T.R., Scott, G.J., Kurup, G.T., Balagopalan, C. (Eds.), sweet potato in South Asia: post-harvest handling, storage, processing and use. Proceedings of a workshop held at CICRI, Trivandrum, 9-13 September, pp. 23-28.

Hue, S.M., Boyce, A.N., & Somasundram, C. (2012). Antioxidant activity, phenolic and flavonoid contents in the leaves of different varieties of sweet potato (*Ipomoea batatas*). Australian Journal of Crop Science, 6(3), 375-380.

Hall, A. J., & Devereau, A. D. (2000). Low-cost storage of fresh sweet potatoes in Uganda: lessons from participatory and on-station approaches to technology choice and adaptive

testing. Outlook on Agriculture, 29(4), 275-282.

Hoang, M.L., Verboven, P., De Baerdemaeker, J., & Nicolaï, B.M. (2000). Analysis of the airflow in a cold store by means of computational fluid dynamics. International Journal of Refrigeration, 23, 127-140.

Henderson, S.M., & Miller Jr., G.E. (1972). Hop drying – Unique problems and some solutions. Journal of Agricultural Engineering Research, 17, 281-287.

INNOTECH Ingenieursgesellschaft GmbH (2016). Solarer Tunneltrockner ‘‘Hohenheim. Ausgereifte Technik für tropische und subtropische Länder. Online. http://www.innotech-ing.de/de/index.php/tunneltrockner (accessed on 09.07.2016).

International Potato Center (CIP) (2010). Facts and figures about sweetpotato. Online. http://192.156.137.121:8080/cipotato/publications/pdf/005448.pdf (accessed on 09.07.2016).

Islam, S. (2006). Sweetpotato (*Ipomoea batatas* L.) leaf: Its potential effect on human health and nutrition. Journal of Food Science, 71(2), R14-R21.

Islam, S. M., Yoshimoto, Y., & Yamakawa, O. (2003). Distribution and physiological functions of caffeoylquinic acid derivatives in leaves of sweet potato genotypes. Journal of Food Science, 68(1), 111-116.

Ishida, H., Suzuno, H., Sugiyama, N., Innami, S., Tadokoro, T., & Maekawa, A. (2000). Nutritive evaluation on chemical components of leaves, stalks and stems of sweet potatoes (*Ipomoea batatas poir*). Food Chemistry, 68(3), 359-367.

Johnson, A.C., & Gurr, G.M. (2016). Invertebrate pests and diseases of sweetpotato (*Ipomoea batatas*): A review and identification of research priorities for smallholder production. Annals of Applied Biology, 168(3), 291-320.

Jeng, T. L., Lai, C.C., Liao, T.C., Lin, S. Y., & Sung, J. M. (2015). Effect of drying on caffeoylquinic acid derivative content and antioxidant capacity of sweet potato leaves. Journal of Food and Drug Analysis, 23(4), 701-708.

Johnson, M., & Pace, R.D. (2010). Sweet potato leaves: Properties and synergistic interactions that promote health and prevent diseases. Nutrition Reviews, 68(10), 604-615.

Janjai, S., Lamlert, N., Intawee, P., Mahayothee, B., Bala, B. K., Nagle, M., & Müller, J. (2009) Experimental and simulated performance of a PV-ventilated solar greenhouse dryer for drying of peeled longan and banana. Solar Energy, 83, 1550-1565.

Janjai, S., Khamvongsa, V., & Bala, B. K. (2007). Development, design, and performance of a

PV-ventilated greenhouse dryer. International Energy Journal, 8(4), 249-258.

Kumar, R., Kumar, A., & Murthy, U. N. (2008). Heat transfer during forced air precooling of perishable food products. Biosystems Engineering, 99, 228-233.

Lareo, C., Ferrari, M.D., Guigou, M., Fajardo, L., Larnaudie, V., Ramírez, M.B., & Martínez-Garreiro, J. (2013). Evaluation of sweet potato for fuel bioethanol production: Hydrolysis and fermentation. SpringerPlus, 2:493.

Lebot, V. (2009). Tropical root and tuber crops: Cassava, sweet potato, yams and aroids. Crop production Science in Horticulture Series (17), CAB books, CABI Wallingford, UK.

Lewicki, P.P. (2006). Design of hot air drying for better foods. Trends in Food Science and Technology, 17(4), 153-163.

Moureh, J., Tapsoba, S., Derens, E., & Flick, D. (2009). Air velocity characteristics within vented pallets loaded in refrigerated vehicle with and without air ducts. International Journal of Refrigeration, 32(2), 220-234.

Müller, J. (2007). Convective drying of medicinal, aromatic and spice plants. A review. Stewart Postharvest Review, 4(2), 1-6.

Minke, G. (2006). Building with earth – Design and technology of a sustainable architecture. Birkhauser publishers for Architecture, Basel, Berlin, Boston.

Müller, J., & Heindl, A. (2006). Drying of medicinal plants. In R. J. Bogers, L. E. Craker, & D. Lange (Eds.), Medicinal and aromatic plants-agricultural, commercial, ecological, legal, pharnmacological and social aspects (Vol. 17, pp. 237-258). Berlin, Germany: Wageningen UR Frontis Series.

Mühlbauer, W., & Esper, A. (1999). Solar energy: Present situation, principles of solar energy applications, solar drying. CIGR - Handbook Vol. V: Energy and Biomass Engineering, St. Joseph, Mich.: ASAE. pp. 53-66.

Mathioulakis, E., Karathanos, V.T., & Belessiotis, V. G. (1998). Simulation of air movement in a dryer by computational fluid dynamics: Application for the drying of fruits. Journal of Food Engineering, 36(2), 183-200.

Mukhopadhyay, S.K., Sen, H., & Jana, P.K. (1991). Storage of sweetpotato tubers using locally available materials. Journal of Root Crops, 17, 71-72.

Norton, T., & Sun, D.-W. (2006). Computational fluid dynamics (CFD) – An effective and efficient design and analysis tool for the food industry: A review. Trends in Food Science and Technology, 17(11), 600-610.

Öztekin, S., & Martinov, M. (2013). Medicinal and aromatic crop drying. Stewart Postharvest Review, 2(3), 1-5.

Picha, D.H. (1986). Weight loss in sweet potatoes during curing and storage. Contribution of transpiration and respirations. Journal of the American Society for Horticultural Science, 111 (6), 889-892.

Ray, R.C., & Nedunchezhiyan, M. (2012). Postharvest fungal rots of sweet potation tropics and control measures. Fruits, Vegetables and Cereal Science and Biotechnology, 6(1), 134-138.

Román, F., Strahl-Schäfer, V., & Hensel, O. (2012). Improvement of air distribution in a fixed bed dryer using Computational Fluid Dynamics. Biosystems Engineering, 112, 359-369.

Reisinger, G., Müller, J., & Mühlbauer, W. (1987). Development of an air conditioning system for green houses in hot and dry climates. Solar and Wind Technology, 4(1), 17-20.

Roger, J. A. (1979). Theory of the direct coupling between DC motors and photovoltaic solar arrays. Solar Energy, 23, 193-198.

Sugiura, R. (2012). Production of dried sweet potato leaves and stems with high polyphenol content using airflow drying and steam blanching. Transactions of the ASABE, 55(5), 1887-1892.

Sagar, V.R., & Suresh, K.P. (2010). Recent advances in drying and dehydration of fruits and vegetables. A review. Journal of Food Science and Technology, 47(1), 15-26.

Samarasinghe, S.H.M.C. (1991). Production, post-harvest handling and utilization of sweet potato in Sri Lanka. In Dayal, T.R., Scott, G.J., Kurup, G.T., Balagopalan, C. (Eds.), sweet potato in South Asia: Post-harvest handling, storage, processing and use. Proceedings of a workshop held at CICRI, Trivandrum, 9-13 September, pp. 29-31.

Tortoe, C., Obodai, M., Amoa-Awua, W., Oduro-Yeboah, C., & Vowotor, K. (2008). Effectiveness of three different storage structures and curing process for the storage of sweet potato (*Ipomoea batatas* L) in Ghana. Ghana Journal of Agricultural Science, 41 (2), 227-236.

USDA (2016). USDA National Nutritional Database for Standard Reference, Release 28. Nutrient Database Laboratory. Online. https://ndb.nal.usda.gov/ndb/foods/show/3207 (accessed on 30.06.2016).

Vashisth, T., Singh, R.K., & Pegg, R.B. (2011). Effect of drying on the phenolics content and antioxidant activity of muscadine pomace. LWT-Food Science and Technology, 44(7), 1649-1657.

World Bank (2011). Missing food: The case of post-harvest grain losses in Sub-Saharan Africa. Washington, DC: The World Bank, Report No. 60371-AFR.

Wilhelm, L.R., Suter, D.A., & Brusewitz, G.H. (2004). Drying and dehydration. Food and Process Engineering Technology. St. Joseph, Michigan: ASAE. Chapter 10, pp. 259-284.

Wang, S. Tang, J., & Cavalieri, R. P. (2001). Modeling fruit internal heating rates for hot air and hot water treatments. Postharvest Biology and Technology, 22, 257-270.

Woolfe, J. A. (1992). Sweet potato: An untapped food resource. Cambridge, UK: Cambridge University Press.

Xia, B., & Sun, D.-W. (2002). Application of computational fluid dynamics (CFD) in the food industry: A review. Computers and Electronics in Agriculture, 34(1-3), 5-24.

3 Resistance to airflow through sweet potato aerial vine components

J.K. Korese[1,2)], O. Hensel[1)]

[1)] Department of Agricultural Engineering, University of Kassel, Nordbahnhofstr. 1a, 37213 Witzenhausen, Germany

[2)] Department of Agricultural Mechanisation and Irrigation Technology, University for Development Studies, Post Office Box 1882, Nyankpala Campus, Tamale, Ghana

3.1 Abstract

Designers of forced air handling systems require data on resistance to airflow for accurate selection of fans and mathematical prediction of pressure drop and airflow patterns. In this research, resistance to airflow of sweet potato leaves and chopped sweet potato aerial vines dried in an experimental cabinet dryer was measured to determine the effect of airflow rate, moisture content and bulk depth. Five levels of moisture contents (88.7%, 74.7%, 52.9%, 26.8%, and 11.0% w.b.) for sweet potato leaves and (88.1%, 69.1%, 52.2%, 35.0%, and 12.2% w.b.) for chopped sweet potato aerial vines, respectively, and four levels of bulk depths (0.30, 0.45, 0.60, and 0.75 m) were investigated at airflow rates ranging from 0.0206 to 0.2342 m^3 s^{-1} m^{-2}. Results indicated that airflow, moisture content, and bulk depth have significant ($P < 0.01$) effect on airflow resistance of sweet potato leaves and chopped sweet potato aerial vines. Equations that relate pressure drop to airflow rate, moisture content, and bulk depth were developed based on the Hukill and Ives (1955) equation through the implementation of empirical “de-rating” factors and the coefficients obtained by regression analysis. The developed models provided a good fit to the experimental pressure drop data obtained in the range of conditions investigated. Also, comparison of the pressure drop data in this study with marigold flowers cited in the literature shows that the resistance to airflow for both sweet potato leaves and chopped sweet potato aerial vines was lower than that of marigold flowers. The pressure drop curves for sweet potato leaves however had a steeper slope than the marigold flowers. Bulk density which varied from 29.57 to 112.63 kg m^{-3} for sweet potato leaves and 83.99 to 317.23 kg m^{-3} for chopped sweet potato aerial vines was significantly affected by moisture content.

Keywords. Bulk depth, Bulk density, Chopped aerial vines, Curves, Leaves, Moisture content, Sweet potato.

3.2 Introduction

Sweet potato (*Ipomoea batatas* L.) is an important food and feed crop in most developing countries because of its nutritional advantages. The tops of sweet potato plants can be continuously harvested over many months, not just once like many other commercial vegetables or forage crops. The aerial vines of the plant are rich in polyphenols such as caffeic acid, chlorogenic acid, and other caffeoylquinic acid derivatives, as well as many nutrients including protein, dietary fiber, carotenoids (carotenes and xanthophylls), vitamins, and minerals (Sugiura and Watanabe, 2011; Ishida et al., 2000). It has been documented that the aerial vines of the plant can be used as a direct feed or as a feed supplement for animals (Farrell et al., 2000; Teguia et al., 1997; Brown and Chavalimu, 1985). Carotene and xanthophyll is used in the poultry industry as a feed supplement for the coloration of egg yolks and chicken skin. As an alternative, sweet potato aerial vine components could be used to enhance the yellow color produced in the skin and yolk of broilers or for other domestic and industrial applications. Sugiura and Watanabe (2011) reported that great amounts of sweet potato aerial vines are produced as a by-product after harvesting of the roots. Most of these are however discarded in the current sweet potato production systems in tropical and subtropical climates where it is mostly cultivated. It is therefore anticipated that if the aerial parts of sweet potato plants are collected and preserved, local farmers can earn additional revenue.

The leaves and stems of sweet potato have high moisture content and are perishable (Sugiura and Watanabe, 2011). Since they have a short shelf-life, they must be processed or preserved for future processing or for use as a functional animal feed. One of the methods of preservation is to dry the plant parts by forcing heated air through them to remove moisture (Müller and Heindl, 2006; Janjai and Tung, 2005). Due to the variety of agricultural products, namely leaves, stems, flowers, roots and fruits of food/feed, herbal and medicinal plants, dryers of different designs exist and are often configured to specific needs (Müller and Heindl, 2006). For instance, many of the plants are heat sensitive and tend to loose quality during drying. As a result, dryer designs must conform to the plant parts to be dried. This implies that drying must be carried out under specific conditions in order to obtain the desired final product quality. To carry out drying, harvested products are usually bulked up on a grated floor of a dryer and dried by forcing heated air through the product using ventilators. During this phase, there will

be gradients for moisture content, temperature, and relative humidity as a function of bulk height, which changes as drying progresses. The drying time depends mostly on the bulk height, air velocity, and the applied temperature and relative humidity of the inlet air. Therefore, for the operation of such drying systems several decision variables must be taken into account. For instance, airflow can be reduced to decrease the pressure head and the power required to operate a dryer ventilator. Moreover, a commercial dryer should be monitored continuously to adjust the fan speed and airflow direction to achieve the right moisture content efficiently without over-drying (Iqbal et al., 2015). High moisture content and smaller particle size result in higher bulk density, which increases the pressure drop across the drying plenum. High airflow speed also increases the pressure drop due to more resistance of the material. Therefore, airflow through bulk products during drying provides a means of environmental control for the chemical changes likely to occur as well as moisture removal. To optimally design a forced air ventilation system for drying bulk aerial vines of sweet potato, the resistance to airflow data is required and must be estimated realistically in order to appropriately match a fan to the drying system and its content.

A number of research workers have studied airflow resistance of various biological products, ranging from woody biomass (Grubecki, 2015; Iqbal et al., 2015; Sadaka et al., 2002; Kristensen and Kofman, 2000; Suggs and Lanier, 1985) to milkweed pod (Jones and Von Bargen, 1992). Pressure drop data for more common products like grains and seeds, as well as other agricultural products, have also been documented in ASABE standard D272.3 (ASABE Standards, 2011). To determine airflow relationships for a biological material, it is common to include some physical characteristics of the material (Reed et al., 2001; Li and Sokhansanj, 1994; Gunasekaran and Jackson, 1988). Cooper and Sumner (1985) reported that biomass pressure drop characteristics are often affected by bulk density and particle size. For example, bulk density, moisture content, particle size, and shape were shown to influence the pressure drop curves for chopped miscanthus and alfalfa leaves (Iqbal et al., 2015; Rabe and Currence, 1975) and density and leaf orientation were the determining parameters for pressure drop in fresh tobacco leaves (Anderson et al., 1998; Suggs et al., 1985). For whole potatoes, Irvine et al. (1993) reported that pressure drop was affected by potato size and airflow direction for different potato types while airflow resistance in sugar beet roots was influenced by root size and presence of foreign materials (Tabil et al., 2003). To date, limited

data on the resistance to airflow of sweet potato leaves and chopped sweet potato aerial vines have been reported in literature or compiled in ASABE standard D272.3 (ASABE Standards, 2011), which presents resistance to airflow for about 40 agricultural commodities. Considering that the cost of acquisition and operation of ventilation fan are related to its power which is a function of airflow and static pressure to be supplied, it is important to understand the factors that influence its power demand.

The objectives of this study were: (1) to measure and evaluate the pressure drop as a function of airflow through bulk sweet potato leaves and chopped sweet potato aerial vines at different moisture contents and bulk depths, (2) to establish the relationship between bulk density and bulk depths at different moisture contents, and (3) to develop model equations based on the experimental data to predict pressure drop across bulk sweet potato leaves and chopped sweet potato aerial vines for a range of drying conditions.

3.3 Materials and methods

3.3.1 Plant material

Sweet potatoes (*Ipomoea batatas* L. cv. CRI-Apomuden) used in this study were grown in summer 2014 at the Experimental and Demonstration farm of the Department of Agricultural Engineering, University of Kassel, Witzenhausen, Germany. The sweet potatoes were grown according to organic production practices and the aerial vines were harvested before flowering. Figure 3-1 shows a sweet potato plant and its major components.

Two different samples were investigated in this study: sweet potato leaves and chopped sweet potato aerial vines. The leaves, here refers to the sweet potato aerial vine components formed by a single leaf and a petiole. For each sample, the matured aerial vine components were randomly harvested by hand in early morning to avoid shrinkage due to environmental drying. After harvesting, the samples were immediately transported to the research laboratory. The leaves were manually separated from the vines. The entire aerial vines of the plants were also collected and chopped into particles of between 1.5 to 3.0 cm long pieces using a straw cutting machine (FLORICA E-1800, Germany). The mixture of the leaves and the stem material (petiole and stem) was 24.6% and 75.4% by weight, respectively. Almost all experiments were performed within one or a maximum of two days and consisted of several experimental

measurements.

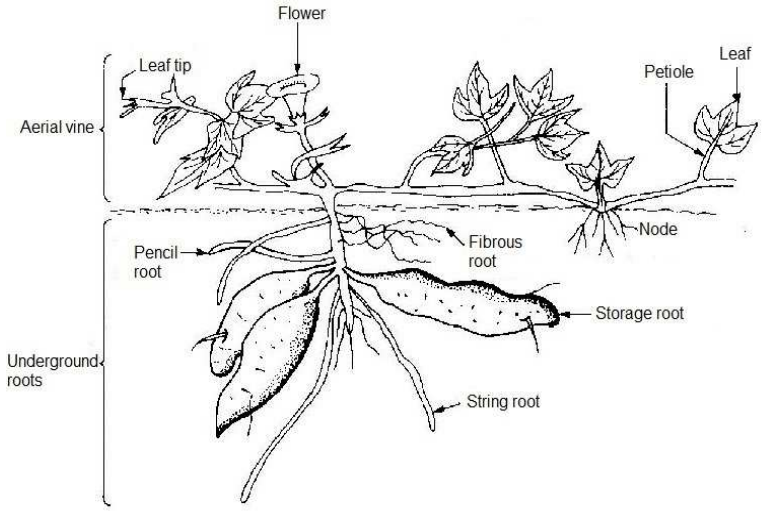

Figure 3-1 A drawing showing the morphology of a sweet potato plant (Woolfe, 1992). In practice, the proportion of foliage to root is somewhat greater than that shown here.

3.3.2 Test equipment

The arrangement of the apparatus used for the study was similar in dimensions (except the test chamber), though not necessarily in concept, to that used by Román and Hensel (2014) and is shown in figure 3-2. The main parts of the apparatus are air inlet duct, butterfly valve, centrifugal in-line duct fan (type KRW315/4F, Helios Ventilatoren, Germany), air plenum, and test chamber. The entrance to the apparatus consisted of a round galvanized steel air duct with a diameter of 0.15 m and a length of 0.85 m. At 0.3 m downstream from the duct inlet, a honeycomb flow straightener with tube diameter of 0.005 m and tube length of 0.05 m was installed to remove any tangential velocity components. The butterfly valve was installed immediately upstream of the fan in order to reduce the airflow to the desired test conditions. Below the perforated plate which formed the bottom of the test chamber, three additional perforated plates with a space of 0.05 m between them were installed to improve the flow uniformity after the change of direction in the plenum chamber. The test column consisted of a cylindrical container constructed from transparent acrylic material of 1 m long and 0.45 m internal diameter.

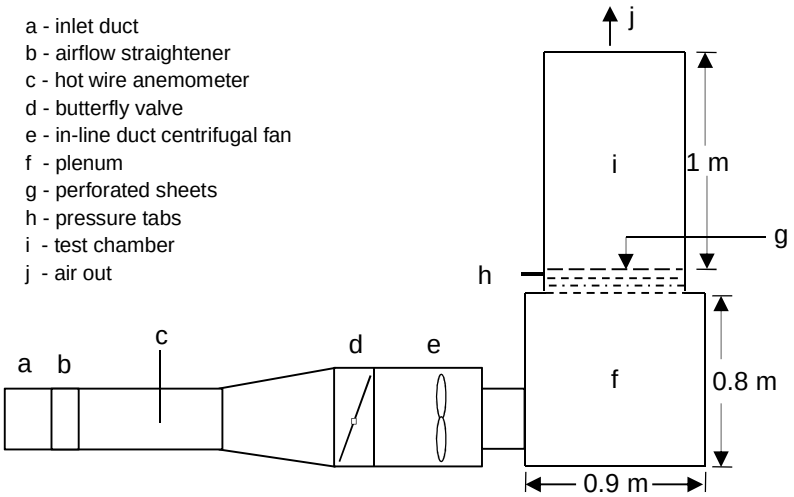

Figure 3-2 Schematic diagram of the apparatus used for airflow resistance measurement.

Hot wire anemometer (Airflow TA-5, Airflow Lufttechnik GmbH, Germany) was inserted through a port located at the duct center and 0.4 m downstream of the flow straightener to measure the air velocity profile. To determine the airflow rate in the system, the guideline of VDI/VDE 2640 part 3 (1983) was used as detailed by Román and Hensel (2014). Static pressure was measured across bulk sweet potato aerial vine components using an electronic differential pressure meter (Testo 510, Testo AG, Germany). The device was connected to four pressure tabs by a flexible rubber tubing located immediately below the test chamber base.

3.3.3 Pressure drop test

Measurements of pressure drop were obtained for sweet potato leaves and chopped sweet potato aerial vines at various moisture contents and bulk depths. To obtain samples of different moisture content conditions, sweet potato leaves and sweet potato aerial vines were dried in a laboratory cabinet dryer. The cabinet dryer consisted of 24 square-shaped trays which were stacked on a rack at 0.1 m intervals. Each tray had a drying area of 0.308 m^2. The trays of the dryer were loaded with approximately 0.03 m thickness of drying material in order to ensure uniform drying. The drying air temperature during samples drying was set at 60 °C for all experiments in order to reduce the drying time (Sugiura and Watanabe, 2011). Nevertheless, adjusting the drying air temperature from 60 °C to 36 °C is reported to improve the polyphenol content of dried sweet potato leaves (Sugiura and Watanabe, 2011). For a given experimental material, the samples were dried for a couple of hours (table 3-1), removed, and placed in the

airflow resistance measurement system (fig. 3-2). After each measurement, the samples were placed back in the cabinet dryer for additional drying and the same sequence of pressure drop measurement repeated as reported by Reed et al. (2001). The duration required to obtain a given moisture content condition was based on preliminary drying test that were conducted. Drying experiments were performed once for each moisture condition.

Pressure drop measurements for each test condition were conducted as follows. The test chamber was filled manually with non-compacted material to a desired depth. Once the chamber was filled, the fan was switched on. Then the pressure drop was measured by throttling the fan at predetermined series of increasing airflow rates, from 0.0206 to 0.2342 m^3 s^{-1} m^{-2}. Three replications were performed for a given moisture content and depth, and a randomized approach was used for the sequencing of test within each experiment. Although it was not possible to keep the moisture contents as desired due to the handling and test runs, moisture differences were not significant in all cases. The bulk density of the material was obtained by dividing the mass required to fill a given depth of the chamber by its volume. Moisture content of the test material after each drying phase was determined in triplicate according to ASABE S358.3 (ASABE Standards, 2012). Due to shrinkage during the drying phase, the maximum bulk depth that could be tested decreased at moisture content levels of 52.9% to 11.0% w.b. for leaves and 52.2% to 12.2% w.b. for chopped aerial vines. As a result, additional drying tests were performed and combined with previously dried material to create enough volume for testing. The drying interval, moisture contents, and bulk depths are presented in table 3-1.

Table 3-1 Sweet potato aerial vine components moisture contents and test depths for pressure drop measurements during drying at 60°C.

Test Depths (m)	Drying Interval (hr)	Leaves MC (% w.b.)	Chopped Aerial Vines MC (% w.b.)
	0 [a]	87.7	88.1
0.30, 0.45,	2.2	74.7	69.1
0.60, 0.75	4.2	52.9	52.2
	6.2	26.8	35.0
	7.2	11.0	12.2

[a] Fresh samples

3.3.4 Analysis of airflow resistance data

Several models have been used to describe the relationship between airflow and pressure drop data, including Shedd (1953) equation, Hukill and Ives (1955) equation, and the Ergun (1952) equation. The Hukill and Ives (1955) equation was selected as an ASABE standard (ASABE Standards, 2011) and is used to represent a wide range of materials. Therefore, the airflow resistance results for each data of fixed moisture content and bulk depth were fitted into the Hukill and Ives (1955) equation:

$$\frac{\Delta P}{L} = \frac{av^2}{\mathrm{Log_e}(1+bv)} \tag{3-1}$$

where ΔP is the pressure drop (Pa), L is the bulk depth (m), v is the airflow ($m^3\ s^{-1}\ m^{-2}$) and a and b are constants for a particular material (regression coefficients).

The model constants of equation (3-1) were estimated by fitting the model to the experimental data by non-linear regression using the statistical analysis program, IBM SPSS Statistics 22. The effect of different variables (airflow, moisture content, and bulk depth) on the resistance to airflow of bulk sweet potato leaves and chopped sweet potato aerial vines were determined using completely randomized design (CRD) method with three replications. The data were analyzed using univariate analysis of variance (ANOVA) in SPSS. Pressure drop was treated as the depended variable.

3.4 Results and discussion

3.4.1 Resistance to airflow

A laboratory test stand was used to determine the resistance to airflow through sweet potato leaves and chopped sweet potato aerial vines over airflow rate range of 0.0206 to 0.2342 $m^3\ s^{-1}\ m^{-2}$. The pressure drop across the empty test chamber of the test stand was found as 0.66 to 44.74 Pa for airflow rates ranging from 0.0206 to 0.3095 $m^3\ s^{-1}\ m^{-2}$. To evaluate the pressure drop due to the sweet potato leaves and chopped sweet potato aerial vines only, the pressure drop values of the empty test chamber were subtracted from the pressure drop measurements for the chamber with sweet potato leaves and/or chopped sweet potato aerial vines at similar velocities. Figures 3-3 and 3-4 exemplify pressure drop data of sweet potato leaves and

chopped sweet potato aerial vines in the moisture content range of 88.7% to 11.0% w.b. and 88.1% to 12.2% w.b., respectively, and for bulk depths of 0.30, 0.45, 0.60, and 0.75 m. The dotted lines in all the figures are model fitting results based on an empirical modification of Hukill and Ives (1955) equation. This is discussed in the section empirical improvement of model and fitting. Pressure drop increased linearly with increasing airflow rate as shown in the figures. As expected, the slope of pressure drop curves is observed to decrease as moisture content is reduced for a given bulk depth. Similar trends have been reported by Rabe and Currence (1975) for alfalfa leaves. The difference in the slope of the curves is only marginal at MC ≤ 52.9% w.b. and MC ≤ 52.2% w.b. for the leaves and chopped aerial vines, respectively, except in the bulk depth of 0.30 m (fig. 3-4). In general, the pressure drop for sweet potato leaves was lower compared to chopped sweet potato aerial vines, except at moisture content levels of 88.7% and 74.7% and bulk depth of 0.75 m for sweet potato leaves. One possible cause for the trend observed in 0.75 m bulk depth (fig. 3-3) is compaction due to the loading of the leaves in the airflow resistance measuring system. Generally, loading of the leaves in the chamber of the airflow resistance measuring system was a task that cannot be performed with greater consistency. However, Swetnam et al. (1990) stated that such inconsistency during loading should reflect what would occur in the field and is therefore an essential design consideration.

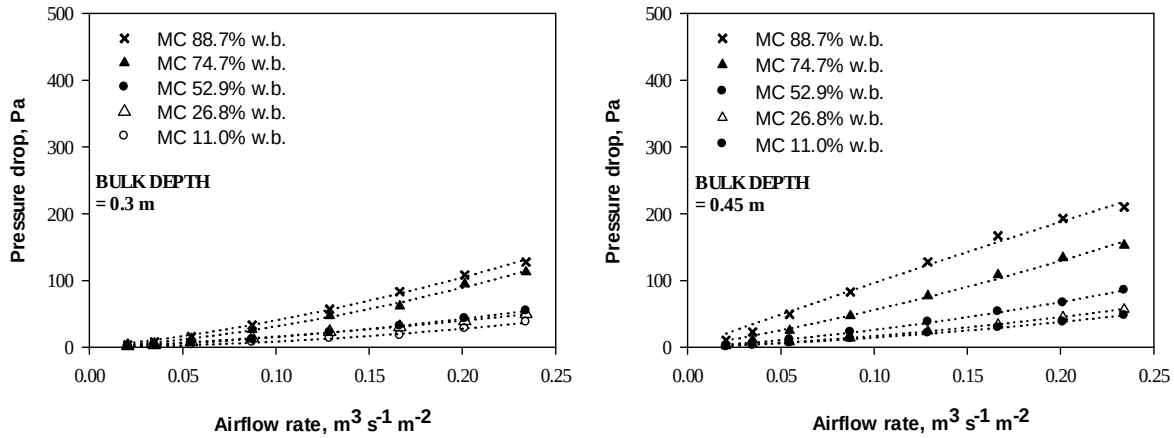

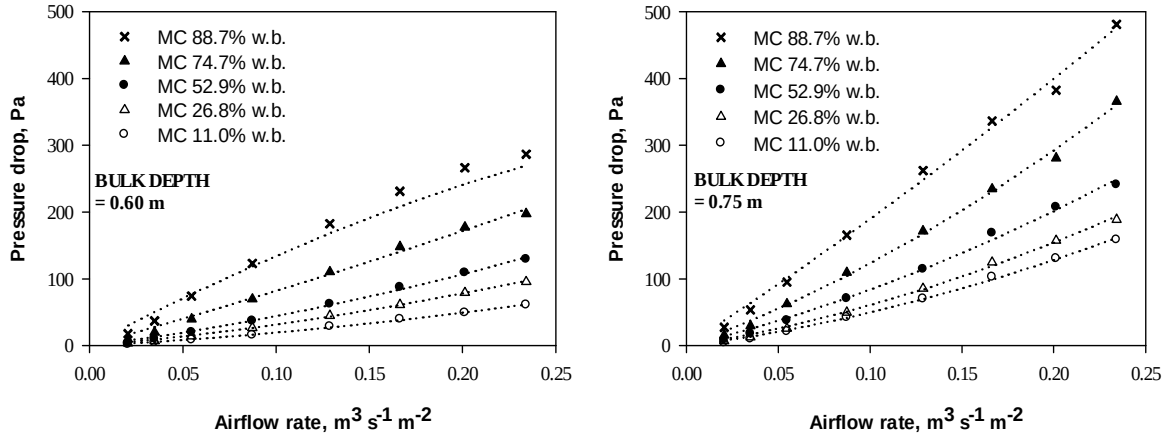

Figure 3-3 Relationship between pressure drop and airflow for sweet potato leaves at different moisture contents and bulk depths.

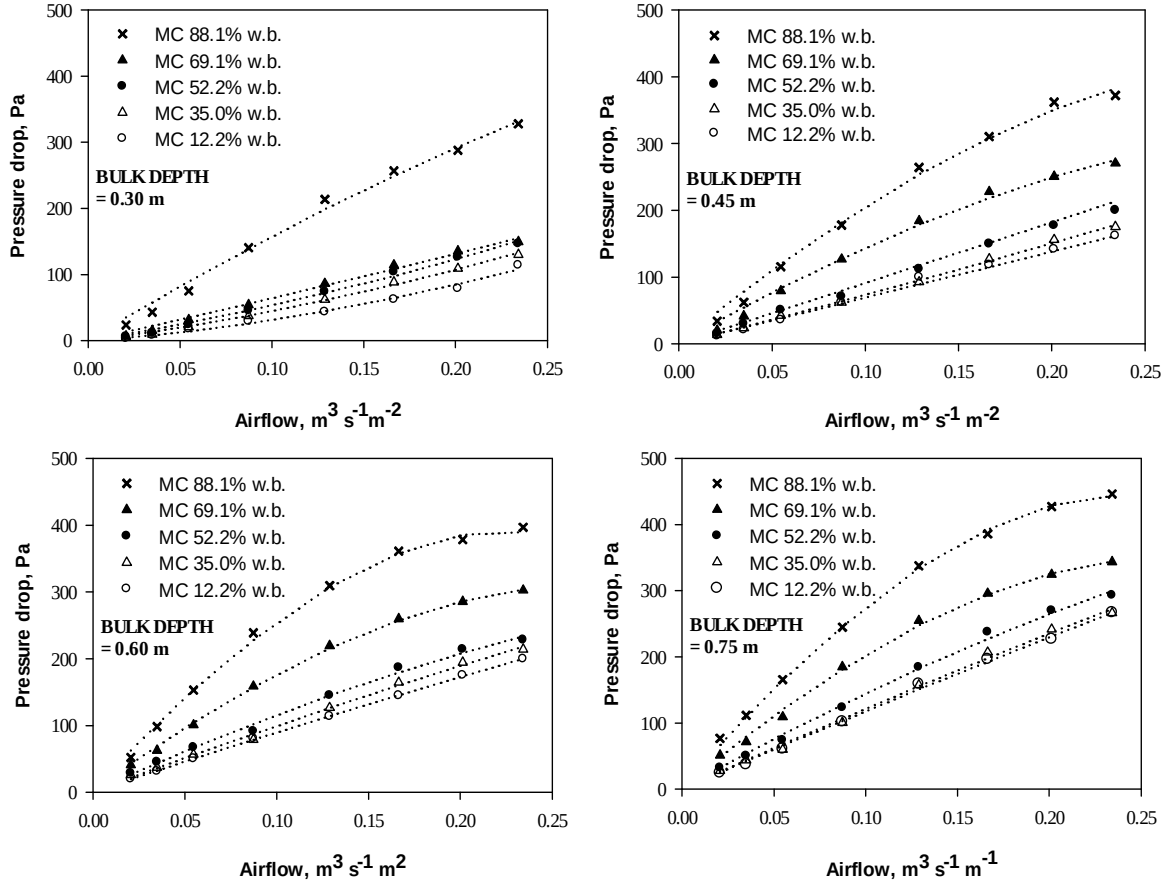

Figure 3-4 Relationship between pressure drop and airflow for chopped sweet potato aerial vines at different moisture contents and bulk depths.

For comparison purposes, sweet potato leaves and chopped sweet potato aerial vines in the moisture content range of 88.7% to 11.0% w.b. and 88.1% to 12.2% w.b., respectively, and bulk depth of 0.75 m were compared with Reed et al. (2001) data for marigold flowers (fig. 3-5). The marigold flowers moisture conditions and bulk depth ranged from 84.8% to 10.3% and 0.15 to 1.0 m, respectively. Note the near linear relationship on a typical log-log plots of pressure drop per unit depth versus airflow rate for sweet potato leaves and chopped aerial vines. The pressure drop as a function of airflow for both sweet potato leaves and chopped sweet potato aerial vines was found below the values for marigold flowers. A closer look at figure 3-5 indicates a steep slope for sweet potato leaves when compared with the cited data. The curves for chopped sweet potato aerial vines are almost parallel, indicating a fairly constant slope in comparison with marigold flowers.

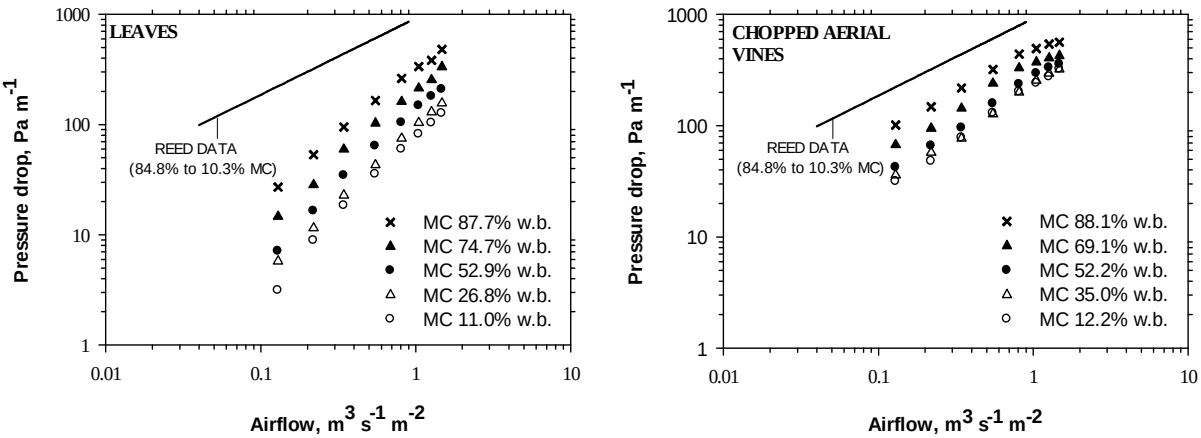

Figure 3-5 Pressure drop per unit bulk depth of sweet potato leaves and chopped sweet potato aerial vines at various moisture contents.

Table 3-2 summarizes the analysis of variance of the effects of airflow rate, moisture content, and bulk depth on pressure drop for both sweet potato leaves and chopped sweet potato aerial vines. All three variables and their interactions significantly ($P < 0.01$) affected pressure drop, but airflow had the most significant effect on pressure drop for both sweet potato leaves and chopped sweet potato aerial vines followed by moisture content and bulk depth.

Table 3-2 Results of statistical analysis showing the effects of airflow rate (v), bulk depth (L), and moisture content (MC) on pressure drop for sweet potato leaves and chopped sweet potato aerial vines.

Sweet Potato Components	Variable	DF[a]	Sum of Squares	F-Value[b]
leaves	v	7	943109.986	2544.681
	L	3	212821.926	1339.875
	MC	4	541730.399	2557.951
	v x L	21	94109.187	84.641
	v x MC	28	229354.103	154.710
	MC x L	12	61930.090	97.474
Chopped aerial vines	v	7	2972015.922	1830.284
	L	3	540996.788	777.390
	MC	4	1194636.034	1287.482
	v x L	21	89933.043	18.461
	v x MC	28	277367.451	42.703
	MC x L	12	29723.725	10.678

[a] Degrees of freedom.
[b] All variables and their interactions significantly affected the static pressure drop at P = 0.01.

Bulk density, which varied from 29.57 to 112.63 kg m^{-3} for sweet potato leaves and from 83.99 to 317.23 kg m^{-3} for chopped sweet potato aerial vines, was found to increase with increasing bulk depth (fig. 3-6). In the case of sweet potato leaves, at moisture content of 88.7% to 11.0% w.b., the change in bulk density was less noticeable, as depicted by the lower slope of the regression lines. Conversely, at moisture content of 88.1% and 69.1% w.b. for chopped sweet potato aerial vines, the change in bulk density with bulk depth was more obvious, defined by the larger slope of the regressions lines. At moisture contents below 50% w.b. in all test cases, the slope was the lowest underscoring the reduced influence on bulk density. Interestingly, as the drying process progresses for a given bulk depth of sweet potato leaves, their bulk density increases to a maximum value at 74.7% w.b. moisture content and suddenly starts to decline with further drying. The sweet potato leaves tend to mat from the beginning of the drying process (at 74.7% w.b), a phenomenon best ascribed to the large shrinkage that occurs as a result of significant changes in the leaf structure. Similar observation has being reported for air-dried leaves of *Mellisa officinalis* L. (Argyropoulos and Müller, 2014) and marigold flowers, var. I822 and EI236 (Reed et al., 2001). Bulk density of the chopped sweet potato aerial vines continue to drop up to the minimum moisture content (12.2% w.b.) as the products dry for a

given initial bulk depth. In all experimental batches, bulk density continues to decline but at varying rates with further drying.

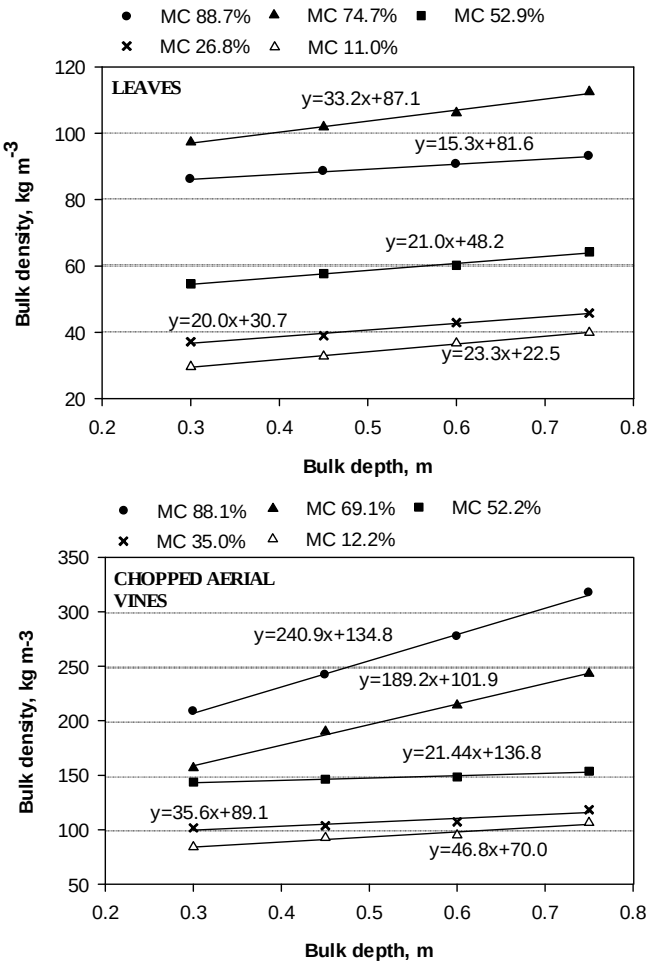

Figure 3-6 Bulk density vs. bulk depth at different moisture contents for sweet potato leaves and chopped sweet potato aerial vines. With three replicates at each data point, r^2 was at least 0.9943 for leaves and 0.8652 for chopped aerial vines in each of the five regression equations for the charts (leaves and chopped aerial vines).

3.4.2 Empirical improvement of model and fitting

Initial model fitting based on equation (3-1) (model fitting results not shown) shows that the Hukill and Ives (1955) equation can be used to accurately describe airflow resistance through sweet potato leaves and chopped sweet potato aerial vines. The coefficient of determination values was $r^2 \geq 98.8\%$ in all the test cases. Though the initial model fitting proved accurate, this only provides airflow resistance information in limited operation conditions. In practice, forced-air dryers are designed to be operated in more general conditions with products of

different moisture conditions and bulk depth values. In order to apply the results of this work to broader applications, de-rating factors are inserted into the Hukill and Ives (1955) equation. Equations (3-2) and (3-3) are the empirical de-rating modification of equation 3-1 for sweet potato leaves and chopped sweet potato aerial vines, respectively.

$$\frac{\Delta P}{L} = \frac{av^2}{\mathrm{Log_e}(1+bv)}[1 + c(MC - 50.82)] \times [1 + d(L - 0.3)] \quad (3\text{-}2)$$

$$\frac{\Delta P}{L} = \frac{av^2}{\mathrm{Log_e}(1+bv)}[1 + c(MC - 51.34)] \times [1 + d(L - 0.3)] \quad (3\text{-}3)$$

where MC is the moisture content of sweet potato leaves or chopped sweet potato aerial vines (% w.b.), c and d are empirical constants.

Equations (3-2) and (3-3) are based on the following observations. The moisture content for sweet potato leaves and chopped sweet potato aerial vine components ranged from 88.7% to 11.0% w.b. and 88.1% to 12.2% w.b., respectively. The average (50.82% w.b. for leaves and 51.34% w.b. for chopped aerial vines) was set as the base point. According to Yang et al. (2011), the de-rating factor will affect the final results if the average expected moisture content is much greater. In addition, 0.3 m was selected as the baseline bulk thickness to account for possible compactions, especially when designing forced-air dryers to be operated up to 1.5 m bulk depth as indicated by Müller and Heindl (2006) for medicinal plants. Based on the above considerations, all the resistance to airflow results were fitted into equations (3-2) and (3-3) for each data set of fixed moisture content and depth. The estimated parameters a, b, c, and d, along with statistical parameters, are summarized in table 3-3. The values of r^2 and RMSE obtained are ranging, respectively, from 97.9% to 100% and from 0.31 to 17.67 for the sweet potato leaves and from 97.2% to 99.9% and from 2.51 to 16.88 for chopped sweet potato aerial vines. The P-values were below 10% in 35 test cases with maximum P ≤ 11.76%. It is generally considered that (P) values below 10% indicate an adequate fit for practical purposes (Park et al., 2002). The statistical analysis of the improved Hukill and Ives (1955) equation indicates that it can be used to predict airflow resistance through sweet potato aerial vine components. Therefore, the 40 data set listed in table 3-3 can be used by designers for predicting the airflow resistance to overcome when designing forced-air drying systems for sweet potato aerial vine components. Once the airflow resistance has been determined, a requisite fan for forcing the air through bulk sweet potato aerial vine components can be selected.

Table 3-3 Estimated parameters and comparison criteria of equation (3-2) and (3-3) at various moisture content and bulk depth for sweet potato leaves and chopped sweet potato aerial vines.

Depth (m)		Moisture Content (% w.b)									
		88.7	74.7	52.9	26.8	11.0	88.1	69.1	52.2	35.0	12.2
		Leaves					Chopped Aerial Vines				
0.30	a	1963.437	3274.073	1139.061	635.784	1868.641	-2669.282	426.314	3505.199	757.708	3888.749
	b	14.484	37.241	29.839	9.922	400.394	-1.298	0.563	4.514	6.908	20.556
	c	0.021	0.019	0.384	-0.029	-0.015	-0.005	-0.010	-0.503	-0.128	0.003
	d	1.000	1.000	1.000	1.000	1.000	0.500	0.500	0.500	0.500	0.50
	r^2	0.996	0.995	0.999	0.998	0.993	0.991	0.991	0.995	0.997	0.988
	RMSE	2.65	2.84	0.50	0.71	1.05	10.49	4.94	3.74	2.51	3.92
	P (%)	4.68	6.97	7.17	5.68	5.66	7.18	5.95	5.64	5.62	7.11
0.45	a	125.088	2567.103	1953.094	2109.615	1071.184	-2700.049	-456.011	123.130	1092.673	1893.370
	b	0.002	4.889	14.426	19.602	16.307	-2.262	0.001	0.014	0.652	0.002
	c	-0.023	0.005	-0.163	-0.008	0.011	-0.073	-0.064	-1.077	0.022	0.025
	d	-5.868	-1.573	5.140	-1.918	8.582	-14.415	-6.525	2.220	-2.102	-6.434
	r^2	0.989	0.993	0.997	1.000	0.992	0.993	0.972	0.997	0.998	0.994
	RMSE	8.20	4.52	1.43	0.31	0.95	10.26	16.88	3.42	4.46	4.09
	P (%)	8.37	5.65	3.88	8.15	7.60	5.76	6.48	6.81	11.76	10.74
0.60	a	156.125	1319.359	2418.920	1649.670	1531.051	-3528.294	-6041.266	91.869	155.393	85.611
	b	0.001	1.146	7.513	9.319	11.586	-3.204	-2.724	0.001	0.001	0.001
	c	-0.024	-0.024	-0.235	-0.028	0.012	-0.073	-0.106	0.580	0.057	0.024
	d	-3.026	1.881	3.286	-0.847	2.955	-8.863	-6.828	-3.306	-3.036	-2.763
	r^2	0.979	0.992	0.996	0.998	0.997	0.996	0.999	0.983	0.994	0.999
	RMSE	17.67	5.87	2.70	1.30	1.47	8.10	3.39	14.16	5.29	3.56
	P (%)	8.62	5.72	5.59	5.58	8.48	4.40	1.89	10.94	4.47	10.00
0.75	a	1331.277	2009.868	1707.572	4021.799	3470.859	-4465.420	-3620.858	-3105.986	73.937	8.019
	b	1.217	5.839	6.813	11.668	13.289	-3.012	-2.788	-1.461	0.001	0.001
	c	0.020	0.018	0.495	0.022	0.014	-0.068	0.039	-1.992	0.055	0.044
	d	-0.167	2.135	0.558	3.164	3.734	-5.478	0.178	-4.522	-1.872	-2.688
	r^2	0.995	0.997	0.994	0.997	0.998	0.999	0.997	0.996	0.995	0.997
	RMSE	11.05	6.89	6.06	3.49	2.69	5.17	5.80	5.92	6.26	9.44
	P (%)	9.42	3.44	10.96	5.67	7.61	2.36	4.00	5.81	5.12	10.67

3.5 Conclusions

The study provides information on the resistance to airflow through sweet potato leaves and chopped sweet potato aerial vines at various moisture contents and bulk depths. The resistance to airflow was significantly affected by all three variables (airflow, moisture content, and bulk depth) and their interaction, but airflow rate had the most significant effect on pressure drop of both sweet potato leaves and chopped sweet potato aerial vines. Comparing the data in this study with marigold flowers cited in literature, the curves of sweet potato leaves and chopped sweet potato aerial vines at the studied moisture content range were found below the values for marigold flowers. Bulk density is greatly affected by moisture content and ranged from 29.57 to 112.63 kg m^{-3} for sweet potato leaves and from 83.99 to 317.23 kg m^{-3} for chopped sweet potato aerial vines. Since moisture content and bulk depth were significant in determining airflow resistance, an empirical ‘‘de-rating’’ modification of Hukill and Ives (1955) equation was developed and used to predict pressure drop across the various samples investigated. The developed models provided a good fit to the experimental pressure drop data obtained in the range of airflows, moisture contents, and bulk depth under consideration.

3.6 Acknowledgements

The first author, Joseph Kudadam Korese, wishes to acknowledge financial support from the German Academic Exchange Service (DAAD) for his research stay in Germany. This study is part of an ongoing Global Food Supply (GlobE) project RELOAD (FKZ 031A247 A), funded by the German Federal Ministry of Education and Research (BMBF). We gratefully acknowledge their financial contributions. Thanks also to the Council for Scientific and Industrial Research (CSIR)-Crops Research Institute (CRI), Kumasi-Ghana for providing sweet potato planting material for the study.

3.7 References

Argyropoulos, D., & Muller, J. (2014). Effect of convective, vacuum and freeze drying on sorption behaviour and bioactive compounds of lemon balm (*Melissa officinalis* L.). Journal of Applied Research on Medicinal and Aromatic Plants, 1(2), 59-69.

ASABE Standards. (2012). D358.3: Moisture measurements-Forages. St. Joseph, MI: ASABE.

ASABE Standards. (2011). D272.3: Resistance to airflow of grains, seeds, other agricultural

products and perforated metal sheets. St. Joseph, MI: ASABE.

Anderson, D. S., Abubakar, Y., Young, J. H., & Johnson, W. H. (1998). Pressure vs. airflow characteristics through fresh intact and cut-strip tobacco. Transactions of the ASAE, 41(6), 1747-1753.

Brown, D. L., & Chavalimu, E. (1985). Effects of ensiling or drying on five forage species in western Kenya: *Zea mays* (maize stover), *Pennisetum purpureum* (Pakistan napier grass), *Pennisetum sp.* (bana grass), *Impomea batata* (sweet potato vines) and *Cajanus cajan* (pigeon pea leaves). Animal Feed Science and Technology, 13(1), 1-6.

Cooper, S. C., & Sumner, H. R. (1985). Airflow resistance of selected biomass materials. Transactions of the ASAE, 28(4), 1309-1312.

Ergun, S. (1952). Fluid flow through packed columns. Chemical Engineering Progress, 48, 89-94.

Farrell, D. J., Jibril, H., Perez-Maldonado, R. A., & Mannion, P. F. (2000). A note on a comparison of the feeding value of sweet potato vines and lucerne meal for broiler chickens. Animal Feed Science and Technology, 85(1), 145-150.

Grubecki, I. (2015). Airflow versus pressure drop for a mixture of bulk wood chips and bark at different moisture contents. Biosystems Engineering, 139, 100-110.

Gunasekaran, S., & Jackson, C. Y. (1988). Resistance to airflow of grain sorghum. Transactions of the ASAE, 31(4), 1237-1240.

Hukill, W. V., & Ives, N. C. (1955). Radial airflow resistance of grain. Agricultural Engineering, 36(5), 332-335.

Iqbal, T., Eckhoff, S. R., Syed, A. F., Nizami, A.-S., & Sadef, Y. (2015). Airflow resistance of chopped miscanthus on drying platform. Transactions of the ASABE, 58(2), 487-492.

Ishida, H., Suzuno, H., Sugiyama, N., Innami, S., Tadokoro, T., & Maekawa, A. (2000). Nutritive evaluation on chemical components of leaves, stalks and stems of sweet potatoes (*Ipomoea batatas poir*). Food Chemistry, 68(3), 359-367.

Irvine, D. A., Jayas, D. S., & Mazza, G. (1993). Resistance to airflow through clean and soiled potatoes. Transactions of the ASAE, 36(5), 1405-1410.

Janjai, S., & Tung, P. (2005). Performance of a solar dryer using hot air from roof-integrated solar collectors for drying herbs and spices. Renewable Energy, 30(14), 2085-2095.

Jones, D., & Von Bargen, K. L. (1992). Some physical properties of milkweed pods. Transactions of the ASAE, 35(1), 243-246.

Kristensen, E. F., & Kofman, P. D. (2000). Pressure resistance to air flow during ventilation of different types of wood fuel chip. Biomass Bioenergy, 18(3), 175-180.

Li, W., & Sokhansanj, S. (1994). Generalized equation for airflow resistance of bulk grains with variable density, moisture content and fines. Drying Technolology, 12(3), 649-667.

Müller, J., & Heindl, A. (2006). Drying of medicinal plants. In R. J. Bogers, L. E. Craker, & D. Lange (Eds.), Medicinal and aromatic plants-agricultural, commercial, ecological, legal, pharnmacological and social aspects (Vol. 17, pp. 237-258). Berlin, Germany: Wageningen UR Frontis Series.

Park, K. J., Vohnikova, Z., & Brod, F. P. R. (2002). Evaluation of drying parameters and desorption isotherms of garden mint leaves (*Mentha crispa* L.). Journal of Food Engineering, 51(3), 193-199.

Román, F., & Hensel, O. (2014). Real-time product moisture content monitoring in batch dryer using psychrometric and airflow measurements. Computer and Electronics in Agriculture, 107, 97-103.

Reed, S. D., Armstrong, P. R., Brusewitz, G. H., & Stone, M. L. (2001). Resistance of marigold flowers to airflow. Transactions of the ASAE, 44(3), 639-642.

Rabe, D. L., & Currence, H. D. (1975). Air flow resistance and density of alfalfa leaves. Transactions of the ASAE, 18(5), 932-934.

Sugiura, R., & Watanabe, T. (2011). Effect of airflow drying and steam blanching on polyphenol retention in sweet potato leaves. Transactions of the ASABE, 54(2), 563-569.

Sadaka, S., Magura, C. R., & Mann, D. D. (2002). Vertical and horizontal airflow characteristics of wood/compost mixtures. Applied Engineering in Agriculture, 18(6), 735-741.

Swetnam, L. D., Casada, M. E., & Walton, L. R. (1990). Airflow through densely packed burley tobacco leaves. Applied Engineering in Agriculture, 6(3), 334-336.

Suggs, C. W., & Lanier, A. (1985). Resistance of wood chips and sawdust to airflow. Transactions of the ASAE, 28(1), 293-295.

Suggs, C. W., Zimmer, A. L., & Gore, J. W. (1985). Pressure vs. air flow through fresh tobacco leaves. Transactions of the ASAE, 28(5), 1664-1667.

Shedd, C. K. (1953). Resistance of grains and seeds to airflow. Journal of Agricultural Engineering, 34(9), 616-619.

Tabil, L. G., Kienholz, J., Hong, Q. P., & Eliason, M. V. (2003). Airflow resistance of sugarbeet. Journal of Sugar Beet Research, 40(3), 68-86.

Teguia, A., Njwe, R. M., & Nguekouo Foyette, C. (1997). Effects of replacement of maize with dried leaves of sweet potato (*Hypomoea batatas*) and perennial peanuts (*Arachis glabrata* Benth) on the growth performance of finishing broilers. Animal Feed Science and Technology, 66(1), 283-287.

VDI/VDE. (1983). Netzmessungen in strömungsquerschnitten (Blatt 3): Bestimmung des Gasstromes in Leitungen mit Kreis-, Kreisring- oder Rechteckquerschnitt. Düsseldorf, Germany: VDI-Verlag.

Woolfe, J. A. (1992). Sweet potato: An untapped food resource. Cambridge, U. K.: Cambridge University Press.

Yang, L., Wang, X., Funk, T. L., & Gates, R.S. (2011). Biofilter media characterization and airflow resistance test. Transactions of the ASABE, 54(3), 1127-1136.

4 Airflow resistance through bulk sweet potato roots

J.K. Korese[1,2)], U. Richter[1)], O. Hensel[1)]

[1)] Department of Agricultural Engineering, University of Kassel, Nordbahnhofstr. 1a, 37213 Witzenhausen, Germany

[2)] Department of Agricultural Mechanisation and Irrigation Technology, University for Development Studies, Post Office Box 1882, Nyankpala Campus, Tamale, Ghana

4.1 Abstract

Storage of sweet potato roots in bulk is common in tropical and subtropical countries. Hot spots and mold damage may occur during storage, especially if the roots are not ventilated. Airflow resistance data are therefore required to predict the uniformity of airflow and to design optimum ventilation systems. This study presents the resistance to airflow through unwashed and clean sweet potato roots over a superficial velocity range of 0.08 to 1.70 m s^{-1}. The results were correlated by a physically meaningful modified Ergun model and compared with the modified Shedd's model. In the modified Ergun model, the physical properties of the roots, such as porosity, shape factor, and surface roughness, were explicitly incorporated into the model. The modified Ergun model exhibited higher values for coefficient of determination, lower root mean square error, and lower percentage error and therefore provided the best fit when compared with the modified Shedd's model. The model can therefore be used to predict resistance to airflow through bulk sweet potato roots realistically. The differences in the pressure drop between sweet potato roots arranged differently to airflow and with or without soil fraction on the surfaces of the roots were further explained by the contribution of particle drag and surface friction. The pressure drop through unwashed and clean sweet potato roots was observed to increase with higher airflow, bed depth, root grade composition, and presence of soil fraction. The results for the effect of soil fraction stress the importance of cleaning sweet potato roots before storage. Airflow was the most significant factor affecting pressure drop of unwashed and clean sweet potato roots compared with root grade composition and presence of soil fraction for all batches studied. The results obtained from this study are comparable to those reported by other researchers, particularly for other agricultural roots.

Keywords. Models, Resistance to airflow, Shape factor, Surface roughness, Sweet potato roots.

4.2 Introduction

Sweet potato (*Ipomoea batatas* L.) is grown throughout the tropics and subtropics, and ranks fifth as a staple food crop after rice, wheat, maize, and cassava (Lin et al., 2007). The fleshy roots of the crop are used as food, animal feed, and to some extent as raw material for the production of alcoholic beverages, starch, and organic acids (Woolfe, 1992). However, the short shelf-life of the crop is a major constraint both for food security and for marketing of the roots, especially in the developing world where the use of temperature and humidity control is often not feasible. Storage in bulk piles is a common practice in the sweet potato processing industry (Woolfe, 1992). Sufficient ventilation of the bulk during storage is important to maintain root quality. Boyette (2009) reported that poor environmental control and insufficient airflow rates during ventilation can result in mold damage and temperature buildup brought about by respiration of the roots in bulk. Higher airflow rates, on the other hand, can result in excessive moisture loss, resulting in shriveling and causing large pressure drops that require more powerful fan systems. Therefore, knowledge of the relationship between pressure drop and airflow rate is needed for optimal design and operation of ventilated curing and cooling systems.

Many studies have described the relationships among static pressure drop, airflow rates, fluid properties, foreign materials, flow direction, and other physical parameters (Giner and Dinisienia, 1996; Irvine et al., 1993; Chau et al., 1985; Abrams and Fish, 1982; Brooker et al., 1974). In most of these studies, pressure drop data are analyzed using empirical equations, such as the Shedd (1953) and Hukill and Ives (1955) models. These non-linear models easily fit many experimental data sets; however, the constants in these models have a purely empirical nature without physical meaning (Verboven et al., 2004). A more adaptable expression is the Ergun model (1952), which is based on fluid-dynamic principles (Kashaninejab and Tabil, 2009). The modified Ergun model describes pressure drop as a function of particle diameter, porosity of the packed bed, air density, and viscosity. This model has been used successfully to describe the pressure drop of several agricultural and horticultural stored products (Amanlou and Zomorodian, 2011; Verboven et al., 2004; van der Sman, 2002; Chau et al., 1985).

Although empirical equations have been derived and used in estimating pressure loss through various agricultural products, information relating to the effects of shape factor, surface roughness, orientation to airflow, and presence of soil fraction on sweet potato roots on airflow resistance is limited. Hayes et al. (2014) indicated that producers in the sweet potato processing industry are adapting to potato (*Solanum tuberosum*) bulk harvesting systems. Inevitably, soil is usually transported to storage with the roots, especially when harvesting is done under unfavorable weather conditions. Woodruff et al. (1983) suggested that soil adhering to the surfaces of potatoes during storage accounts for about 3% of the tuber weight. This soil tends to loosen from the tuber surfaces and partially fill the voids between tubers, which increases the resistance to airflow through the voids. The objectives of this study were therefore to (1) calculate the surface roughness and shape factor of sweet potato roots in order to realistically predict the variation in static pressure of an irregular product such as sweet potato roots, (2) fit the experimental data to the modified Ergun model and compare it with the modified Shedd's model, and (3) elucidate the effect of alignment to airflow, bed depth, airflow rate, grade composition, and presence of soil fraction on the variation in pressure drop across bulk sweet potato roots

4.3 Materials and methods

4.3.1 Plant material

Sweet potatoes (*Ipomoea batatas* L. cv. CRI-Apomuden) used in this study were grown in summer 2014 at the experimental and demonstration farm of the Department of Agricultural Engineering, University of Kassel, Witzenhausen, Germany. The sweet potatoes were grown according to organic agriculture production standards, and the roots were harvested 90 days after seedling transplantation. After harvest, damaged or severely bruised roots were sorted out. The remaining roots were cured by storing them at 30 °C and 85% RH for seven days in a controlled environment room. Both unwashed and clean roots were studied. The mass percentage of soil fraction that adhered to the surfaces of the roots from harvest was computed according to Verboven et al. (2004) and was found to be 6.5% on a wet basis (w.b.). The true density of the roots was calculated as the mass divided by the true volume of the products. Bulk density was determined by weighing the mass of the products needed to fill the test column. The porosity (ε) of the bulk of sweet potato roots was determined using the following

equation (Mohsenin, 1996):

$$\varepsilon = 1 - \frac{\rho_b}{\rho_p} \tag{4-1}$$

The average effective diameter (d_{eff}) of the roots was calculated according to Pérez-Alegría et al. (2001) and was 62.4 and 72.8 mm for mixed and hand-graded roots, respectively. Table 4-1 summarizes the average effective diameter and bulk porosities of the batches of sweet potato roots used in the study.

Table 4-1 Average effective diameter and bulk porosity of batches of sweet potato roots at three different batch arrangement to airflow.

Product	Batch Arrangement	d_{eff} (mm)	Bulk Porosity
Unwashed roots (mixed)	Random	62.4	0.554
	Parallel	62.4	0.491
	Perpendicular	62.4	0.485
Unwashed roots (graded)	Random	72.8	0.550
	Parallel	72.8	0.480
	Perpendicular	72.8	0.455
Clean roots (mixed)	Random	62.4	0.557
	Parallel	62.4	0.488
	Perpendicular	62.4	0.497
Clean roots (graded)	Random	72.8	0.564
	Parallel	72.8	0.496
	Perpendicular	72.8	0.490

4.3.2 Experimental set-up

The apparatus used in this study is shown in figure 4-1. Román and Hensel (2014) provide a detailed description of the experimental apparatus, which is similar in dimensions except for the test chamber and the concept. The test chamber was constructed of 0.0185 m plywood box sections, each with internal dimensions of 0.49×0.50 m and a height of 0.5 m to simulate the conditions within a box of larger cross-sectional area (Maw et al., 2002). The overall height of the test chamber was 1 m. Pressure taps were located immediately below the test chamber base and above it at 1 m.

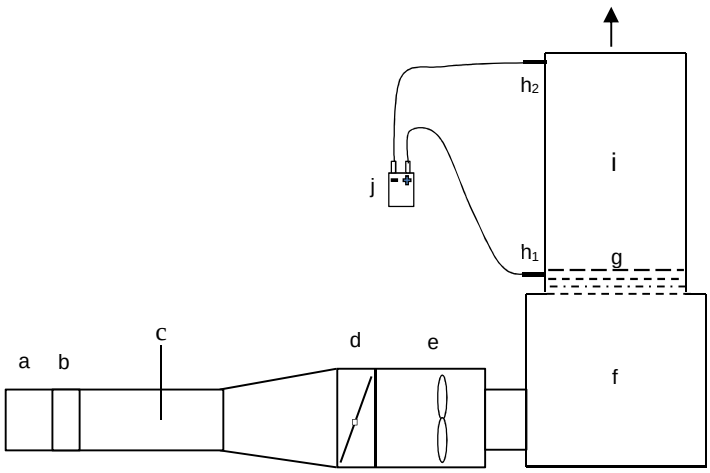

Figure 4-1 Schematic diagram of the apparatus used for airflow resistance measurement. (a) inlet duct, (b) airflow straightener, (c) hot wire anemometer, (d) butterfly valve, (e) in-line duct centrifugal fan, (f) plenum, (g) perforated sheet, (h_1-h_2) pressure tabs, (i) sample holding chamber (j) pressure transducer.

The airflow was measured with a hot-wire anemometer (TA-5, Airflow Lufttechnik GmbH, Germany) located at the duct center and 0.4 m downstream of the flow straightener. To determine the airflow rate in the system, the guideline of VDI/VDE 2640 Part 3 (VDI/VDE, 1983) was used, as detailed by Román and Hensel (2014). The superficial velocity, which was used in all calculations for the models, is the volumetric flow rate per unit cross-section of the test column. The pressure drop across the bed of sweet potato roots was measured using a pressure transducer (DMU/A, FuehlerSysteme eNET International GmbH, Germany). The differential pressure transducer was connected by flexible rubber hoses to aluminum probes that penetrated the test chamber wall through 0.006 m ports. The probes were made of hollow aluminum tubes with 0.006 m outside diameter and extended 0.2 m toward the center of the box section in order for static pressure readings to be taken away from the interior surface of the box section (Maw et al., 2002). The hot-wire anemometer and the pressure transducer were both connected to a data acquisition unit (34970a, Agilent Technologies, Santa Clara, Cal.), which was connected to a computer. For each experimental configuration, measurements were carried out and averaged over a 5 min period.

4.3.3 Measurement procedure

The resistance to airflow through beds of unwashed and clean sweet potato roots, expressed as the pressure drop per unit depth of column, was measured for a superficial velocity range

from 0.08 to 1.70 m s^{-1}. At each fan speed, the static pressure was measured in the lower and upper parts of the column. In each set of experiments, measurements were made for randomly filled beds of sweet potato roots. To investigate the influence of root orientation during loading on pressure drop, the sweet potato roots were arranged with their axis parallel or perpendicular to the airflow direction, as shown in figure 4-2. Both unwashed (soil fraction of 6.5% w.b.) and clean roots were used in this study for mixed and hand-graded sweet potato roots. The mixed roots had an effective diameter ranging from 33.0 to 87.4 mm. The hand-graded roots had an effective diameter ranging from 62.1 to 87.4 mm. Each test case was replicated three times to check the reproducibility of the measurements. The channel-to-particle diameter ratio in this study was 10.23 for sweet potato roots using the maximum possible curvature of the roots near the wall, i.e., 48.4 mm (Verboven et al., 2004); therefore, the wall effect was neglected (Amanlou and Zomorodian, 2011; Verboven et al., 2004; Eisfeld and Schnitzlein, 2001).

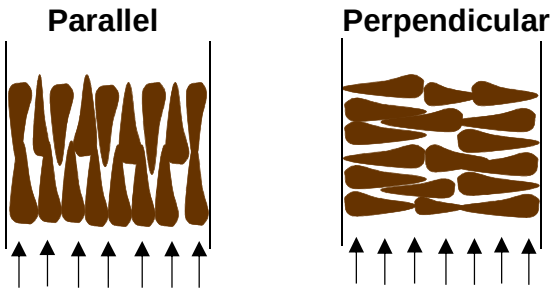

Figure 4-2 Parallel and perpendicular arrangements of sweet potato root batches to direction of airflow (shown by arrows).

4.3.4 Modeling pressure drop through bulk sweet potato roots

Mathematical modeling of the experimental data was based on two alternative models, sourced from the literature: Shedd's model (1953), which is frequently mentioned in the literature, and the physically meaningful model starting from the basic Darcy-Forchheimer theory. Shedd's model is:

$$v = A(\Delta P)^B \tag{4-2}$$

Equation (4-2) can be rewritten by considering pressure drop as a function of airflow rate (Nimkar and Chattopadhyay, 2002). Equation (4-3) is referred to as the modified Shedd's

equation to avoid confusion:

$$\Delta P = A_1(v)^{B_1} \tag{4-3}$$

According to Shedd (1953), this model is adequate for prediction over a narrow range of airflow rates due to the non-linearity of the log-log plot.

The relationship between pressure drop and air velocity is also governed by Darcy's law, which states that for small airflows the airflow rate is proportional to the applied pressure drop (van der Sman, 2002). At higher airflow rates, i.e., particle Reynolds number ($\rho|v|d_{eff}/\mu$, where d_{eff} is the effective diameter of the particles in m) exceeding 1, the airflow is described by the well-known Darcy-Forchheimer equation (eq. (4-4)), which includes a quadratic term. This range of Reynolds number corresponds to most food cooling applications (Verboven et al., 2004; van der Sman, 2002):

$$\Delta P = -\frac{\mu}{K}v - C\rho|v|v \tag{4-4}$$

The first term in equation (4-4) originates from Darcy's law, i.e., $\Delta P = -[(\mu/K)v]$, which holds in the range of small airflow velocities, indicated by the particle Reynolds number $Re_p < 1$. The first term in the Darcy-Forchheimer equation relates to friction forces, which involve fluid viscosity, while the second term expresses drag resistance and involves fluid density. Parameters K and C depend on the geometrical shape of the product (λ), their surface roughness (α_r), the product effective diameter (d_{eff}), and the porosity (ε). Since the physical properties of the fluid and the product were considered in the modified Ergun model, realistic results can be expected (Amanlou and Zomorodian, 2011; Verboven et al., 2004).

For near-spherical products, the Ergun expression applies and the coefficients are well known in the literature (Ergun, 1952):

$$\frac{1}{K} = \frac{150(1-\varepsilon)^2\lambda^2}{d_{eff}^2\varepsilon^3} \tag{4-5}$$

$$C = \frac{1.75(1-\varepsilon)\lambda}{d_{eff}\varepsilon^3} \tag{4-6}$$

where λ is a shape factor. Amanlou and Zomorodian (2011) and Verboven et al. (2004) considered the particle shape and roughness for calculating K and C:

$$\frac{1}{K} = \alpha_r \frac{K_1(1-\varepsilon)^2\lambda^2}{d_{eff}^2\varepsilon^3} \quad (4\text{-}7)$$

$$C = \frac{C_1(1-\varepsilon)\lambda}{\alpha_r d_{eff}\varepsilon^3} \quad (4\text{-}8)$$

Before their publications, shape and roughness effect had been absorbed into the values of coefficients K_1 and C_1 without taken into account parameters λ and α_r. Verboven et al. (2004) fitted λ and α_r values to experimental measurements of pressure drop and airflow rate over bulk chicory roots while maintaining values of K_1 = 150 and C_1 = 1.75. In the present study, the shape factor and surface roughness were estimated directly from the experimental pressure drop data using equations (4-4), (4-7), and (4-8) and assuming K_1 = 150 and C_1 = 1.75.

The experimental data of resistance to airflow for all experimental batches were fitted to the modified Shedd's and modified Ergun equations using the procedure of non-linear regression analysis with the Marquardt algorithm of SPSS Statistics 22 software. Statistical criteria, such as coefficient of determination (r^2), root mean square error (RMSE), and percentage relative error (E), were employed to select the best model. The effects of different parameters (airflow, root grade composition, and presence of soil fraction) on airflow resistance of bulk sweet potato roots were determined using a factorial completely randomized design (CRD) following the analysis of variance (ANOVA) method. Pressure drop was treated as the dependent variable. Significant differences of variable means were compared using the least significant difference (LSD) test at 5% level using SPSS Statistics 22 software.

4.4 Results and discussion

Resistance to airflow over unwashed and clean sweet potato roots was measured at superficial velocities ranging from 0.08 to 1.70 m s^{-1}. Random batches as well as batches with their longitudinal axis oriented perpendicular or parallel to the airflow were studied for both mixed and hand-graded sweet potato roots. Results of model fitting using equations (4-4), (4-7), and (4-8) are shown in figures 4-3 and 4-4 for each set of data. A good fit was obtained for predicting the resistance to airflow for all experimental data sets. For unwashed roots, the RMSE values for the random, perpendicular, and parallel arrangements were respectively 2.4, 2.0, and 3.4 Pa for mixed roots and 2.3, 1.6, and 0.7 Pa for hand-graded roots. For clean

roots, the RMSE values for the random, perpendicular, and parallel arrangements were respectively 1.2, 2.4, and 2.0 Pa for mixed roots and 1.1, 1.4, and 1.8 Pa for hand-graded roots. For comparison purposes, figures 4-3 and 4-4 also show plots of data from Abrams and Fish (1982) for clean hand-graded sweet potato roots. The dashed lines in figures 4-3 and 4-4 are extrapolations of the Abrams and Fish (1982) data.

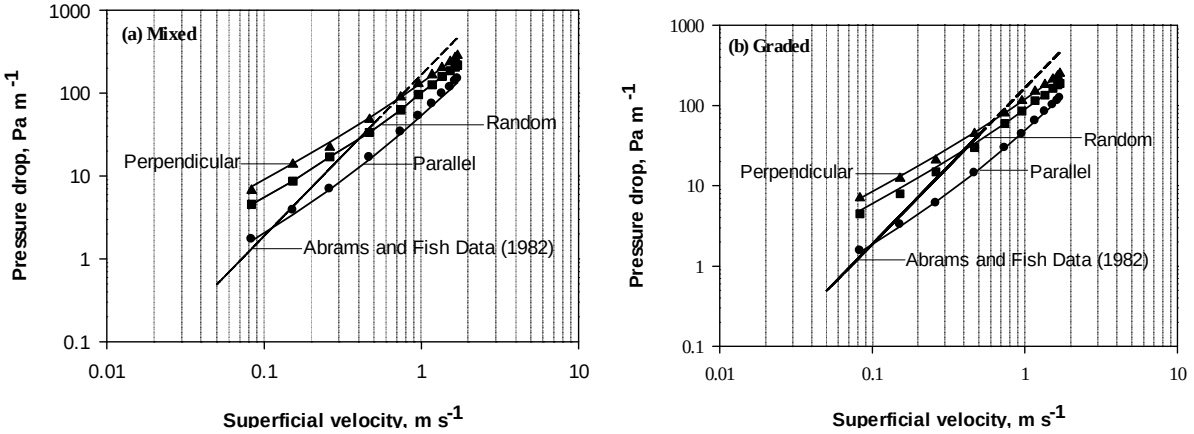

Figure 4-3 Pressure drop through batches of (a) mixed and (b) hand-graded unwashed sweet potato roots as a function of superficial velocity for different arrangements of the roots to airflow compared to data from Abrams and Fish (1982). Solid black line represents fit by modified Ergun model taking into account the root shape factor and surface roughness factor of each arrangement.

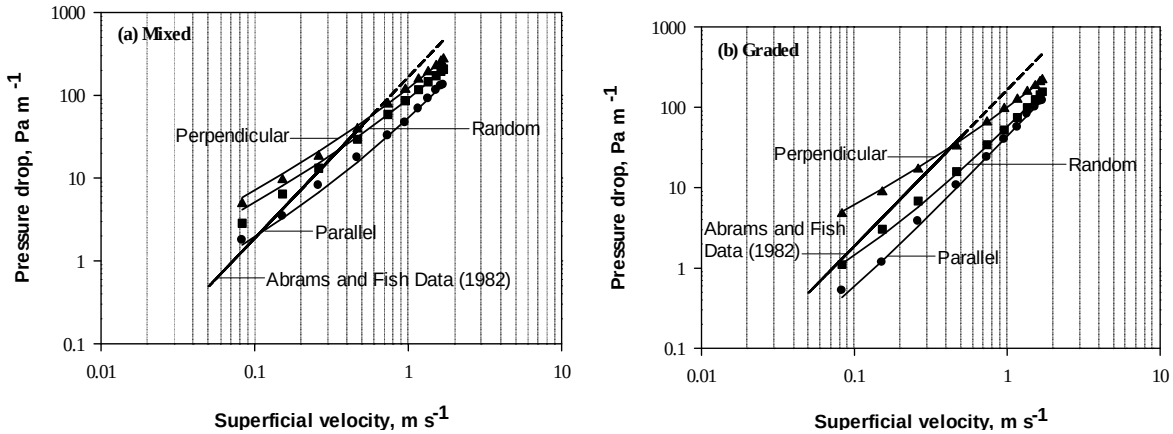

Figure 4-4 Pressure drop through batches of (a) mixed and (b) hand-graded clean sweet potato roots as a function of superficial velocity for different arrangements of the roots to airflow compared to data from Abrams and Fish (1982). Solid black line represents fit by modified Ergun model taking into account the root shape factor and surface roughness factor of each arrangement.

Using randomly filled batches of sweet potato roots as illustration, figures 4-3a, 4-3b, and 4-4a shows that the pressure drop in our study is a little greater than the Abrams and Fish (1982) data at superficial velocity ranges of 0.08 to 0.39 m s^{-1}, 0.08 to 0.40 m s^{-1} and 0.08 to 0.36 m s^{-1}, respectively. However, the pressure drop for clean graded roots, as shown in figure 4-4b, was less than that of Abrams and Fish (1982) for the entire range of superficial velocities tested.

As the object of this study was also to observe how the two models adapt to the entire superficial velocity range, we calculated the percentage error of prediction as a function of superficial velocity for randomly filled clean mixed and hand-graded roots. The error at each velocity was defined by

$$E = \left(\frac{P_i - E_i}{E_i}\right) \times 100 \tag{4-9}$$

Figure 4-5 shows the relative errors for the two models. The modified Ergun model had lower errors at low airflow and had better fit to the entire range of data as compared to the modified Shedd's model. The modified Ergun model covers both laminar flow and turbulent regimes and seems to explain the data best. The coefficient of determination for the modified Ergun model was greater than 99%, while that of the modified Shedd's model ranged from 97.34% to 98.62%. However, both models had RMSE values less than 5 Pa.

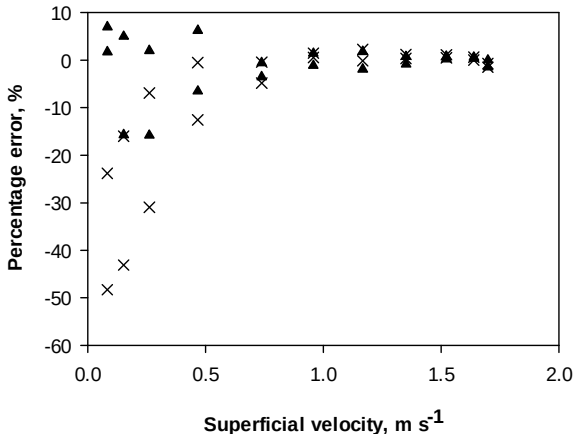

Figure 4-5 Percentage error in prediction of the pressure drop for combined data of randomly filled mixed and graded clean sweet potato roots as a function of superficial velocity using two models (× = Shedd's model; ▲ = modified Ergun model).

The shape and surface roughness factors were computed using equations (4-4), (4-7), and (4-8). Table 4-2 summarizes the corresponding values with standard errors for the shape and roughness factors for each experimental set. Table 4-2 shows that the effect of shape depends on the orientation of the product to the direction of airflow. Sweet potato roots filled randomly (λ = 2.207 to 1.346) appear to have a more dramatic effect of shape than perpendicular batches (λ = 1.806 to 1.549), while the smallest effect was found for products oriented parallel to airflow (λ = 0.987 to 0.467). These results correspond to those of Verboven et al. (2004), who found high values for the shape factor in random batches of chicory roots compared with transverse and parallel arrangements to airflow. In the case of complex products like sweet potato roots, the open structure in the randomly filled batch creates a boundary layer separation phenomenon on individual roots, which increases particle drag with reference to perpendicular alignment (Verboven et al., 2004). For roots oriented parallel to airflow, surface friction is more relevant than particle drag, as clearly shown in table 4-2.

The surface roughness of sweet potato roots is significant for the whole set of experimental batches, since $\alpha_r > 1$. This is because the flow path is much obstructed by the solid surfaces due to the irregular shape of the roots. However, the data reported here contradict the findings of Verboven et al. (2004), who found surface roughness to be less important for chicory roots transverse to airflow. For each of the root batches in this study, parallel arrangement had smaller surface roughness (α_r = 5.590 to 6.064 for unwashed roots and α_r = 2.360 to 5.268 for clean roots), underscoring the importance of the channeling effect as compared to the random and perpendicular batches. Interestingly, the roughness factor was greater for unwashed roots (α_r = 5.590 to 8.097 for mixed and α_r = 6.064 to 9.201 for graded) than for clean roots (α_r = 5.268 to 7.419 for mixed and α_r = 2.360 to 7.517 for graded). The unwashed sweet potato roots had loamy soil adhering to their surfaces. The soil tended to loosen and fill the voids between the sweet potato roots, thereby plugging the airflow paths between them. The larger confidence bounds for the estimated structural parameters (table 4-2), especially for surface roughness, point to the natural variation of the roots and from one batch to other. This variation may be important to consider in the design of forced-air ventilation systems for perishable horticultural products, especially those often stored in packages.

Table 4-2 Shape factor (λ) and roughness factor (α_r) estimated from pressure drop through batches of sweet potato roots, fitted from equations (4-4), (4-7), and (4-8).

		Factors		Standard Error	
Product	Arrangement	λ	α_r	λ	α_r
Unwashed roots (mixed)	Random	2.207	6.680	0.010	0.379
	Parallel	0.932	5.590	0.029	0.415
	Perpendicular	1.806	8.097	0.007	0.322
Unwashed roots (graded)	Random	1.975	8.038	0.012	0.517
	Parallel	0.722	6.064	0.012	0.224
	Perpendicular	1.549	9.201	0.007	0.330
Clean roots (mixed)	Random	2.130	6.039	0.010	0.203
	Parallel	0.987	5.268	0.042	0.492
	Perpendicular	1.745	7.419	0.005	0.275
Clean roots (graded)	Random	1.346	3.351	0.063	0.229
	Parallel	0.467	2.360	0.231	1.264
	Perpendicular	1.565	7.517	0.004	0.248

Typical linear-scale plots of pressure drop as a function of airflow for all arrangements of sweet potato roots are shown in figure 4-6, from which differences can be more clearly observed than in the previous log-log plots. The differences were statistically significant ($p < 0.05$) for each data set of mixed and graded sweet potato roots. The pressure drop for randomly filled, unwashed, mixed and graded roots was 13% and 40% higher, respectively, as compared to clean roots (fig. 4-6). This can be ascribed to the high estimated values of the shape and surface roughness factors. Furthermore, pressure drop measurements were low for parallel roots in comparison with random batches. This was expected because roots oriented parallel to the airflow have larger pores and channels. Conversely, the pressure drop was almost double for roots aligned perpendicular to airflow in all cases, as compared to randomly filled roots, due to the lower void fraction in the perpendicular arrangement (table 4-1).

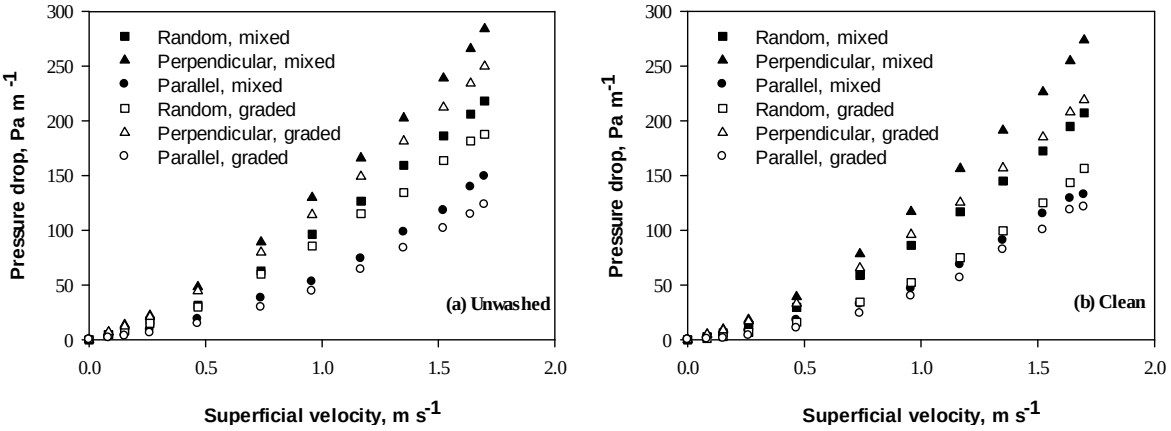

Figure 4-6 Linear-scale plots of pressure drop for different arrangements of (a) unwashed (6.5% wet basis soil) and (b) clean sweet potato roots, both mixed and graded, as a function of superficial velocity.

To illustrate the effect of bed depth on pressure drop, data on only randomly filled, mixed, clean roots were considered, and the results are shown in figure 4-7. Similar trends were obtained for the other experimental data sets. Doubling the bed depth for the same airflow had less effect on pressure drop than doubling the airflow for the same bed depth. For example, the dotted lines in figure 4-7 indicate that doubling the bed depth from 0.5 to 1 m at 0.15 m s^{-1} airflow increased the pressure drop from 4.8 to 9.2 Pa. However, doubling the airflow from 0.15 to 0.30 m s^{-1} for the 0.5 m bed depth more than doubled the pressure drop from 4.8 to 10.9 Pa. Therefore, it can be stated that, in general, pressure drop increases more rapidly with increasing air velocity than with increasing bed depth. Similar observations were reported by Kashaninejad and Tabil (2009) for pistachio nuts.

Table 4-3 summarizes the analysis of variance of the effects of airflow, root grade composition, and presence of soil fraction on pressure drop per unit depth of unwashed and clean sweet potato roots. All three variables had significant ($p < 0.05$) effects on pressure drop. Of the three variables, airflow had the greatest effect on pressure drop. For the interactions, there was no significant ($p < 0.05$) effect on pressure drop.

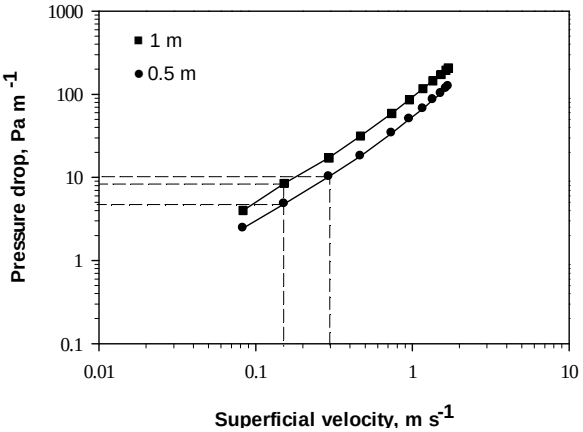

Figure 4-7 Airflow and pressure drop relationship for randomly filled, mixed, clean sweet potato roots at different bed depths.

Table 4-3 Influence of airflow rate, grade composition, and presence of soil fraction on static pressure of bulk sweet potato roots.

Variable	Sum of Squares	F-Value[a]	Probability (p-value)
Airflow (Q)	1256398.228	102.019*	0.00
Grade composition (G)	17258.001	14.013*	0.00
Presence of soil fraction (S)	7977.822	6.478*	0.01
Q × G	9430.337	0.766	0.66
Q × S	2155.076	0.175	1.00
G × S	921.002	0.748	0.39

[a]Asterisk (*) indicates a significant effect on pressure drop ($p < 0.05$).

4.5 Conclusions

Sweet potato roots, harvested and cured, were subjected to airflow resistance tests in a laboratory. The pressure drop for each of the studied batches was measured over a wide range of superficial velocities. The effects of product shape, surface roughness, and porosity were incorporated into a physically meaningful model based on Darcy-Forchheimer theory for both unwashed and clean sweet potato roots. By comparing the entire experimental data set, the modified Ergun model fitted the data well, with root mean square error (RMSE) less than 4 Pa and in most cases less than 2 Pa for the measurement range of 0.52 to 284 Pa and superficial velocity range of 0.08 to 1.70 m s^{-1}. Among the two predictive models studied (modified Shedd's and modified Ergun), the modified Ergun model provided the best fit to the experimental data for the entire range of airflow rates. This could be attributed to the two additive terms representing laminar and turbulent flows in the Ergun model. Accordingly, the modified Ergun model was able to account for different structural parameter values and hence

predicted the pressure drop of irregular sweet potato roots realistically.

Pressure drop was highly affected by the void fraction of the bulk sweet potato roots. At the same time, shape factor and surface roughness were physically explained by the presence of soil fraction on the roots, which resulted in higher surface roughness. Moreover, the presence of channels stresses the importance of surface roughness for friction losses, while vertical airflow obstruction in all experimental batches was strongly attributed to the shape factor through drag losses. Roots aligned parallel to airflow were considerably affected by channeling and low porosity (as low as 48% for hand-graded unwashed roots). The resistance to airflow by roots oriented perpendicular to airflow was more than double and almost three times higher, respectively, than the resistance of parallel and randomly filled roots due to the low porosity (45.5% to 49.7%) as well as blockage of vertical airflow. Randomly filled batches had the highest porosity (>50%). This study emphasizes the importance of the shape and surface roughness factors, which are not easily determined for irregularly shaped products such as sweet potato roots. Based on the estimated shape and roughness factors of sweet potato roots, interpretation of the pressure drop measurements can be made with much confidence. Hence, the results can aid in the design of ventilated cooling systems considering the large variations that exist within and among agricultural products.

The resistance to airflow increased more rapidly with airflow than with bed depth of sweet potato roots, as doubling the bed depth nearly doubled the resistance to airflow, but doubling the airflow more than doubled the resistance. Airflow, root grade composition, and presence of soil fraction significantly ($p < 0.05$) affected pressure drop, but airflow had the greatest effect on pressure drop for both unwashed and clean sweet potato roots compared to grade composition and soil fraction. The presence of soil fraction has to be taken into account when choosing fans for ventilating sweet potato root piles, as it will affect the fan static pressure and the uniformity of airflow. The results for the effect of soil fraction therefore stress the importance of cleaning sweet potato roots before storage.

4.6 Acknowledgements

The first author, Joseph Kudadam Korese would wish to acknowledge financial support from the German Academic Exchange Service (DAAD) for his research stay in Germany. This study is part of Global Food Supply (GlobE) project RELOAD (FKZ 031A247 A), funded by the

German Federal Ministry of Education and Research (BMBF). We gratefully acknowledge their financial contributions. Thanks also to the Council for Scientific and Industrial Research (CSIR) Crops Research Institute (CRI) in Kumasi, Ghana, for providing sweet potato germplasm for this study.

4.7 References

Amanlou, Y., & Zomorodian, A. (2011). Evaluation of air flow resistance across a green fig bed for selecting an appropriate pressure drop prediction equation. Food and Bioproducts Processing, 89(2), 157-162.

Abrams Jr., C. F., & Fish Jr., J. D. (1982). Air flow resistance characteristics of bulk piled sweet potatoes. Transactions of the ASAE, 25(4), 1103-1106.

Boyette, M. D. (2009). The investigation of negative horizontal ventilation for long-term storage of sweetpotatoes. Applied Engineering in Agriculture, 25(5), 701-708.

Brooker, D. B., Bakker-Arkema, F. W., & Hall, C. W. (1974). Drying cereal grains. Westport, CT: AVI Publishing.

Chau, K. V., Gaffney, J. J., Baird, C. D., & Church II, G. A. (1985). Resistance to air flow of oranges in bulk and in cartons. Transactions of the ASAE, 28(6), 2083-2088.

Eisfeld, B., & Schnitzlein, K. (2001). The influence of confining walls on the pressure drop in packed beds. Chemical Engineering Science, 56(14), 4321-4329.

Ergun, S. (1952). Fluid flow through packed columns. Chemical Engineering Progress, 48, 89-94.

Giner, S. A., & Denisienia, E. (1996). Pressure drop through wheat as affected by air velocity, moisture content, and fines. Journal of Agricultural Engineering Research, 63(1), 73-85.

Hayes, B. H., Ward, J. K., Lowe, J. W., Davis, J. D., Shankle, M. W., & Arancibia, R. A. (2014). Development of a mechanical undercutting system to minimize sweetpotato skinning during harvest. Applied Engineering in Agriculture, 30(3), 355-360.

Hukill, W. V., & Ives, N. C. (1955). Radial airflow resistance of grain. Agricultural Engineering, 36(5), 332-335.

Irvine, D. A., Jayas, D. S., & Mazza, G. (1993). Resistance to airflow through clean and soiled potatoes. Transactions of the ASAE, 36(5), 1405-1410.

Kashaninejad, M., & Tabil, L. G. (2009). Resistance of bulk pistachio nuts (Ohadi variety) to airflow. Journal of Food Engineering, 90(1), 104-109.

Lin, K. H., Lai, Y., Chang, K., Chen, Y., Hwang, S., & Lo, H. (2007). Improving breeding efficiency for quality and yield of sweet potato. Botanical Studies, 48(3), 283-292.

Maw, B. W., Williams, E. J., & Mullinix, B. G. (2002). Resistance of sweet onions to airflow. Transactions of the ASAE, 45(1), 39-45.

Mohsenin, N. N. (1996). Physical characteristics. In Physical properties of plants and animal materials. Newark, NJ: Gordon and Breach Science.

Nimkar, P. M., & Chattopadhyay, P. K. (2002). Airflow resistance of green gram. Biosystems Engineering, 82(4), 407-414.

Pérez-Alegría, L. R., Ciro V, H. J., & Abud, L. C. (2001). Physical and thermal properties of parchment coffee bean. Transactions of the ASAE, 44(6), 1721-1726.

Román, F., & Hensel, O. (2014). Real-time product moisture content monitoring in batch dryer using psychrometric and airflow measurements. Computers and Electronics in Agriculture, 107, 97-103.

Shedd, C. K. (1953). Resistance of grains and seeds to airflow. Journal of Agricultural Engineering, 34(9), 616-619.

van der Sman, R. G. (2002). Prediction of airflow through a vented box by the Darcy-Forchheimer equation. Journal of Food Engineering, 55(1), 49-57.

VDI/VDE. (1983). Netzmessungen in Strömungsquerschnitten (Blatt 3): Bestimmung des Gasstromes in Leitungen mit Kreis-, Kreisring-, oder Rechteckquerschnitt. Dusseldorf, Germany: VDI-Verlag.

Verboven, P., Hoang, M. L., Baelmans, M., & Nicolai, B. M. (2004). Airflow through beds of apples and chicory roots. Biosystems Engineering, 88(1), 117-125.

Woodruff, D. W., Hyde, G. M., & Thornton, R. E. (1983). A high-frequency soil riddling device for potato harvesters. ASAE Paper No. 831074. St. Joseph, MI: ASAE.

Woolfe, J. A. (1992). Sweet potato: An untapped food resource. Cambridge, UK: Cambridge University Press.

5 Simulation of transient heat transfer during cooling and heating of whole sweet potato (*Ipomoea batatas* (L.) Lam.) roots under forced-air conditions

Joseph Kudadam Korese[1, 2], Barbara Sturm [1, 3], Franz Román[1], Oliver Hensel[1]

[1] Department of Agricultural Engineering, University of Kassel, Nordbahnhofstr. 1a, 37213 Witzenhausen, Germany

[2] Department of Agricultural Mechanisation and Irrigation Technology, University for Development Studies, Post Office Box 1882, Nyankpala Campus, Tamale, Ghana

[3] School of Agriculture, Food and Rural Development, Newcastle University, Newcastle upon Tyne, NE1 7RU, UK

5.1 Abstract

In this work, we investigated how different air velocity and temperature affect the cooling and heating rate and time of individual sweet potato roots. Additionally, we modified and applied a simulation model which is based on the fundamental solution of the transient equations for estimating the cooling and heating time at the centre of sweet potato roots. The model was adapted to receive input parameters such as thermo-physical properties of whole sweet potato roots as well as the surrounding air properties, and was verified with experimental transient temperature data. The experimental results showed that the temperature at the centre and the under skin of sweet potato roots is almost homogeneous during forced convection cooling and heating. The cooling and heating time was significantly ($P < 0.05$) affected by high air velocity and sweet potato root size. The simulation results quantitatively agreed with the experimental transient data. This research, thus provides a reliable experimental and theoretical basis for understanding the temperature variations as well as estimating the cooling and heating times in individual sweet potato roots under forced convection cooling and heating. The result from this study could be applied to design and optimize forced-air treatment equipments with improved energy efficiency as well as ensuring safety and the maintenance of sweet potato roots quality.

Keywords. Cooling, Heating, Simulation model, Whole sweet potato root, Air velocity, Size.

5.2 Introduction

Sweet potato (*Ipomoea batatas* (L.) Lam.) is a valuable, nutritious crop which is widely grown in tropical, subtropical and even in some warm temperate regions (Woolfe, 1992). It is a staple food in many developing countries and is often consumed both fresh and in the processed forms. It has a great potential as a raw material for the manufacturing of a wide range of industrial products such as starch, liquid glucose, citric acid and ethanol (Woolfe, 1992). Despite the many advantages, sweet potato is subject to substantial losses, caused particularly by fungal pathogens, insect pests and breakdown of the produce as a result of the environmental conditions (Ray and Ravi, 2005). The emphasis on year-round, transregional and transnational long-distance marketing of sweet potato roots, particularly for food service applications and processing coupled with grower concern for risk management has prompted a re-examination of traditional postharvest treatment facilities and practices (Boyette, 2009; Edmunds et al., 2008). Further, sweet potato roots are subject to quarantine restrictions and are treated with methyl bromide (MeBr) before shipment to the mainland United States and international markets. However, MeBr production, importation and use are being phased out, because it is an ozone-depleting substance (Browner, 1999). A market window exists for fresh sweet potato roots if precise control of the thermal processes during postharvest handling as well as alternatives to MeBr fumigation are available (Boyette, 2009; Valenzuela et al., 1994).

Familiarity with forced-convective cooling and heating processes of sweet potato roots is necessary before a thermal treatment process can be developed. This includes knowledge of how rapidly the commodity cools down or heats up in a given thermal environment depending on its size and the air velocity. Many researchers have discussed forced-air cooling and heating of foodstuffs or food products (Han et al., 2016; Kumar et al., 2008; Glavina et al., 2007; Hoang et al., 2003; Wang et al., 2001; Gaffney and Armstrong, 1990). Fikiin (1983) and Wang et al. (2001) studied the influence of air velocity in cooling and heating of food products and concluded it is one of the most important factors for intensifying these processes. Temperature variations within agricultural commodities reduce the efficiency of a thermal treatment and may cause severe thermal damage to its quality and adversely affect product safety (Heldman and Lund, 2007). Also, a failure to cool or heat to the required temperature can result in potential growth of unwanted fungal pathogens, insect pests and spoilage. Therefore, research on cooling and heating of individual sweet potato roots is needed to better

understand the temperature variations of sweet potato roots under forced-convective cooling and heating. Moreover, a reliable theoretical basis is needed to optimize cooling and heating temperatures and related durations for different treatment media in order to ensure the maintenance of sweet potato roots quality and safety.

The subject of heat transfer theory is well-established in the literature (Holman, 2010; Heldman and Lund, 2007; Cengel, 2006) and has been widely used in the study of cooling and heating rates of horticultural products (Uyar and Erdoğdu, 2012; da Silva et al., 2010; Kumar et al., 2008; Wang et al., 2001). Some of the methods employed in analysing heat transfer were mostly empirical while the tests involved were labor-intensive, costly and the results obtained are only applicable to the specific condition under which such tests were carried out (Wang et al., 2001). Investigation on the influence of physical parameters on heat transfer based on computer and numerical studies have been carried out (Uyar and Erdoğdu 2012; da Silva et al., 2010). A major advantage of these computer simulations and numerical procedures is their ability to assess the effect of various physical parameters on cooling and heating profiles of fruits and vegetables (Wang et al., 2001). However, a drawback of the available modeling tools is that they need a high level of mathematical sophistication for solutions and applications (da Silva et al., 2010; Lin et al., 1996). The efficient design of optimal cooling or heat treatments devices, however, requires the use of simple mathematical models which will enable processes to be described or estimated accurately.

The objective of this study, was therefore, to provide insight into the influence of root size, air velocity and temperature on the treatment rate and time under forced-air cooling and heating conditions. Davey (2015) developed a generalized computational procedure, based on fundamental solution of the transient equations for simulating the cooling time of fish in ice slurry. Due to the complex composition and behaviour of biological products like sweet potato roots, calculations of cooling/or heating time are made difficult. An additional aim of the study was to modify the transient model procedure of Davey (2015) and ascertain its suitability in simulating the cooling and heating time of whole sweet potato roots under forced-air conditions. The results of the simulation are validated using experiments.

5.3 Materials and methods

5.3.1 Raw material

Sweet potato of the variety CRI-Apomuden was cultivated in summer 2014 at the Experimental and Demonstration farm of the Department of Agricultural Engineering, University of Kassel, Witzenhausen, Germany. The plants were cultivated according to organic agriculture production standards and the roots were harvested 90 days after planting. After harvest, damaged or severely bruised roots were sorted out and the roots that presented the visual match to a cylindrical shape selected for the experiments. The roots were then cured at 30 °C and 85% relative humidity (RH) for 7 days in a walk-in, temperature and RH controlled, room and subsequently stored at a cooling temperature range of 13-14.5 °C and 85-90% RH (Blankenship and Boyette, 2002) for consecutive test experiments. Prior to the start of the experiments, the sweet potato roots were graded into medium and large sizes with an average mass of 315.6 g and 551.1 g, respectively. The average moisture content of the roots at the time of the experiments was 81.2 ± 1.7% w.b.

5.3.2 Experimental methodology

The experiments were carried out using a laboratory scale climate chamber (VCL 4010, Vötsch Industrietechnik, Germany) with a maximum temperature and RH deviation of ±0.5 K and ±3% respectively. To accomplish the given objective, a rectangular ventilated box with dimensions 320 mm x 300 mm x 300 mm was built using 19 mm MR grade plywood, and consisted of an axial fan (ebm-papst 4412F/2M, ebm-papst St. Georgen GmbH & Co. KG, Germany), a variable fan speed controller (Aerocool X-Vision 5.25", Aerocool Advanced Technologies Corp., Taiwan), air inlet duct, air plenum and a test chamber. The MR grade plywood exterior was insulated with 60 mm thick glass wool. The installed fan was capable of delivering air velocity in the range of 0.8 -1.7 m s^{-1} at the test humidity level. A perforated plate was installed, 65 mm from the bottom of the box to improve the flow uniformity after the change of direction in the plenum chamber. The air velocity was measured with a hot wire anemometer (TA-5, Airflow Lufttechnik GmbH, Germany) with a full scale accuracy of ±1% (FS of 15 m s^{-1}).

The experimental regimes were fixed as follows:

i. For cooling: the temperature of cooling air was 14.5 °C, the RH was kept at 85% and the air velocity set to 0.8 m s^{-1} and 1.7 m s^{-1}. Uniform initial product temperature was 30 °C.
ii. For heating: the temperature of the heating air was 30, 40 and 50 °C, the RH was kept at 85% and the air velocity set to 0.8 m s^{-1} and 1.7 m s^{-1}. Uniform initial product temperature was 14.5 °C.

The temperature at the centre and under the skin of the sweet potato roots, as well as the temperature of the surrounding air were measured using K-type thermocouples with ±1.5 K accuracy. Probe sheaths of diameter 1 mm were prepared by fixing the thermocouples on the probes via connectors. These probes were then inserted in the sweet potato roots to measure the temperature change. The thermocouple probes were inserted at the centre, through the length of each root and at 5 mm under the skin. The actual locations of the thermocouples were obtained by cutting thin slices from the roots after the cooling and heating processes were completed and measuring using a vernier caliper with ±0.02 precision. This method has being used in earlier studies (Uyar and Erdoğdu, 2012; Fasina and Fleming, 2001).

In a group of 8 thermocouples, 4 were used to measure the temperature change at the centre of the sweet potato roots, 2 for measuring temperature change under the skin while the rest were used to record the medium temperature as shown in figure 5-1. After the thermocouples were located, the roots were placed on small supports inside the ventilated box so that the airflow around the sample was not impeded. Depending on the experimental set-up, the ventilated box which contained the sweet potato root was always placed inside the pre-cooled or pre-heated climatic chamber and the air-tight door of the chamber was quickly closed. A schematic drawing of the experimental set-up is shown in figure 5-1. All the thermocouples were connected to an Agilent 34970a data acquisition device and temperature-time data was recorded. The temperature change at the centre and under the skin for each experimental set was measured every 5s. Five replications were run for each given test condition (80 measurements in total) and averaged to produce a single mean experimental history.

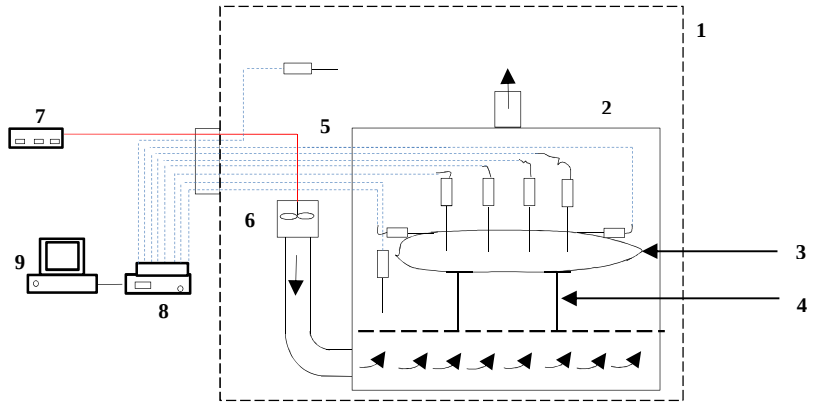

Figure 5-1 Schematic diagram of the experimental apparatus; 1- climate chamber, 2- ventilated box, 3-sweet potato root, 4- supports, 5- thermocouples inserted in sweet potato roots, 6- axial fan, 7- variable fan controller, 8- data logger, 9- computer.

5.3.3 Transient model for whole sweet potato root cooling and heating

For evaluation of the cooling or heating process of sweet potato roots, transient heat transfer principles must be analysed. Therefore, assumptions and a set of equations describing the model of the transient heat transfer in forced-convection cooling and heating process of whole sweet potato root are presented. The following basic assumptions have been made to drive the mathematical model: (1) fresh sweet potato roots hold the geometrical shape of a cylinder where heat transfer in the longitudinal direction might be neglected; (2) the sweet potato root was considered to have a uniform initial temperature T_i and to be subjected suddenly (Baïri and Laraqi, 2003) to an environment with a constant temperature T_a; (3) the roots are considered as homogenous and the radius of the cylinder is constant during the heat transfer process; (4) there is negligible moisture loss due to the rather short time of the test; (5) Choi and Okos models are adequate for estimating the thermo-physical properties of sweet potato roots (Choi and Okos, 1986); (6) the changes in the air temperature and humidity from the inlet to the outlet of the testing device are small enough to produce a negligible effect on the thermo-physical properties of the air. On this basis, the properties of the airflow are calculated at the conditions of dry air entering the ventilated box, see Section 5.3.2; (7) the external surface of each cylindrical root is supposed to be surrounded by this cold or heated air with constant properties. This assumption was based on an air velocity range (0.5-3 m s^{-1}) in forced-air applications (Zou et al., 2006); (8) the convective heat transfer coefficient is calculated as the area average value of the local heat transfer coefficient (Becker and Fricket,

2004).

Based on the assumptions above, the transient model procedure developed by Davey (2015) is modified and utilized. Parts of the model are reproduced here for ease of comprehension of this article. The terms used in the model are carefully defined in the Nomenclature. The target temperature of the cooled or heated sweet potato root, T, is the centreline temperature. The solution for the centreline temperature of a cylinder with cooling or heating (Holman, 2010) is

$$\frac{\theta_0}{\theta_i} = C_B \exp\left(-A_B^2 \frac{\alpha_{sp} t}{r^2}\right) \tag{5-1}$$

where equation (5-2) and equation (5-3) defines the two temperature difference terms:

$$\theta_0 = T - T_a \tag{5-2}$$

$$\theta_i = T_i - T_a \tag{5-3}$$

C_B and A_B are constants that are defined using Bessel functions J_0 ( ) and J_1 ( ), of the first kind such that:

$$\frac{A_B J_1}{J_0(A_B)} = Bi = \frac{h.r}{k_{sp}} \tag{5-4}$$

and

$$C_B = \frac{2}{A_B}\left(\frac{J_1(A_B)}{J_0^2(A_B)+J_1^2(A_B)}\right) \tag{5-5}$$

where Bi is the Biot number, h is the convective heat transfer coefficient from the sweet potato root to the cooling or heating surrounding environment (W m^{-2} $°C^{-1}$) and k_{sp} is thermal conductivity of the sweet potato roots (W m^{-1} $°C^{-1}$).

For a cylindrical food product undergoing cooling or heating process where air movement is involved, the correlation (eq. (5-6)) developed by Dincer (1994) can be applied to compute the heat transfer coefficient.

$$h = \frac{Nuk_a}{D_{sp}} = \left(0.291 Re^{0.592} Pr^{1/3}\right)\frac{k_a}{D_{sp}} \tag{5-6}$$

where k_a and D_{sp} refer to the thermal conductivity of air (W m^{-1} °C^{-1}) and the sweet potato root diameter (m) respectively. The diameter of sweet potato root was calculated according to Pérez-Alegría et al. (2001). Nu is the dimensionless Nusselt number. Re and Pr are the Reynolds and Prandtl dimensionless numbers and are determined as follows:

$$\mathrm{Re} = \frac{\rho_a V_a D_{sp}}{\mu_a} \tag{5-7}$$

$$\mathrm{Pr} = \frac{C_a \mu_a}{k_a} \tag{5-8}$$

where ρ_a, v_a, μ_a and C_a are the air density, air velocity, air viscosity and specific heat of air.

The Fourier number (Fo) is critical when evaluating cooling and heating processes. It is defined in equation (5-1) and given as:

$$\frac{\alpha_{sp} t}{r^2} = \mathrm{Fo} \tag{5-9}$$

where t is the time elapsed during the cooling and heating process. The thermal diffusivity of sweet potato root α_{sp}, (m^2 s^{-1}), defined in equation (5-9) is given as

$$\alpha_{sp} = \frac{k_{sp}}{\rho_{sp} C_{sp}} \tag{4-10}$$

where ρ_{sp} is the density (kg m^{-3}) and C_{sp} is the heat capacity of sweet potato roots (J kg^{-1} °C^{-1}).

The radius of the equivalent cylinder of the sweet potato root is expressed in terms of root mass, m_{sp}. This can be calculated as $m_{sp} = \rho_{sp} V_{sp} = \rho_{sp}(\pi r^2 L_{sp})$, with L_{sp} = the characteristic length of the sweet potato root. For a range of sizes, the sweet potato root radius (r) will reasonally be approximated by

$$r = K_{sp}\sqrt{m_{sp}/\rho_{sp}} \tag{5-11}$$

where K_{sp} , a characteristic constant for a particular sweet potato size/or variety at harvest ($m^{-1/2}$) is defined as:

$$K_{sp} = \sqrt{1/(\pi L_{sp})} \quad (5\text{-}12)$$

Now, substituting Fo as defined in equation (5-9) into equation (5-1) and rearranging gives:

$$\frac{\theta_0}{\theta_i} = C_B \exp(-A_B^2 Fo) \quad (5\text{-}13)$$

Equations 5-2 through to 5-13 define the generalized transient model which can be used to estimate the desired cooling or heating time (t) of sweet potato root of size m_{sp} from an initial uniform temperature (T_i) to a target temperature (T) at the centre in a thermal environment with constant air temperature (T_a). Model simulations were carried as follows (Davey, 2015): T_i, T, T_a, and m_{sp} are specified and the other model parameters are obtained from tables 5-1 to 5-3; r is obtained from equation (5-11); Bi is computed from the RHS of equation (5-4), and; an iterative procedure is used to calculate A_B and the Bessel function J_0 ( ) and J_1 ( ); C_B is obtained from equation (5-5), and θ_0 and θ_i from equations (5-2) and (5-3), respectively; Fo is computed from rearranged equation (5-13); α_{sp} is obtained from equation (5-10); and, cooling or heating time t is obtained from rearranged equation (5-9). The computations were performed in Microsoft Excel™ (2013). The *solver* function is used for step 3 such that

$$Bi - \frac{A_B J_1(A_B)}{J_0(A_B)} = 0 \quad (5\text{-}14)$$

Table 5-1 summarizes the air medium properties while tables 5-2 and 5-3 list the density, thermal conductivity, heat capacity and heat transfer coefficient values at the different test conditions.

Table 5-1 Cooling and heating air properties (Cengel, 2006).

T_a, (°C)	ρ_a, (kg m^{-3})	μ_a, (kg m^{-1} s^{-1})	C_a, (J kg^{-1} °C^{-1})	k_a, (W m^{-1} °C^{-1})
14.5	1.225	1.802 x 10^{-5}	1007	2.476 x 10^{-2}
30	1.164	1.872 x 10^{-5}	1007	2.588 x 10^{-2}
40	1.127	1.918 x 10^{-5}	1007	2.662 x 10^{-2}
50	1.092	1.963 x 10^{-5}	1007	2.735 x 10^{-2}

Table 5-2 Thermo-physical properties of whole sweet potato roots.

Parameter	Medium size root	Large size root
Density, ρ_{sp} (kg m^{-3}) (Eq. (5-15))	1027	990
Heat capacity, C_{sp} (J kg^{-1} $°C^{-1}$)[a]		
at T_a = 14.5 °C	3684.4	3729.3
at T_a = 30 °C	3687.8	3730.5
at T_a = 40 °C	3690.1	3731.5
at T_a = 50 °C	3692.6	3732.7
Thermal conductivity, k_{sp} (W m^{-1} $°C^{-1}$)[a]		
at T_a = 14.5 °C	0.597	0.578
at T_a = 30 °C	0.619	0.600
at T_a = 40 °C	0.633	0.613
at T_a = 50 °C	0.645	0.625

[a]Choi and Okos (1986) model

Table 5-3 Dependency of heat transfer coefficient with medium air velocity and sweet potato roots size (eqs. (5-6) to (5-8)).

Sweet potato root size	h, (W m^{-1} $°C^{-1}$)	
	v_a = 0.8 m s^{-1}	v_a = 1.7 m s^{-1}
Medium temperature (Ta = 14.5 °C)		
Medium size	14.140	22.093
Large size	12.461	19.469
Medium temperature (Ta = 30 °C)		
Medium size	13.991	21.860
Large size	12.330	19.264
Medium temperature (Ta = 40 °C)		
Medium size	13.899	21.716
Large size	12.248	19.137
Medium temperature (Ta = 50 °C)		
Medium size	13.807	21.572
Large size	12.167	19.010

5.3.3.1 Thermo-physical properties of whole sweet potato root

The apparent density of sweet potato roots was determined by the water displacement method (Rahman, 1995) and computed using equation (5-15). The density is assumed to be constant during the treatment process.

$$\rho_{\text{apparent}} = m_{sp}/V_{sp} \quad (5\text{-}15)$$

The heat capacity and thermal conductivity of sweet potato roots were estimated according to the Choi and Okos (1986) models, which account for the chemical components making up the sweet potato roots. Since the thermal conductivity and heat capacity are sensitive to the amount of air inside the porous structure of biological materials, the mass fraction of the air for the individual sweet potato roots was estimated. The true density of sweet potato roots was calculated based on equation (5-16) (Choi and Okos, 1986).

$$\rho_{true} = \frac{1}{\sum x_i/\rho_i} \tag{5-16}$$

where x_i is the mass fraction of the various component i (kg kg^{-1}) and the values ρ_i are the densities (kg m^{-3}) of the constituents of component i (water, protein, carbohydrate, fat, fibre and ash respectively). The component of the raw sweet potato root were obtained from USDA (2016): 77.28% water, 1.57% protein, 20.12% carbohydrate, 0.05% fat, 3% fibre and 0.99% ash. The density of each constituent (ρ_i) can be obtained from the models of Choi and Okos (1986). The apparent density of sweet potato roots is thus expressed as (Lu et al., 2009):

$$\rho_{apparent} = \left[\frac{1-x_a}{\rho_{true}} + \frac{x_a}{\rho_a}\right]^{-1} \tag{5-17}$$

The mass fraction of air (x_a) can be estimated using equation (5-18).

$$x_a = \frac{\rho_a(\rho_{true}-\rho_{apparent})}{\rho_{apparent}(\rho_{true}-\rho_a)} \tag{5-18}$$

where ρ_a is the density of air.

5.3.3.2 Error of the simulated cooling and heating time

In the different air velocities and sweet potato root grades investigated in this study, the error between the experimental and the simulated cooling and heating times at the centreline was determined using equation (5-19). The experimental cooling or heating time was defined as the time at which all the thermocouples in a given sweet potato root registered the T = 15 °C (for cooling) and T = 29.5, 39.5 and 49.5 °C, respectively (for heating).

$$e(\%) = \left|100\left(\frac{t_{sim}-t_{exp}}{t_{exp}}\right)\right| \tag{5-19}$$

5.4 Results and discussion

5.4.1 Cooling and heating profiles

A comparison of the temperature-time histories of medium and large size sweet potato roots in the centre and under the skin using T_a = 14.5 °C and only T_a = 30 °C is shown in figures 5-2 and 5-3 using different air velocities. Similar curves were obtained at the other heating temperatures. At first sight, one can see that the temperature at the centre and the under the skin of the roots is almost homogeneous during forced-convective cooling or heating. This is very important from the point of view of sweet potato roots quality and insect pest control. As indicated in figure 5-2a and b for cooling, the average temperature at the centre and under the skin of the roots decreases with increasing air velocity. This result is attributed to the higher heat transfer coefficients (table 5-3). Statistical tests based on quantitative comparison of the time required to cool a given sweet potato root to its centreline (table 5-5) further revealed significant difference between 0.8 m s^{-1} and 1.7 m s^{-1} air velocity and among the root grades investigated (one-way analysis of variance (ANOVA); α = 0.05; IBM SPSS Statistics 22). This result is similar to the previously reported cooling rates of apple, oranges and tomatoes (Han et al., 2016; Kumar et al., 2008). Generally, the temperature difference between the centre and under the skin is bigger at the beginning of the cooling process (fig. 5-2a and b). However, this variation became smaller and smaller as the temperature at centre and under the skin approaches the medium air temperature. The temperature difference between the centre and under the skin is however marginal at air velocity of 0.8 m s^{-1} in the medium size sweet potato roots.

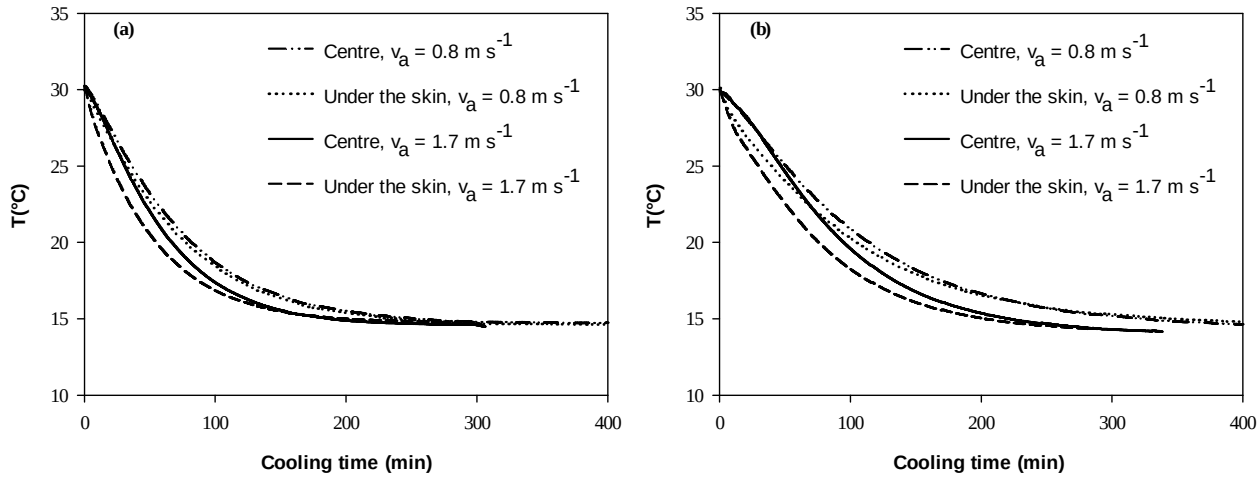

Figure 5-2 Temperature change at the centre and under the skin of (a) medium size and (b) large size whole sweet potato roots during forced-air cooling at 14.5 °C.

Figure 5-3a and b shows the measured sweet potato roots centre and under the skin temperatures when exposed to forced hot air with air velocity of 0.8 m s^{-1} and 1.7 m s^{-1}. When the air velocity increased from 0.8 to 1.7 m s^{-1}, the heating time to reach the medium air temperature is reduced. This is in accordance with the literature (Wang et al., 2001; 1992; Gaffney and Armstrong, 1990). Slower heating rates were obtained in the large size roots. Quantitative comparison (table 5-5) of the time required to heat a given sweet potato root to its centreline revealed significant difference between the air velocities tested and among the sweet potato grades on specific medium air temperature (one-way analysis of variance (ANOVA); α = 0.05; IBM SPSS Statistics 22). Temperature differences between the centre and under the skin during heating is comparable to the observations made in figure 5-2a and b.

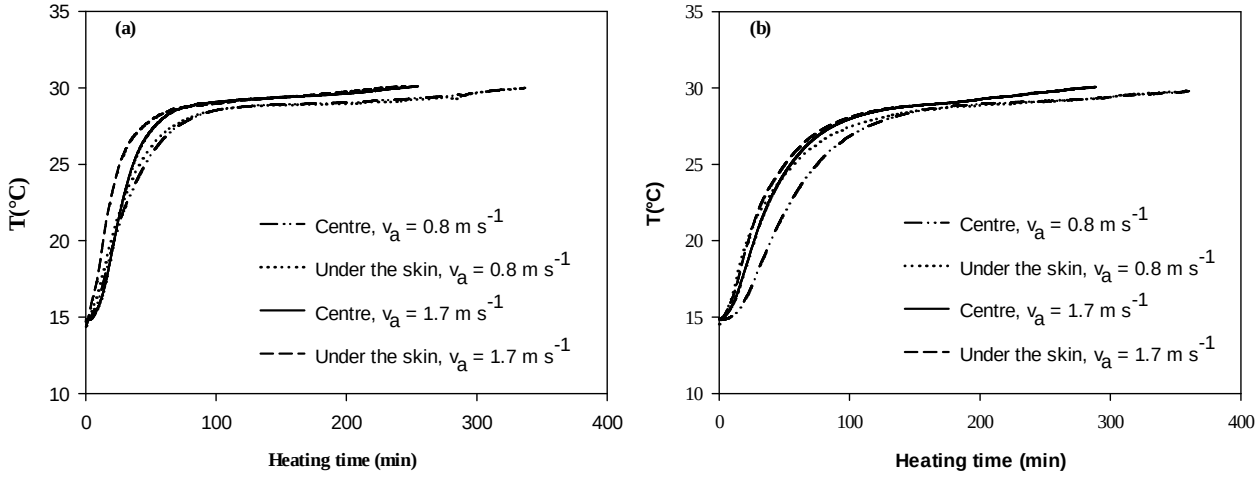

Figure 5-3 Temperature change at the centre and under the skin of (a) medium size and (b) large size whole sweet potato roots during forced-air heating at 30 °C.

5.4.2 Model validation using experimental temperature-time data

The simulation model was validated by experiments. As an example, table 5-4 shows a summary of the simulation carried out in Excel for large size sweet potato root, from an initial uniform temperature of T_i = 30 °C subjected to cooling medium temperature of 14.5 °C under a uniform air velocity of 0.8 m s^{-1}. The target temperature is 15 °C at the centreline. In the table row 12 shows the Bi number while the time (t) required for cooling at the centreline of a whole sweet potato is depicted in row 22.

Table 5-4 The simulation constructed using Microsoft Excel™ spread sheet tools for medium air velocity (v_a) of 0.8 m s^{-1}.

Inputs				
Row 1	T_a	14.5	°C	
2	T_i	30	°C	
3	T	15	°C	
4	C_{sp}	3729.32	J kg^{-1} $°C^{-1}$	
5	ρ_{sp}	990	Kg m^{-3}	
6	k_{sp}	0.5781	W m^{-1} $°C^{-1}$	
7	h	12.46091417	W m^{-2} $°C^{-1}$	
8				
9	K	1.2615	$m^{-1/2}$	
10	m_{sp}	0.5511	kg	
Calculations				
11	r	0.03	m	
12	Bi	0.6416	dimensionless	(eq.(5-4))
13	A_B	1.047993678	5.33521 x 10^{-7}	**Solver™**
14	J_0	0.743709608	dimensionless	
15	J_1	0.455276946	dimensionless	
16	C_B	1.142656491	dimensionless	(eq.(5-5))
17	θ_0	0.5	°C	(eq.(5-2))
18	θ_i	15.5	°C	(eq.(5-3))
19	Fo	3.248	dimensionless	(eq.(5-13))
20	α_{sp}	1.56579 x 10^{-7}	m^2 s^{-1}	(eq.(5-10))
Outputs				
21	t	18376.1	s	(eq.(5-9))
22		**306.27**	min	

Table 5-5 shows a comparison between repeated simulations and the experimental average and standard deviation of time required for cooling or heating of individual whole sweet potato roots to a target temperature in the centreline. Clearly, the simulated time estimates are in agreement with the experimental data required at the centreline (table 5-5). The average error

between the simulated and the experimental times is between -1.17 to 0.97% and -1.29 to 1.29% for cooling and heating, respectively within the conditions investigated. A possible explanation for the discrepancies between the simulated and the experimental results could be due to minor variations in the sweet potato roots size as well as issues such as thermocouple location imprecision. Nevertheless, such minor variations can be considered negligible in industrial applications.

Table 5-5 Comparison between simulated time estimates and experimental time (t) [a] require to reach a centreline temperature of: (a) 15 °C during cooling from an initial uniform temperature of 30 °C; (b) 29.5, 39.5 and 49.5 °C during heating from an initial uniform temperature of 14.5 ° of two grades of sweet potato roots under air velocity of 0.8 m s^{-1} and 1.7 m s^{-1}, respectively. The **bold text** is the particular simulation demonstrated in table 5-4.

Sweet potato roots size	Medium temperature (T_a), (°C)	Centreline temperature (T), (°C)	Time (t) taken to reach centreline temperature (min)					
			v_a = 0.8 m s^{-1}			v_a = 1.7 m s^{-1}		
			sim	exp	e(%)	sim	exp	e(%)
(a) Cooling	14.5	15						
Medium size			248.82	252.67 ± 1.82^{aA}	-1.52	175.52	177.59 ± 2.65^{bA}	-1.17
Large size			**306.27**	308.92 ± 1.66^{aB}	-0.86	216.20	214.13 ± 3.47^{bB}	0.97
(b) Heating	30	29.5						
Medium size			249.61	248.02 ± 3.11^{aA}	0.64	175.41	175.75 ± 1.51^{bA}	-0.19
Large size			307.04	305.33 ± 1.12^{aB}	0.56	215.92	218.75 ± 2.78^{bB}	-1.29
	40	39.5						
Medium size			285.23	281.61 ± 2.01^{aA}	1.29	199.64	200.37 ± 3.17^{bA}	-0.36
Large size			350.70	348.21 ± 1.32^{aB}	0.72	245.64	248.24 ± 1.71^{bB}	-1.05
	50	49.5						
Medium size			309.43	312.41 ± 1.32^{aA}	-0.95	215.93	216.82 ± 1.24^{bA}	-0.41
Large size			380.31	383.55 ± 2.62^{aB}	-0.84	265.59	267.80 ± 2.51^{bB}	-0.83

Different small letters in the row indicated significant difference in medium and large size values between different air velocities and different capital letters in the column indicated significant difference among the sweet potato root sizes on specific medium air temperatures.

[a] Experimental values are means ± standard deviation of 5 repetitions.

5.4.3 Analysis of Biot number

The Bi number is defined as the ratio of the external to internal heat transfer resistance and is an important parameter to be examined in transient heat transfer processes (Holman, 2010; Reinheimer et al., 2010). A low value of Bi (typically < 0.1) means that the internal conduction resistance is negligible compared with the surface convection resistance. The Bi numbers for forced convection cooling and heating presented in table 5-6 are characterized by values greater than 0.1 but less than 10. This indicates that the external and internal resistance to heat transfer in the sweet potato roots are on the same order as previously illustrated in figures 5-2 and 5-3. Lower Bi numbers correspond to medium size sweet potato roots, slower air velocity as well as higher air temperatures.

Table 5-6 Simulated Biot number during forced-air cooling of two grades of sweet potato roots.

Sweet potato root size	Biot number	
	v_a = 0.8 m s^{-1}	v_a = 1.7 m s^{-1}
Medium temperature (Ta = 14.5 °C)		
Medium size	0.636	0.993
Large size	0.642	1.002
Medium temperature (Ta = 30 °C)		
Medium size	0.606	0.947
Large size	0.612	0.956
Medium temperature (Ta = 40 °C)		
Medium size	0.589	0.921
Large size	0.595	0.929
Medium temperature (Ta = 50 °C)		
Medium size	0.574	0.896
Large size	0.579	0.905

5.4.4 Generalization of experimental and model results

Experiments and simulation of transient heat transfer were performed under forced convection conditions and multiple air temperatures for development of post-harvest handling and quarantine treatment protocols in the sweet potato production industry. Strictly speaking, the experiments and the simulation method was applied to individual whole sweet potato roots. Therefore, precautions needs to be taken especially when using the model in bulk sweet potato roots handling systems. For example, in a realistic system in which bulk roots are treated, each root may be exposed to different conditions depending on the design of the

forced-air handling system. O'Sullivan et al. (2014) highlighted recommendations prescribed by several authors aimed at ensuring uniform flow distribution during forced-air application. Nevertheless, studying forced-air cooling and heating of individual whole sweet potato roots under laboratory scale serve as a basis for understanding the influence of the flow pattern in a large scale bulk handling system. Importantly, attention should be paid to sorting to help achieve uniform cooling and heating among sweet potato roots under forced-air applications.

Further, there exist a wide range of sweet potato cultivars with noted varying attributes (Lopez-Ramos et al., 1993). As a result, the properties of the roots (density, thermal conductivity and specific heat) used in our simulation model were compared to those values reported by other authors (table 5-7). A closer look at the table reveals that cultivar differences has minor effect on density, thermal conductivity and heat capacity, further underscoring the broader applicability of the estimates in our study.

Table 5-7 Thermo-physical properties of different sweet potato cultivars.

Cultivar	Density, ρ_{sp} (kg m^{-3})	Thermal conductivity, k_{sp} (W m^{-1} °C^{-1})	Heat capacity, C_{sp} (J kg^{-1} °C^{-1})
Beauregard[a]	993	0.481	3729
Hernandez[a]	992	0.536	3704
Jewel[a]	1002	0.597	3616
Sunny II[b]	1212	0.490	3660
CRI-Apomuden[c]	1027	0.597-0.645	3684.4-3692.6
CRI-Apomuden[c]	990	0.578-0.625	3727.3-3732.7

Source: [a]Stewart et al. (2000); [b]Farinu and Baik (2007); [c]This study (medium size roots); [c]This study (large size roots)

5.5 Conclusions

Temperature-time profiles and estimated cooling/or heating times were obtained during forced convection cooling and heating under experimental and transient simulation conditions, respectively. The experimental results asserted that increasing air velocity during cooling and heating influences the cooling and heating rates, thus significantly ($P < 0.05$) affects the cooling and heating times. Furthermore, the cooling and heating times were significantly different ($P < 0.05$) among medium and large size sweet potato roots. Comparison of the simulation results with experimental data confirmed that the transient simulation model can be used to accurately estimate the cooling and heating times of whole sweet potato roots under

forced convection cooling and heating. Although simulations were carried out for individual whole sweet potato roots, studying forced-air cooling and heating of individual whole sweet potato roots under laboratory scale serve as a basis for understanding the influence of the flow pattern in a large scale bulk handling system.

It should however be noted that, the mass of sweet potato root is the controlling variable in successful application of the simulation model. Thus, attention should be paid to sorting of sweet potato roots to guarantee accuracy. The results from this study will be of immediate practical use in designing and evaluating forced-air treatment equipment's. Further investigation is necessary to incorporate microbial reaction and insect mortality in the model for further evaluating the quality of sweet potato roots under forced-convection cooling/heating treatments.

5.6 Acknowledgements

The first author, Joseph Kudadam Korese would wish to acknowledge financial support from the German Academic Exchange Service (DAAD)-Germany for his research stay in Germany. The study is part of two ongoing projects: Global Food Supply (GlobE) project- RELOAD (FKZ 031A247 A), funded by the BMBF-Germany and RE4Food project (EP/L002531/1), funded by EPSRC-United Kingdom, DFID-United Kingdom and DEFRA-United Kingdom. We gratefully acknowledge their financial contributions. We also acknowledge Dr. K. R. Davey, School of Chemical Engineering, the University of Adelaide for his assistance in the simulations.

5.7 References

Boyette, M. D. (2009). The investigation of negative horizontal ventilation for long-term storage of sweetpotatoes. Applied Engineering in Agriculture, 25(5), 701-708.

Becker, B.R., & Fricke, B.A. (2004). Heat transfer coefficient for forced air cooling of selected foods. International Journal of Refrigeration, 27, 540-551.

Baïri, A., & Laraqi, N. (2003). Diagrams for fast transient conduction in sphere and long cylinder subject to sudden and violent thermal effects on its surface. Applied Thermal Engineering, 23, 1373-1390.

Blankenship, S. M., & Boyette, M. D. (2002). Root epidermal adhesion in five sweetpotato cultivars during curing and storage. HortScience, 37(2), 374-377.

Browner, C. M. (1999). Protection of stratospheric ozone: Incorporation of Montreal Protocol adjustment for a 1999 interim reduction in class I, group VI controlled substances. Federal Register, 64(104), 29240-29245.

Cengel, Y. A. (2006). Heat transfer and mass transfer – A practical approach (3rd ed.). New York, NY: McGraw Hill Companies, Inc. (Appendix 1).

Choi, Y., & Okos, M.R. (1986). Effects of temperature and composition on the thermal properties of foods. In: M. LeMaguer & P. Jelen. (Eds.), Food engineering and process applications (pp. 93-101), Elsevier Applied Science Publishers, London.

Davey, K. R. (2015). Development and illustration of a computationally convenient App for simulation of transient cooling of fish in ice slurry at sea. LWT-Food Science and Technology, 60, 308-314.

da Silva, W.P., e Silva, C.M.D.P.S., Farias, W.S.O., & e Silva D.D.P.S. (2010). Calculation of convection heat transfer and cooling kinetics of an individual fig fruit. Heat and Mass Transfer, 46 (3), 371-380.

Dincer, I. (1994). Development of new effective Nusselt-Reynolds correlations for air-cooling of spherical and cylindrical products. International Journal of Heat and Mass Transfer, 37 (17), 2781-2787.

Edmunds, B., Boyette, M., Clark, C., Ferrin, D., Smith, T., & Holmes, G. (2008). Postharvest handling of sweetpotatoes. North Carolina Cooperative Extension Service, pp.53.

Farinu, A., & Baik, O. (2007). Thermal properties of sweet potato with its moisture content and temperature. International Journal of Food Properties, 10, 703-719.

Fasina, O.O., & Fleming, H.P. (2001). Heat transfer characteristics of cucumbers during blanching. Journal of Food Engineering, 47, 203-210.

Fikiin, A.G. (1983). Investigating the factors of intensifying fruits and vegetable cooling. International Journal of Refrigeration, 6(3), 176-181.

Glavina, M., Di scala, K., & del Valle, C. (2007). Effects of dimensions on the cooling rate of whole potatoes applying transfer functions. LWT-Food Science and Technology, 40(10), 1694-1697.

Gaffney, J.J., & Armstrong, J.W. (1990). High-temperature forced-air research facility for heating fruits insect quarantine treatments. Journal of Economic Entomology, 83, 1959-1964.

Han, J-W, Badía-Melis, R., Yang, X-T, Ruiz-Garcia, L., Qian, J-P., & Zhao, C-J. (2016). CFD simulation of airflow and heat transfer during forced-air precooling of apples. Journal of

Food Process Engineering. Online. http://dx.doi.org/doi:10.1111/jfpe.12390.

Holman, J.P. (2010). Heat transfer. (10th ed.). McGraw-Hill Higher Education, New York, NY. (Appendix C, pp. 673).

Heldman, D.R., & Lund, D. B. (2007). Handbook of food engineering (2nd ed.). New York, NY: Taylor & Francis (Chapter 5).

Hoang, M.L., Verboven, P., Baelmans, M., & Nicolaï, B.M. (2003). A continuum model for airflow, heat and mass transfer in bulk of chicory roots. Transactions of the ASAE, 16(6), 1603-1611.

Kumar, R., Kumar, A., & Murthy, U. N. (2008). Heat transfer during forced air precooling of perishable food products. Biosystems Engineering, 99, 228-233.

Lu, J., Dev, S.R.S., Raghavan, G.S.V., & Vigneault, C. (2009). Simulation of a forced-air-twin-chamber for measuring heat treatment uniformity in harvested tomatoes. Journal of Food Engineering, 95, 636-647.

Lin, Z., Cleland, A. C., Cleland, D. J., & Serralach, G.F. (1996). A simple method for prediction of chilling times: Extension to three-dimensional irregular shapes. International Journal of Refrigeration, 19(2), 107-114.

Lopez-Ramos, A. Palmisano, A., Pimentel, J.A., Fayes, D., & Gonzalez-Mendizabal, D. (1993). Thermal properties of tropical fruits and vegetables. Revista espanola de ciencia y technologia de alimentos 33(3), 271-283.

O'Sullivan, J., Ferrua, M., Love, R., Verboven, P., Nicolaï, B., & East, A. (2014). Airflow measurement techniques for the improvement of forced-air cooling, refrigeration and drying operations. Journal of Food Engineering, 143, 90-101.

Pérez-Alegría, L. R., Ciro V, H. J., & Abud, L. C. (2001). Physical and thermal properties of parchment coffee bean. Transactions of the ASAE, 44(6), 1721-1726.

Reinheimer, M.A., Mussati, S., & Scenna, N. J. (2010). Influence of product composition and operating conditions of the unsteady behaviour of hard candy cooling process. Journal of Food Engineering, 101(4), 409-416.

Ray, R.C., & Ravi, V. (2005). Post harvest spoilage of sweetpotato in tropics and control measures. Critical Reviews in Food Science and Nutrition, 45(7-8), 623-644.

Rahman, M. S. (1995). Food properties handbook. New York, NY: CRC press, (Chapter 3).

Stewart, H.E., Farkas, B.E., Blankenship, S.M., & Boyette, M.D. (2000). Physical and thermal properties of three sweetpotato cultivars (*Ipomoea batatas* L.). International Journal of

Food Properties. 3(3) 433-446.

USDA (2016). USDA National Nutritional Database for Standard Reference, Release 28. Nutrient Database Laboratory, Available online at: https://ndb.nal.usda.gov/ndb/foods/show/3207 (accessed on 30.06.2016).

Uyar, R., & Erdoğdu, F. (2012). Numerical evaluation of spherical geometry approximation for heating and cooling of irregular shaped food products. Journal of Food Science, 77(7), 166-175.

Valenzuela, H., Fukuda, S., & Arakaki, A. (1994). Sweet potato production guide for Hawaii. Hawaii Agricultural Experiment Station Research Extension Series 146.

Wang, S. Tang, J., & Cavalieri, R. P. (2001). Modeling fruit internal heating rates for hot air and hot water treatments. Postharvest Biology and Technology, 22, 257-270.

Woolfe, J. A. (1992). Sweet potato: An untapped food resource. Cambridge, UK: Cambridge University Press.

Zou, Q., Opara, L. U., & McKibbin, R. (2006). A CFD modeling system for airflow and heat transfer in ventilated packaging for fresh foods: I. Initial analysis and development of mathematical models. Journal of Food Engineering, 77, 1037-1047.

6 Experimental evaluation of bulk charcoal pad configuration on evaporative cooling effectiveness

Joseph Kudadam Korese[1,2)], Oliver Hensel[1)]

[1)] Department of Agricultural Engineering, University of Kassel, Nordbahnhofstr. 1a, 37213 Witzenhausen, Germany

[2)] Department of Agricultural Mechanisation and Irrigation Technology, University for Development Studies, Post Office Box 1882, Nyankpala Campus, Tamale, Ghana

6.1 Abstract

The purpose of the study was to evaluate the performance of bulk charcoal pad configuration, experimentally. For this, a number of experiments have been conducted in a wind tunnel in order to evaluate the pressure drop, cooling efficiency and specific water consumption as a function of air velocity, water flow rate and pad configuration. The test were carried out at six levels of air velocity (0.12, 0.51, 0.82, 1.05, 1.10 and 1.14 m s^{-1}), three water flow rates (2.2, 3.2 and 5.2 l min^{-1}) and three pad configurations: single layer pad (SLP), double layers pad (DLP) and triple layers pad (TLP) made out of small and large size charcoal particle of equivalent diameter 30 mm and 50 mm, respectively. It was found that pressure drop range of small size charcoal pads is 2.67 to 240.00 Pa while that of pads made out of large size charcoal are much lower with the range of 2.00 to 173.33 Pa, depending on the pad configuration, air velocity and water flow rate. The cooling efficiencies of the small size charcoal pads vary from 56.71% to 96.10% while the cooling efficiencies of large size charcoal pads are 45.41% to 90.06%, depending on the pad configuration, air velocity and the water flow rate. Generally, DLP and TLP configuration with larger wet surface area provide high cooling efficiencies and high pressure drops, though it obviously leads to increase in water consumption. DLP and TLP configurations at low air velocity are therefore recommended for practical applications.

Keywords. Charcoal, Pad configuration, Wind tunnel, Evaporative cooling, Pressure drop, Cooling efficiency, Specific water consumption.

6.2 Introduction

Evaporative cooling is a simple cooling technique that has been used for centuries to provide low-air temperatures and high relative humidity for cooling produce (Thompson and Kasmire, 1981). Rising energy cost, together with scant water resources in most areas of intensive production, urge the use of evaporative cooling systems that are economical and highly water and energy efficient (Franco et al. 2011). Two basic types of evaporative cooling are commonly used: direct and indirect evaporation cooling. Published data concerning both are enormous (Duan et al., 2012; Xuan et al., 2012). The present study focuses on the direct evaporative cooling principle which is the oldest and most widespread form of evaporative air conditioning (Heidarinejad et al., 2009).

Direct evaporative cooling systems are based on the evaporation of water in the air stream; with evaporative cooling pads. The wetted-medium could be porous wetted pads consisting of fibers or cellulose papers (Franco et al., 2010; Koca et al., 1991). According to He et al. (2015a) and Koca et al. (1991), the wetted material behaviour can be classed as aspen pad and rigid media. Aspen pad behaviour is difficult to achieve particularly in rural Africa and rigid media is mostly imported. To reduce investment cost and promote sustainable engineering systems, research on alternative and locally available cheap materials with reasonable thermal performance, comparable or better than rigid media is necessary. A number of researchers have evaluated locally available materials as alternative pad media (Jain and Hindoliya, 2011; Adebisi et al., 2009; Gunhan et al., 2007; Al-Sulaiman, 2002; Liao et al., 1998). However, pad sagging, pad clogging, pad scaling, pad deterioration and mold formation, are big problems thus limiting their useful life and general use.

Several characteristics are used to rate a pad (Koca et al., 1991). Among these characteristics include pressure drop and efficiency which are affected by the pad design, thickness, pad configuration, air velocity and water flow rate (Fanco et al., 2010; Rawangkul et al., 2008; Gunhan et al., 2007; Koca et al., 1991). Pressure drop versus air velocity is essential for selecting a fan and pad area for a particular application while efficiency is the most important physical performance factor. The more efficient a pad at a given air velocity, the more cooling it will provide (Koca et al., 1991). Evaporative cooling pad's water consumption is another essential parameter, especially due to the scarcity of this resource. It enables engineers to

determine the size for the pump and water storage design (Franco et al., 2012; Franco et al., 2010). Franco et al. (2010) reported that the amount of water evaporated from a pad is related to the outside air temperature and relative humidity, as well as pad's structural characteristics and air velocity through the pad.

According to Gunhan et al. (2007), a pad material should have a porous structure that can hold water, light in weight, durable for repeated wetting and drying, inexpensive and locally available. Moreover, it should allow easy construction into required shape and size (Liao et al., 1998). Based on these attributes, we selected locally available and inexpensive material, charcoal of different sizes to test as pad media. Despite the widespread studies conducted in the past on evaporative cooling, there are no experimental investigations on cooling performance of wetted charcoal pad configurations which is useful for system engineering design. The key issue is the trade-off between the wetted medium cooling and the extra pressure drop, both of which are a strong function of the wetted media (pad) configuration. Hence, the performances of charcoal pads made out of small and large size particles are evaluated experimentally and the effect of air velocity, water flow rate and pad configuration on the pressure drop, cooling efficiency and water consumption examined. An additional objective is aimed at identifying suitable wetted pad configuration that provides high cooling efficiency and low pressure drop.

6.3 Materials and methods

6.3.1 Wetted media

The wetted media used in this study is bulk charcoal obtained from a local market in Witzenhausen, Germany. The species of the wood used to produce the charcoal is a pine variety. The charcoal was sorted into two size fraction: small and large. For each size fraction, the equivalent diameter was calculated as average of the three main dimensions (length (L), width (W) and height (H)) of a sample consisting of 150 – 200 particles. The calculated equivalent diameters are 30 mm and 50 mm for small and large sizes charcoal, respectively. Each size fraction of the charcoal material was filled separately into galvanized steel frames to create an evaporative cartridge. The front and the back faces of the cartridges were covered with a wire mesh. The frontal area of these cartridges was 500 mm by 424 mm (H x W) and the thickness was 100 mm.

6.3.2 Wind tunnel system

To determine the performance of a low-cost evaporative cooling pad (charcoal), an open-circuit wind tunnel was designed and fabricated in the Agricultural Engineering Department workshop, University of Kassel, Witzenhausen, Germany. The schematic of the wind tunnel is depicted in figure 6-1.

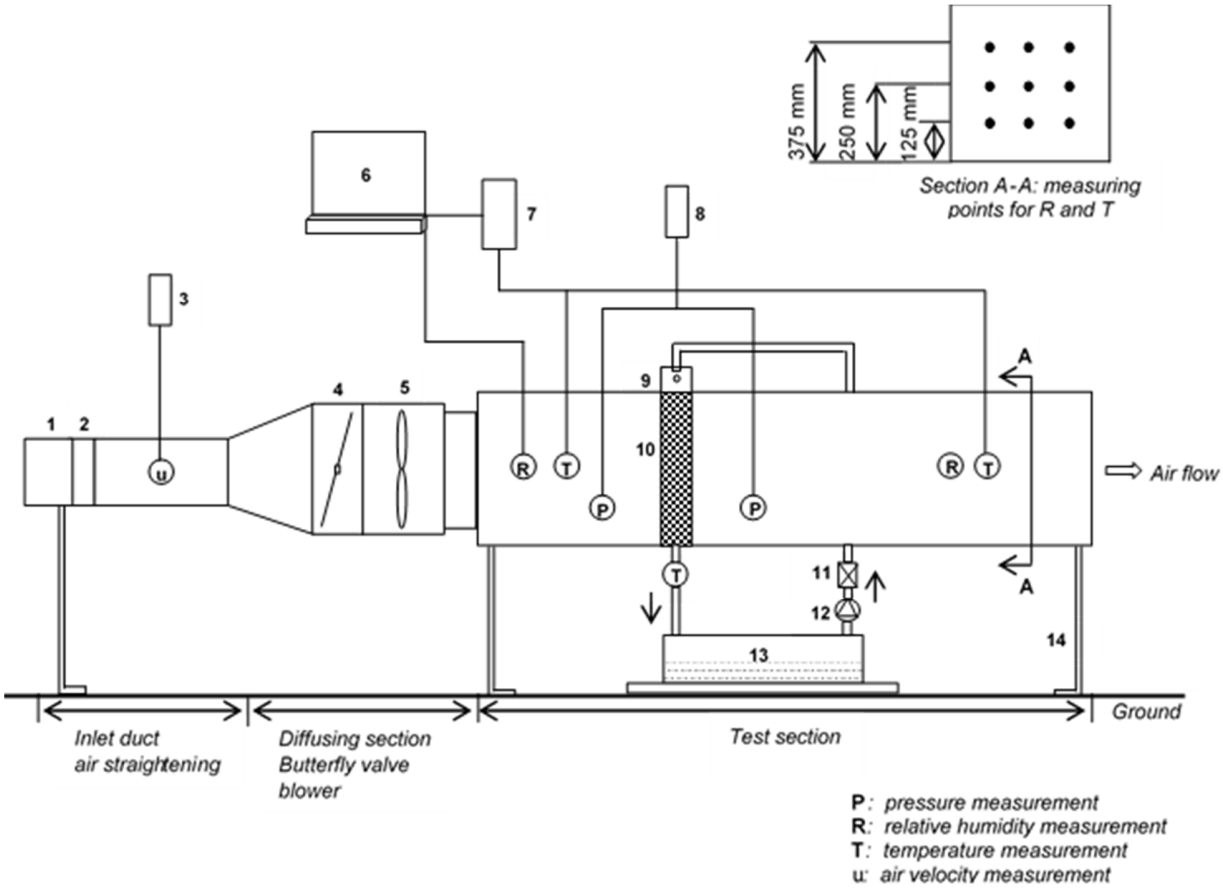

Figure 6-1 Schematic of the wind tunnel with a single layer pad incorporated (not drawn to scale). (1 = inlet duct, 2 = airflow straightener, 3 = hot wire anemometer, 4 = butterfly valve, 5 = in-line duct centrifugal fan, 6 = computer, 7 = data logger, 8 = digital differential pressure meter, 9 = water distributor, 10 = wetted medium, 11 = flowmeter, 12 = water pump, 13 = water tank, 14 = supports).

The apparatus consisted of an inlet induct, butterfly valve, centrifugal in-line duct fan, test section and an air exit section. The entrance to the apparatus consisted of a round galvanized steel air duct with diameter of 150 mm and a length of 850 mm. At 300 mm downstream from the duct inlet, a honeycomb flow straightener with tube diameter of 5 mm and tube length of

50 mm was installed to remove any tangential velocity components (Román and Hensel, 2014). The butterfly valve was installed 202 mm upstream of the fan in order to reduce the airflow to the desired test condition. The test section is a hollow rectangular duct made out of 19 mm thickness MR grade plywood and insulated with 40 mm thick styropor material to minimize heat loss to the surroundings. The dimensions of the test section were 1800 mm x 500 mm x 525 mm.

For the purpose of this study, specific test frames were designed to incorporate different layers of the wetted-medium (fig. 6-1). These frames consisted of a galvanized metal structure with water distribution system incorporated into the top. This system has been used by other researchers (Barzegar et al., 2012; Franco et al., 2010). The distribution pan with perforations at the bottom was located at the top of the media to feed the water to the media more uniformly by gravity. Water was fed to the distribution pan through the distribution pipes, which were constructed of a 20 mm diameter PVC pipe with 2 mm holes, 25 mm apart. Water from the distribution pan was dripped down by gravity to wet the media uniformly. In the lower part of the frames, a water collection system allowed water to drain by gravity into a water tank, before being ceaselessly recycled by a 14 Watts, 12 V DC pump (SP20/20, Solarproject, UK). Water flow at the entrance was controlled by varying the voltage of the pump by a DC power regulator and readings from the flowmeter (GARDENA water smart flowmeter, GARDENA GmbH, Germany) with an average range of 2 to 30 l min^{-1} and an accuracy of ±5%.

6.3.3 Wetted-medium configuration

Three different configurations of the wetted-medium in the wind tunnel were analyzed regarding their capacity for climate conditioning. These were termed as single layer pad (SLP), double layers pad (DLP) and triple layers pad (TLP) configuration. Figure 6-2 shows a perspective of the experimental set-up with pads incorporated at the test section. The wet surface of a single layer pad was 0.212 m^2 and it was identical for the three pad configuration. The distance between the pad layers (fig. 6-2b and c) was 0.3 m.

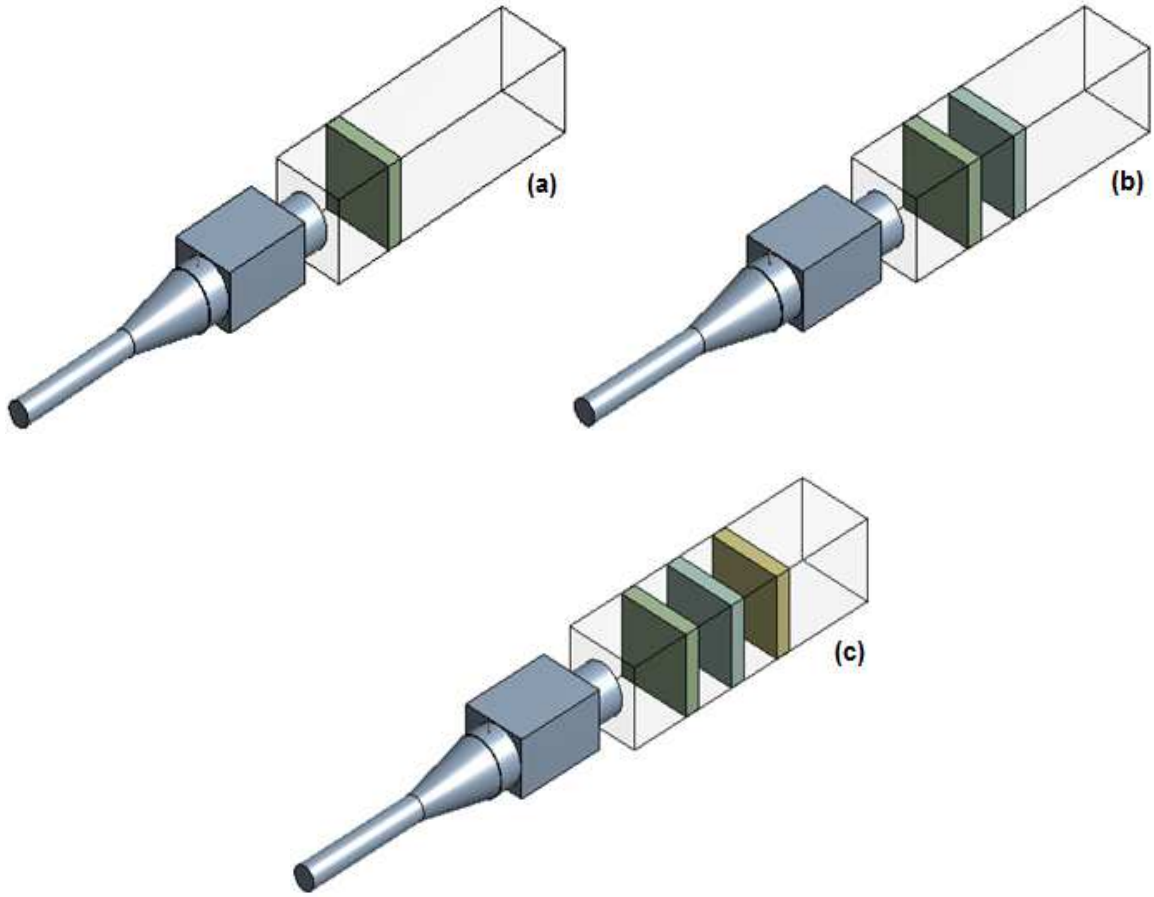

Figure 6-2 A perspective of the experimental set-up of the pad configurations: (a) single layer pad (SLP); (b) double layers pad (DLP); (c) triple layers pad (TLP).

6.3.4 Test procedure and instrumentation

For the purpose of this study, measurements of air velocity and flow of water through the porous medium are required, as well as temperature and humidity of the airflow before and after crossing the wetted-medium to determine the saturation efficiency of the media and the volume of water evaporated. Measurement of the air pressure drop through the porous medium (dry and wet) of the tested cooling pad configurations (SLP, DLP and TLP) is also essential.

For testing of the evaporative pads, control of the test room environmental conditions is necessary. Therefore, in order to keep the room dry-bulb temperature at approximately 31±2 °C and RH of 45±3.2%, which represent long-term averages of dry season months in Northern Ghana, a 2000 W fan heater was placed at the inlet of the system. Measurements were

carried out 200 mm downstream from the fan outlet. Static pressure drop across a given pad configuration was measured with a digital differential pressure meter (Testo 510, Testo AG, Germany) with an accuracy of ±1.5%. The pressure meter was connected by a flexible rubber hose to pressure taps located on the surface of the wind tunnel. One pressure tap was located 350 mm downstream from the fan outlet and the remaining taps 650, 950, and 1250 mm upstream respectively. The average air velocity was measured with a hot wire anemometer (PL-135HAN, Voltcraft, Germany) with a working range of 0.1 to 25 m s^{-1} and accuracy of ±1% full scale. The probe of the hot wire anemometer was placed at the duct center and 400 mm downstream of the flow straightener (fig. 6-1). To determine the air velocity in the wind tunnel from a single measurement point, the guideline of VDI/VDE 2640 part 3 (1983) was used and described by Román and Hensel (2014).

The wet-bulb temperature near the inlet duct of the wind tunnel was recorded manually using a digital hygrometer (model HT-86, Shenzhen Handsome Technology Co., Ltd., China) with accuracy of ±0.8 °C. The temperature and RH of the inlet and outlet air was measured with digital temperature and capacitive humidity data loggers (Testo 174H, testo AG, Germany) with accuracy of ±0.5 °C and ±3%, respectively. For the air inlet conditions, one data logger was located 300 mm upstream from the first pad to be tested. The inserted length of the data logger was 250 mm from the tunnel floor. Nine data loggers were placed at 1700 mm downstream from the fan outlet to measure the outlet dry-bulb temperature and RH. The data loggers were located in groups of three and were mounted across the width of the test section. The inserted length of each group were 125, 250 and 375 mm from the tunnel floor respectively to form a measuring grid (see fig. 6-1, Section A-A).

Water flow rates tested were: 0 (dry), 2.2, 3.2, 5.2 and 7.2 l min^{-1}. However, on analysing the other parameters in the wind tunnel, it was observed that the air stream passing the wetted-medium (for all pad configuration investigated) causes an emergence of water entrainment off the medium at flows of 7.2 l min^{-1}. Therefore, only four flow variables were tested: dry (only for the pressure drop), 2.2, 3.2 and 5.2 l min^{-1}. The air velocity through a given experimental set-up was regulated by throttling the fan at predetermined series and taking measurements with a hot wire anemometer. The range of average air velocity for the test was set between 0.12 and 1.14 m s^{-1}. At the beginning of each test, water flow was fixed. The evaporative cooling pads were wetted before testing begins to ensure saturation (Barzegar et al., 2012;

Liao and Chiu, 2002). The initial air velocity 0.12 m s^{-1} was maintained for 30 min, and then increased to 0.51, 0.82, 1.05, 1.10 and 1.14 m s^{-1} respectively during the test. For each air velocity, at least 10 min waiting period was maintained to ensure equilibrium between the wetted media and the new air and water conditions. All tests were performed in triplicate.

The Testo 174H data loggers were programmed via computer interface. At each velocity, data points were recorded at equilibrium condition by all data loggers at 5 min intervals except pressure drop measurement and the average values were used in data analysis.

6.3.5 System performance analysis

The cooling efficiency of evaporative air cooling is measured by the saturation effectiveness or the evaporative saturation efficiency (ANSI/ASHRAE Standard 133-2001). It is determined as the ratio between the drop in air temperature after passing through the pad and the maximum possible drop under conditions of air saturation using the following equation:

$$\eta_{cool} = \frac{T_1 - T_2}{T_1 - T_{wb}} \times 100 \quad (6\text{-}1)$$

where T_1 is the dry-bulb temperature of the incoming air (°C), T_2 is the dry-bulb temperature of the outgoing air (°C), T_{wb} is the thermodynamic temperature of the wet-bulb at the entrance and η_{cool} is the efficiency. The value of the efficiency depends on the air velocity through the wetted-medium, and the water air ratio (Franco et al., 2010).

The specific water consumption (C_w) of the pads (kg h^{-1} m^{-2} $°C^{-1}$) is expressed as the mass flow of evaporated water (m_e) per unit of the wetted-medium frontal area (A_{mfr}) (i.e., the air flow area) and the maximum thermal difference possible given the conditions of air entering the wetted-medium (Franco et al., 2010).

$$C_w = \frac{m_e}{(T_1 - T_2)A_{mfr}} \quad (6\text{-}2)$$

where the mass flow of evaporated water (m_e) is obtained by applying the water vapour balance:

$$m_e = m_{v2} - m_{v1} \quad (6\text{-}3)$$

m_{v1} and m_{v2} are the flows of vapor at the entrance and exit of the wetted-medium, respectively

in kg h^{-1}. Dividing equation 6-3 by the flow of dry air (m_a) in kg h^{-1} which is constant between the entrance and the exit of the wetted-medium (Franco et al., 2012) gives:

$$m_e = m_a(W_2 - W_1) \quad (6\text{-}4)$$

where W_1 and W_2 are the absolute humidity of the air at the entrance and exit of the pad, respectively ($kg_w\, kg_a^{-1}$) and $m_a = \rho_a Q_a$, in which ρ_a is the air density (kg m^{-3}) and Q_a is the air flow through the pad ($m^3\ h^{-1}$). Substituting expression 6-1 in equation 6-2, the water consumption of the pads depends on the air velocity through it, the saturation efficiency and the air conditions on entering the pad (Franco et al., 2012; Franco et al., 2010):

$$C_w = \frac{m_e}{\eta_{cool}(T_1 - T_{wb})A_{mfr}} \quad (6\text{-}5)$$

6.3.6 Statistical analysis

Duncan test and analysis of variance were carried out to determine the level of significance and the combined effect of pad configuration, water flow rate and air velocity on the cooling efficiency of the pad media.

6.4 Results and discussion

6.4.1 Pressure drop across the media

Figures 6-3a and b depict the effect of inlet air velocity, water flow rate and pad configuration on the pressure drop along the length of the evaporative cooler. A comparison of figure 6-3a with b shows, in general, that the pressure drop across pads made of small size charcoal is larger than that across pads made of large size charcoal at the same pad configuration and water flow rate. The pressure drop increases with the increase in air velocity (fig. 6-3a and b); this is in accordance with the literature (Franco et al., 2010; Gunhan et al., 2007; Liao et al., 1998; Koca et al., 1991).

For all pad configurations, the higher the water flow applied, the greater the pressure drop for a given air velocity. The lower pressure drop in all pad configurations (fig. 6-3a and b) occurs in the dry conditions and it increases with a higher water flow rate. According to El-Dessouky et al. (1996), the increase in water flow increases the films of the water retained on the surface

of the media and thus decreases the volume for the airflow in the media, and as a result increases the pressure drop. The water flow effect on the pressure drop is however small in the test range (fig.6-3) and there is no significant difference ($P > 0.01$) between water flows tested for the two pad media at the studied pad configurations. The result in this study is similar to the results of the study done by Franco et al. (2010), Gunhan et al. (2007), Koca et al. (1991).

Essentially, a greater pressure drop is obtained with TLP configuration compared to DLP and SLP configurations (fig. 6-3a and b). Statistically, the difference between the investigated pad configurations is significantly different ($P < 0.01$) at the same air velocity and water flow rate. For instance, at 0.12 m s^{-1} air velocity and water flow of 5.2 l min^{-1} for small size charcoal pad, the pressure drop increased from 3.67 to 10.67 Pa (+191%) when SLP was changed to DLP configuration while it changed from 3.67 to 12.33 Pa (+236%) when SLP was changed to TLP configuration. In the case of large size charcoal pad, pressure drop increased from 2.66 to 3.33 Pa (+25%) for SLP and DLP and from 2.66 to 5.34 Pa (+101%) respectively, at similar test condition. Similar trends were observed for tests at other air velocity and water flow conditions.

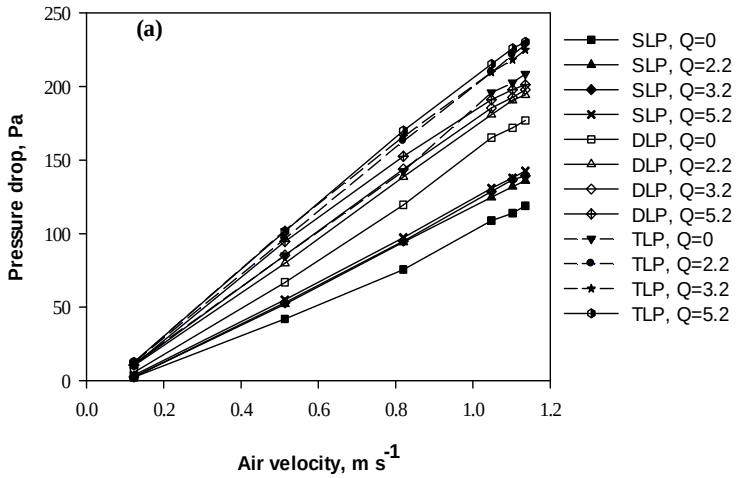

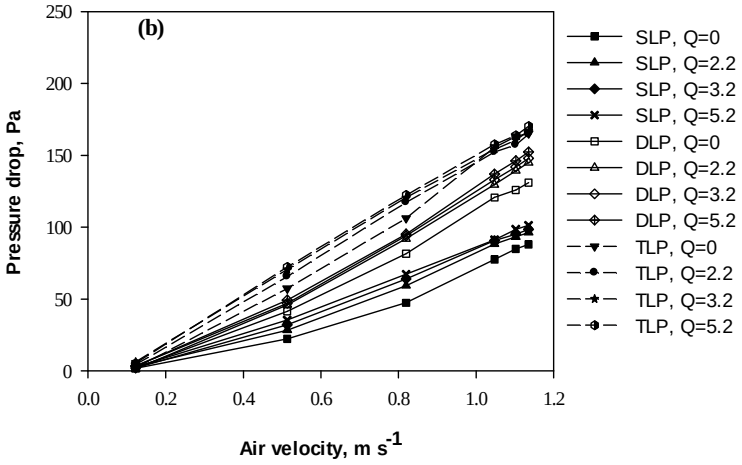

Figure 6-3 Pressure drop across three pad configurations at four water flow rates (water flow rate Q is in l min^{-1}) for (a) small size charcoal; (b) large size charcoal.

6.4.2 Cooling efficiency

Figure 6-4a and b shows the cooling efficiency at different air velocities through the three pad configurations made of small and large size charcoal particles and for all the water flow rates applied. Comparing figure 6-4a with b, one can find that, in general, the cooling efficiency for pads made of small size charcoal particles is higher than that for pads made of large size charcoal at the same pad configuration and the corresponding proportional water flow rate. The results indicate that when the velocity of the air circulated through the cooling pad configurations increases, the cooling efficiency decreases marginally. The results compare to that of Gunhan et al. (2007) closely. With the increase in air velocity, the duration of air-water contact is reduced, and therefore, there is inadequate time for the air to transfer heat and mass with the water, lowering the cooling efficiency.

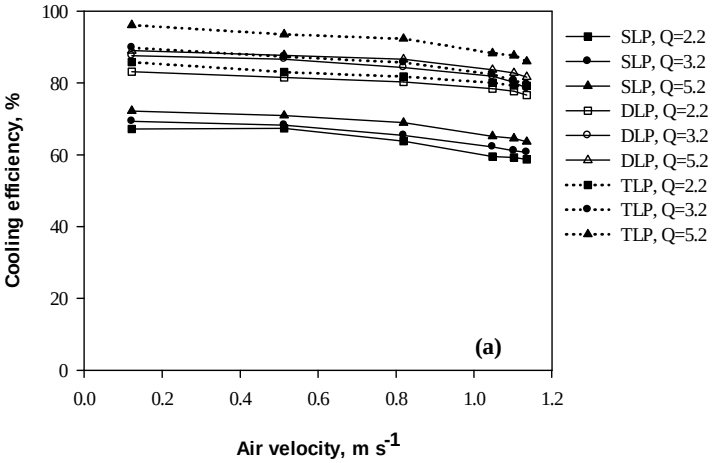

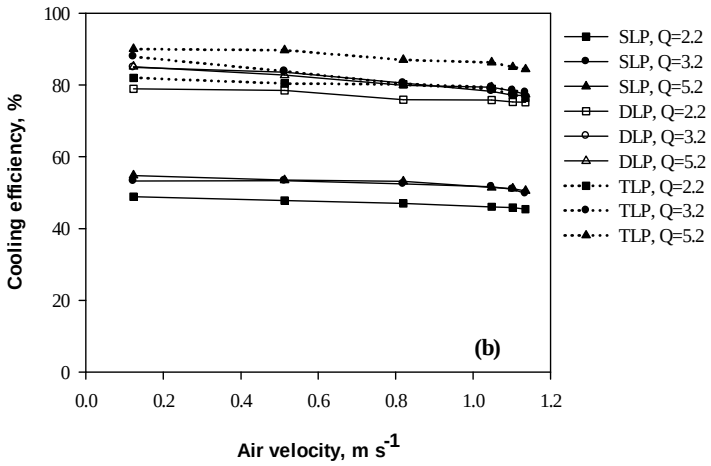

Figure 6-4 Effect of air velocity and pad configuration on cooling efficiency at different water flow rates (water flow rate Q is in l min^{-1}): (a) small size charcoal pad; (b) large size charcoal pad.

Figure 6-4a and b also shows the effect of pad configuration on the cooling efficiency for all water flow rates. According to the analysis of variance, the effect of pad configuration on cooling efficiency is significant at 99% probability level. The results of Duncan tests are given in table 6-1. As a general characteristic, we can say that using SLP configuration allows limited surface area for adiabatic cooling. On the other hand, DLP and TLP configuration exposes larger wet surface area, respectively, thus allowing air to pick up moisture and cool. This type of pad configuration results in cooling efficiency of 76.60% to 89.0% for DLP and 79.21% to 96.10% for TLP for small size charcoal pads and 73.72% to 85.14% for DLP and 73.42% to 90.06% for TLP for large size charcoal pad.

Table 6-1 Effect of pad configuration on the evaporative cooling efficiency.

Pad configuration	Evaporative cooling efficiency (%)	
	Small size	Large size
SLP*	63.55[a]	50.49[a]
DLP*	82.82[b]	79.00[b]
TLP*	85.59[c]	82.56[c]

*Values followed by different letter in the same column are significantly different according to Duncan's test at $P < 0.01$.

Considering the water flow, and according to the test results obtained, the cooling efficiency

increased marginally in most instances when water flow applied to the various pad configurations varies from 2.2 to 5.2 l min^{-1}. This is demonstrated in figure 6-5a and b for air velocities of 0.12 and 1.14 m s^{-1} except TLP configuration made of large size charcoal at 1.14 m s^{-1}. Statistically, the results of the test indicated that there is no significant effect at 99% probability level of water flow rate in the present study on the cooling efficiency at the same pad configuration and the corresponding air velocities. Some earlier studies indicated that cooling efficiency is increased with the increase of water flow rate until the pad is sufficiently moist (Dzivama et al., 1999; Mekonnen, 1996). However, in the present study, the design of the water distribution system (Section 6.3.2) allowed water to be evenly distributed at the chosen water flow rates, thus all pads were fully saturated. The results are supported by past studies (He et al., 2015b; Franco et al., 2010; Gunhan et al., 2007). He et al. (2015a) reported that a further increase in water flow rates than what is practically required for saturation decreases the cooling efficiency as the excess water may block the pore spaces of the medium. The results of the effect of water flow on cooling efficiency are particularly of great importance, since we can reduce water flow supplied to a given pad configuration by providing flow rates that will fully wet the media while the cooling performance remain unchanged. This makes it possible to reduce the designing pump power for wetting media and use less water (He et al., 2015b), thus satisfying an ongoing comprehensive research project that aimed to quantify the potential of using direct photovoltaic powered water pump for evaporative cooling purposes.

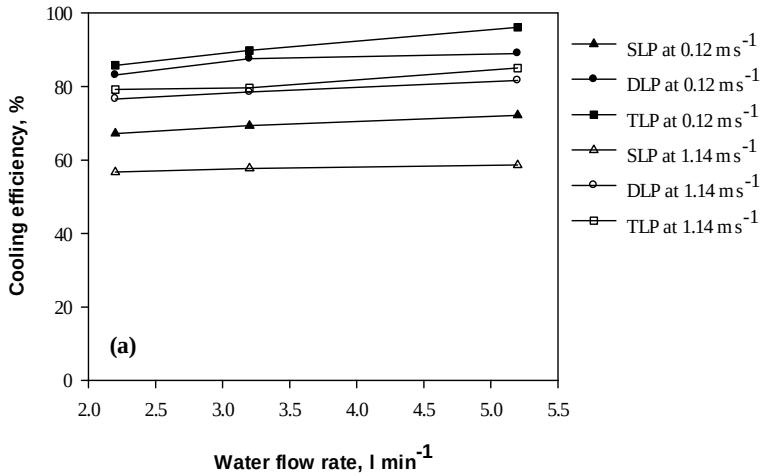

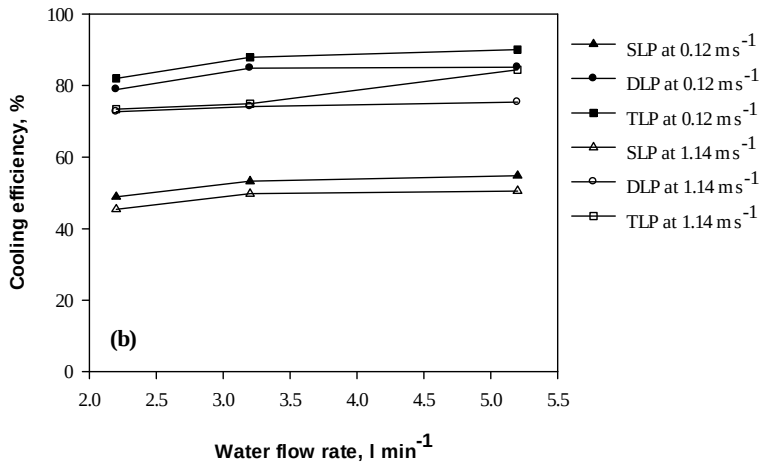

Figure 6-5 Effect of water flow rate on the evaporative cooling efficiency of (a) small size media and (b) large size media for the three pad configuration tested at two air velocities.

6.4.3 Water evaporation rate from the pads

Figures 6-6 and 6-7 reports the calculated water evaporation rate of the two media sizes studied at different air velocities and water flows, expressed in kg of water evaporated per hour per m^2 per degree °C of temperature reduction (eq. 6-5). As the air velocity increases, the rate of evaporation increases. At a given air velocity and water flow, the water evaporation rate of pad made of small size charcoal is higher than its counterpart ($P < 0.01$). For instance, at air velocity of 0.52 m s^{-1} and water flow of 3.2 l min^{-1}, the amount of water evaporated for small size charcoal pads was approximately 0.2280, 0.2594 and 0.5983 kg h^{-1} m^{-2} $°C^{-1}$ per square meter of pad area for SLP, DLP and TLP respectively, while in the case of pads made of large size charcoal these values were 0.1611, 0.2103, and 0.5186 kg h^{-1} m^{-2} $°C^{-1}$ per square meter of pad area for SLP, DLP and TLP respectively. Similar trends can also be observe at the other working conditions investigated.

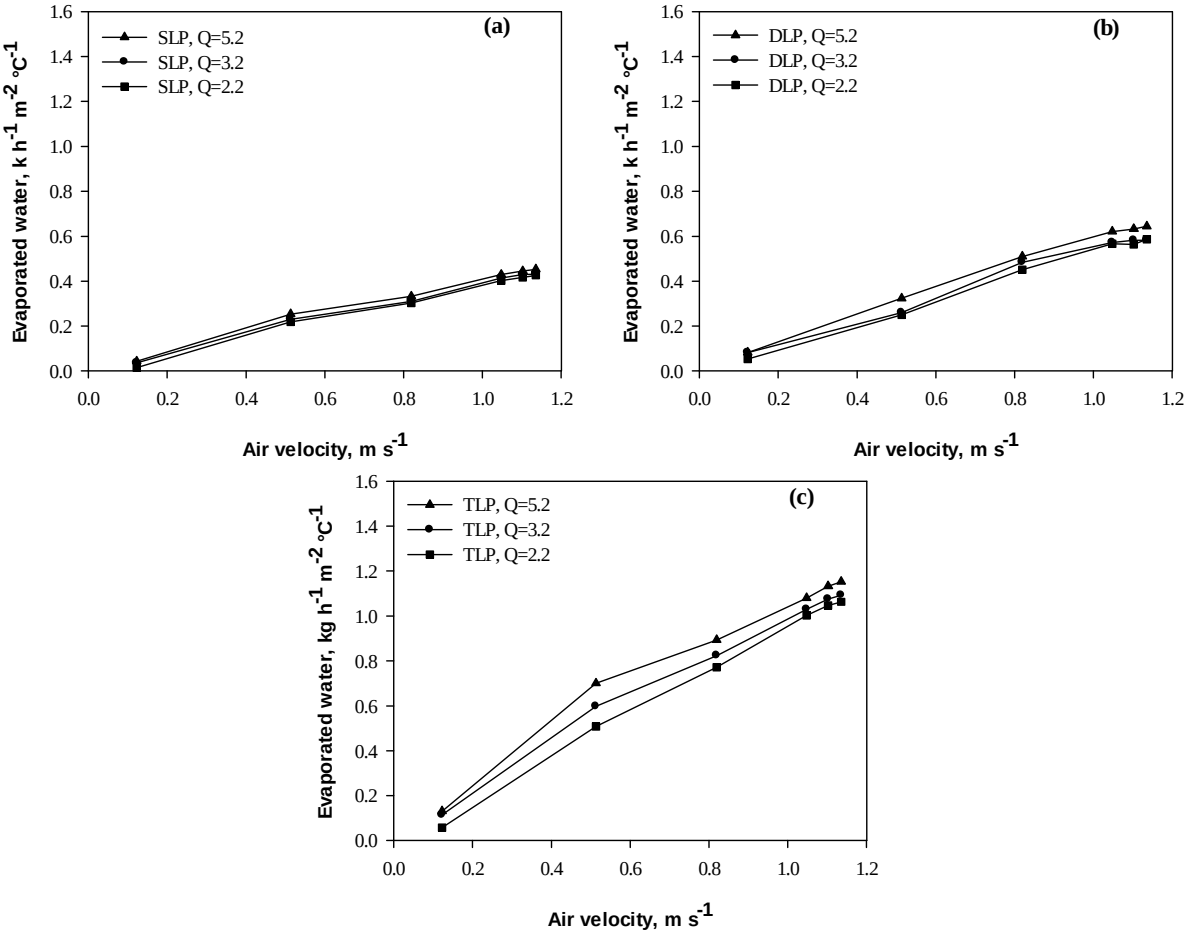

Figure 6-6 Effect of air velocity through small size charcoal pad configuration on specific water consumption at different water flow rates (water flow rate Q is in l min^{-1}): (a) SLP; (b) DLP; (c) TLP.

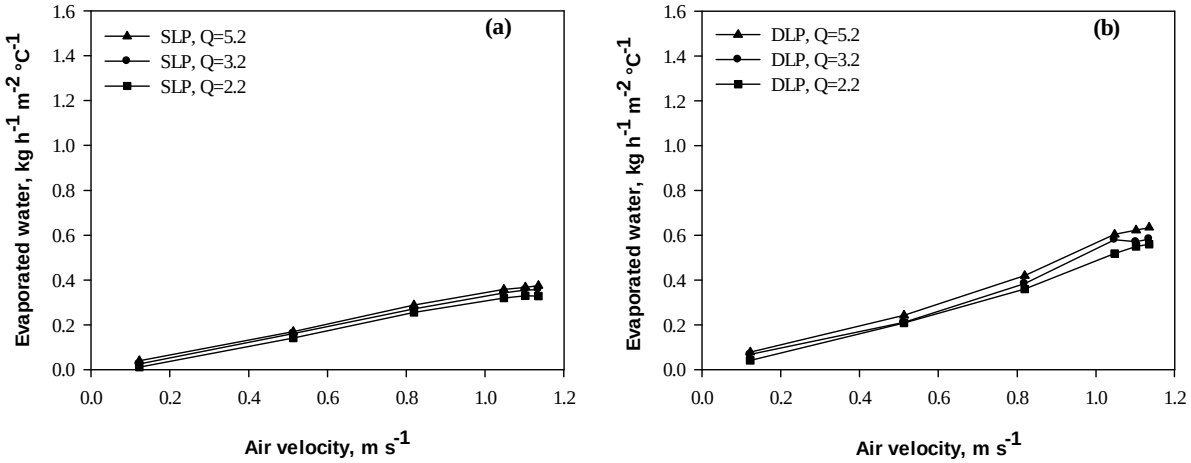

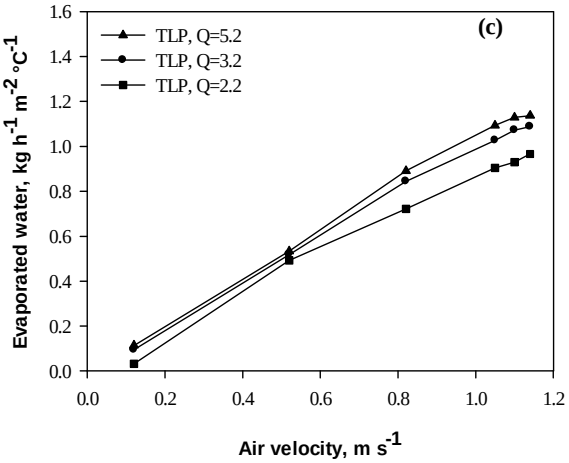

Figure 6-7 Effect of air velocity through large size charcoal pad configuration on specific water consumption at different water flow rates (water flow rate Q is in l min^{-1}): (a) SLP; (b) DLP; (c) TLP.

6.4.4 Comparative view

Table 6-2 shows comparison of the results from the current study to existing local pad materials in the literature. From the table, it can be seen that the charcoal pad material and the tested pad configurations in this study have good prospects to be used as an alternative for cooling purposes. Nevertheless, it is important to mention that it was not easy to a draw comparison amongst several other local pad materials because of the variation in experimental test climatic conditions and type of test rig employed. Gunhan et al. (2007) reported that an ideal pad must provide the highest evaporative cooling efficiency and the lowest airflow resistance. Although increasing the pad thickness increases the cooling efficiency of evaporative coolers, this will increase the fan capacity which will increase costs.

Table 6-2 Comparison of evaporative cooling performance for different materials.

Pad material	Pad thickness (mm)	Air velocity (m s^{-1})	Water flow rate (l min^{-1})	Pressure drop (Pa)	Efficiency (%)	Reference
Palm fruit fiber	30	4	24	N/A	90	Ndukwu et al. (2013)
Jute	N/A	2.4	N/A	N/A	62.10	
Luffa fibers	N/A	2.4	N/A	N/A	55.10	Al-Sulaiman (2002)
Date palm fiber	N/A	2.4	N/A	N/A	38.90	
Rice straw	30	0.3-1.05	1.64	N/A	71.42-76.51	
	100	0.3-1.05	1.64	N/A	68.21-69.57	
	150	0.3-1.05	1.64	N/A	60.24-69.30	Darwesh et al. (2007)
Palm leaf fiber	30	0.3-1.05	1.64	N/A	59.38-65.40	
	100	0.3-1.05	1.64	N/A	58.72-60.98	
	150	0.3-1.05	1.64	N/A	55.49-56.58	
Coarse pumice stones	100	1.6	1.75	266	76.1	
Fine pumice stones	150	1	1.75	225.6	93.1	Gunhan et al. (2007)
Volcanic tuff	100	1.6	1.75	203.9	81.1	
Shading net	150	0.6	1.75	2.9	82.1	
Small size charcoal	SLP*	0.12-1.14	2.2-5.2	2.67-142.67	58.71-72.21	
	DLP	0.12-1.14	2.2-5.2	10.33-201.33	76.60-89.01	
	TLP	0.12-1.14	2.2-5.2	12.22-230.33	79.21-96.10	Current study
Large size charcoal	SLP*	0.12-1.14	2.2-5.2	3.00-101.33	45.41-54.82	
	DLP	0.12-1.14	2.2-5.2	1.33-152.33	75.22-85.14	
	TLP	0.12-1.14	2.2-5.2	4.33-170.33	76.42-90.06	

*Note: The pad thickness for SLP = 100 mm; DLP = 100 mm x 2; TLP = 100 mm x 3

6.5 Conclusions

In this work, three different pad configurations were tested in order to obtain their operational parameters and their suitability to enhance evaporative cooling. The resistance to airflow through the three pad configurations increased at high air velocity and water flows. The largest impacts on pressure drop is however due to the changes in the air velocity. High pressure drop is obtained in TLP configuration compared to DLP and SLP configurations and the differences between the investigated pad configurations is significantly different ($P < 0.01$) at the same air velocity and water flow rate. The cooling efficiency decreases as the air velocity increases but increases as the number of pad layers in the wind tunnel increases. The effect of water flows on the cooling efficiency is small within the range of air velocities tested since the water is evenly distributed and the pads are fully wetted. In general, DLP and TLP configuration with larger wet surface area provide high cooling efficiencies and high pressure drops, though it evidently leads to increase in water consumption. Therefore, DLP and TLP configurations at low air velocity is recommended. Finally, this research showed that low-cost material, such as charcoal, can be used as an alternative material for evaporative media pads based on the multi-layer pad concept developed in this study.

6.6 Acknowledgements

The first author, Joseph Kudadam Korese would wish to acknowledge financial support from the German Academic Exchange Service (DAAD) for his research stay in Germany. The study is part of an ongoing project: Global Food Supply (GlobE) project- RELOAD (FKZ 031A247 A), funded by the German Federal Ministry of Education and Research (BMBF). We gratefully acknowledge their financial contributions.

6.7 References

Adebisi, O. W., Igbeka, J. C., & Olufemi, O. T. (2009). Performance of absorbent materials in evaporative cooling system for the storage of fruits and vegetables. International Journal of Food and Engineering, 5(3), 1-15.

Al-Sulaiman, F. (2002). Evaluation of the performance of local fibers in evaporative cooling. Energy Conversion and Management, 43(16), 2267-2273.

ASHRAE standard. ANSI/ASHRAE 133-2001. (2001). Methods of testing direct evaporative air

coolers. P. 24.

Barzegar, M., Layeghi, M., Ebrahimi, G., Hamzeh, Y., & Khorasani, M. (2012). Experimental evaluation of the performance of cellulosic pads made out of kraft and NSSC corrugated papers as evaporative media. Energy Conversion and Management, 54(1), 24-29.

Duan, Z., Zhan, C., Zhang, X., Mustafa, M., Zhao, X., Alimohammadisagvand, B., & Hassan, A. (2012). Indirect evaporative cooling: Past, present and future potentials. Renewable and Sustainable Energy Reviews. 16(9), 6823-6850.

Darwesh, M., Abouzaher, S., Fouda, T., & Helmy, M. (2007). Effect of using pad manufactured from agricultural residues on the performance of evaporative cooling system. Misr. Journal of Agricultural Engineering, 24(4), 1023-1043.

Dzivama, A.U., Bindir, U. B., & Aboaba, F. O. (1999). Evaluation of pad materials in construction of active evaporative cooler for storage of fruits and vegetables in arid environments. Agricultural Mechanisation in Asia, Africa and Latin America, AMA, 30(3), 51-55.

El-Dessouky, H.T.A., Al-Haddad, A.A., & Al-Juwayhel, F. I. (1996). Thermal and hydraulic performance of a modified two-stage evaporative cooler. Renewable Energy, 7(2), 165-176.

Franco, A., Fernández-Cañero, R., Pérez-Urrestarazu, L., & Velera, D.L. (2012). Wind tunnel analysis of artificial substrates used in active living walls for indoor environment conditioning in Mediterranean buildings. Building and Environment, 51, 370-378.

Franco, A., Valera, D.L., Peña, A., & Pérez, A.M. (2011). Aerodynamic analysis and CFD simulation of several cellulose evaporative cooling pads used in Mediterranean greenhouses. Computers and Electronics in Agriculture. 76(2), 218-230.

Franco, A., Valera, D. L., Madueño, A., & Peña, A. (2010). Influence of water and air flow on the performance of cellulose evaporative cooling pads used in Mediterranean Greenhouses. Transactions of the ASABE, 53 (2), 565-576.

Gunhan, T., Demir, V., & Yagcioglu, A. K. (2007). Evaluation of the suitability of some local materials as cooling pads. Biosystems Engineering, 96(3), 369-377.

He, S., Gurgenci, H., Guan, Z., Huang, X., & Lucas, M. (2015a). A review of wetted media with potential application in the pre-cooling of natural draft cooling towers. Renewable and Sustainable Energy Reviews, 44, 407-422.

He, S., Guan, Z., Gurgenci, H., Hooman, K., Lu, Y., & Alkhedhair, A. M. (2015b). Experimental study of the application of two trickle media for inlet air pre-cooling of natural draft dry

cooling towers. Energy Conversion and Management, 89, 644-654.

Heidarinejad, G., Bozorgmehrm, M., Delfani, S., & Esmaeelian, J. (2009). Experimental investigation of two-stage direct/indirect evaporative cooling system in various climatic conditions. Building and Environment, 44(10), 2073-2079.

Jain, J. K., & Hindoliya, D. A. (2011). Experimental performance of new evaporative cooling materials. Sustainable Cities and Society, 1(4), 252-256.

Koca, R.W., Hughes, W. C., & Christianson, L. L. (1991). Evaporative cooling pads: Test procedure and evaluation. Applied Engineering in Agriculture, 7(4), 785-490.

Liao, C. M., & Chiu, K. H. (2002). Wind tunnel modelling the system performance of alternative evaporative cooling pads in Taiwan region. Building and Environment, 37(2), 177-187.

Liao, C.M., Singh, S., & Wang, T.S. (1998). Characterizing the performance of alternative evaporative cooling pad media in thermal environmental control applications. Journal of Environmental Science and Health, Part A. 33(7), 1391-1417.

Mekonnen, A. (1996). Effectiveness study of local materials as cooling media for shelters in hot climates. Agricultural Mechanisation in Asia, Africa and Latin America, AMA, 27(2), 64-66.

Ndukwu, M. C., Manuwa, S.I. Olukunle, O.J., & Oluwalana, I.B. (2013). Development of an active evaporative cooling system for short-term storage of fruits and vegetable in a tropical climate. Agricultural Engineering International: CIGR Journal, 15(4), 307-313.

Román, F., & Hensel, O. (2014). Real-time product moisture monitoring in batch dryer using psychrometric and airflow measurements. Computers and Electronics in Agriculture, 107, 97-103.

Rawangkul, R., Khedari, J., Hirunlabh, J., & Zeghmati, B. (2008). Performance analysis of a new sustainable evaporative cooling pad made from coconut coir. International Journal of Sustainable Engineering, 1(2), 117-131.

Thompson, J.F., & Kasmire, R.F. (1981). An evaporative cooler for vegetable crops. California Agriculture, March – April: 20 – 21.

VDI/VDE. (1983). Netzmessungen in strömungsquerschnitten (Blatt 3): Bestimmung des Gasstromes in Leitungen mit Kreis-, Kreisring- oder Rechteckquerschnitt. Düsseldorf, Germany: VDI-Verlag.

Xuan, Y.M., Xiao, F., Niu, X. F., Huang, X., & Wang, S. W. (2012). Research and application of evaporative cooling in China: A review (I) – Research. Renewable and Sustainable Energy Reviews, 16(5), 3535-3546.

7 Application of computational fluid dynamics in the simulation of airflow in a low-cost ventilated mud storehouse

Joseph Kudadam Korese[1, 2)], Franz Román[1)], Oliver Hensel[1)]

[1)] Department of Agricultural Engineering, University of Kassel, Nordbahnhofstr. 1a, 37213 Witzenhausen, Germany

[2)] Department of Agricultural Mechanisation and Irrigation Technology, University for Development Studies, Post Office Box 1882, Nyankpala Campus, Tamale, Ghana

7.1 Abstract

In this research, we demonstrated how commercially available engineering tools such as CFD can be used in the design of airflow pattern in a simple mud storehouse for storage of perishable crops such as sweet potato roots under tropical climates. The mud storehouse was envisaged to have a rectangular air plenum built inside for bulk roots storage. Aerodynamically, unfavorable designs often cause non-uniform air distribution. The arrangement of a ventilation fan, the geometric design of the air inlet and outlet and air plenum chamber decisively influence the uniformity of air distribution. To obtain uniform distribution of airflow, which is a prerequisite for quality maintenance of bulk sweet potato roots, different geometries of airflow entries, plenum chamber, and air outlet size and placement were studied theoretically using CFD technique. The most appropriate geometrical sketch with acceptable uniform air distribution in the storehouse was selected and constructed. Experiments were conducted using potatoes to validate the selected design geometry. The potatoes were modelled as a porous media. Results of experimental measurements as well as the CFD simulations show satisfactory distribution of airflow in the headspace of bulk potatoes.

Keywords. Computational fluid dynamics, Air distribution, Design, Bulk storage, Mud storehouse.

7.2 Introduction

Inside forced-ventilation food handling systems such as perishable products storage rooms, it is of paramount importance to control ambient parameters (e.g. temperature and RH) which affect the micro-environment around storage products (Boyette, 2009). The level and uniformity of these parameters are highly governed by the behaviour of airflow patterns and the homogeneity of the ventilation through loaded product. One of the most important factors to achieve uniform distribution of air in forced-air handling systems is the design of the airflow (Tzempelikos et al., 2012). Aerodynamically, unfavorable designs cause non-uniform air distribution. According to Teodorov et al. (2012), the arrangement of a ventilation fan, the geometric design of air inlet and outlet system and the air plenum chamber decisively influence the uniformity of air distribution. Previous studies have asserted that controlling all these parameters experimentally is very tedious and difficult (Amanlou and Zomorodian, 2010). Although computational fluid dynamics (CFD) cannot replace physical experiments completely but it can significantly reduce the amount of time need for experimental works (Yongston et al., 2007). This valuable engineering tool is capable of analyzing the flow patterns of air conditioning systems in short span of time, which is previously impossible from experimental and theoretical procedures (Anderson, 1995). In the present study, the analysis is carried out for a low-cost ventilated mud storehouse presented in Chapter 8 using CFD technique in the ANSYS Fluent software. The distribution of air velocity has been studied to determine the best geometric configuration of the air handling systems (air inlet, plenum chamber and air outlet).

7.3 Materials and methods

7.3.1 The mud storage structure

The mud storage structure was envisaged to have a rectangular shape. Figure 7-1 shows 3D geometry of the mud storehouse. Detail description of the mud storage structure is further presented in Chapter 8.

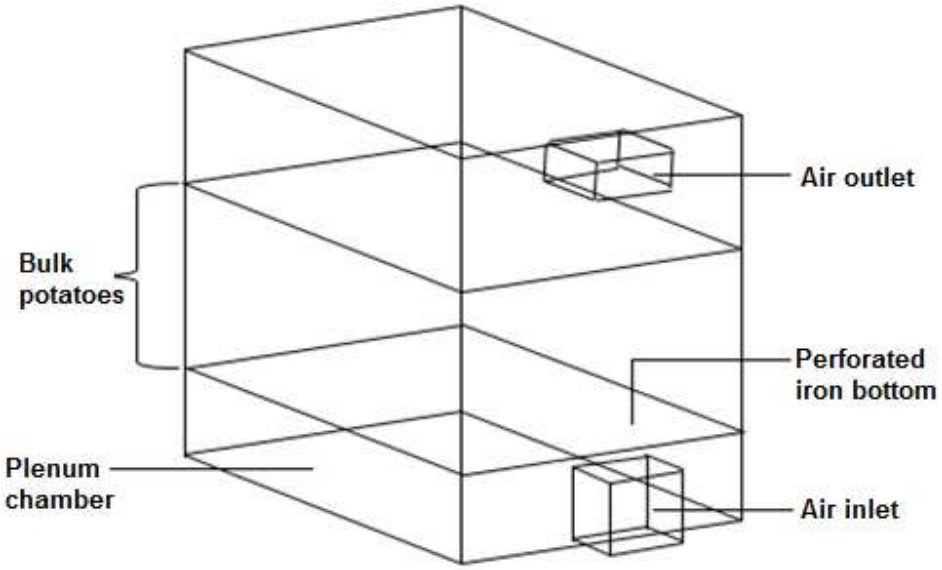

Figure 7-1 3D geometry of the mud storehouse (without gables, door and roof).

7.3.2 CFD simulations

The CFD simulations were conducted using the ANSYS-Fluent in the ANSYS workbench 14.0 platform (ANSYS 14.0 Inc, Canonsbury, USA). The dimensions of the simulation domain is the same as that explained in Chapter 8. In order to find the most appropriate geometrical configuration for achieving uniform distribution of airflow inside the mud storehouse, several geometries of airflow entries, plenum chamber, and air outlet size and placement were simulated in 3D model. The 3D model allows visualization of flow and variation along the plenum chamber and through bulk products which is not assessable in the 2D model. In general, the simulations were carried out with steady state conditions owing to the importance of airflow patterns. The simulations were done for both empty and loaded with products (potatoes) in the mud storehouse. The resistance to airflow through bulk of stored potatoes were modeled using the porous media model (ANSYS Fluent 12.0 User's Guide, 2009). This requires the input of two resistance coefficients to model the pressure drop per unit thickness of the product. The coefficients were obtained from data presented in the ASABE Standard D272.3 (ASAE, 2011) by fitting a second order polynomial function with zero intercept while the value of porosity was taken from Irvine et al. (1993). To simulate the perforated plate in Fluent, the porous jump model was employed. The coefficients were calculated following equations presented by Mühle

(1972). The procedure to obtain these coefficients is illustrated by Román et al. (2012). The simulations served as an aid to design and construct an optimal air inlet and plenum chamber size as well as the air outlet size and its placement. By assuming symmetry, the simulations were done for only half of the mud storehouse. The simulation characteristics, settings and the geometrical configuration with acceptable air distribution is presented in table 7-1.

Table 7-1 Simulation characteristics and settings.

Geometry and grid	Plenum height	0.5 m
	Bulk potato height	1 m
	Grid type	3D, tetrahedral, unstructured
	Number of elements	345028
	Volume of main body	4.61344 m^3
Cell zone and boundary conditions	Inlet	Velocity inlet (normal to boundary), 1.5 m s^{-1}
	Outlet	Pressure outlet, 0 Pa
	Perforated metal plate	Porous jump model (ANSYS Fluent 12.0 user's guide, 2009), resistance coefficient calculated according to Mühle (1972).
	Bulk potatoes	Porous media model (ANSYS Fluent 12.0 user's guide, 2009), resistance coefficients calculated from data presented in ASABE Standard D272.3 (ASAE, 2011) and porosity data taken from Irvine et al. (1993).
Settings	Turbulence model	*k-ε* realizable
	Discretization	Second-order upwind

7.3.3 Validation method

The experimental set-up for the validation is similar to that discussed in Chapter 8 (Section 8.4.2.1). For the purpose of this measurements, a DC power source regulator was used to power the fan such that the inlet air velocity was 1.5 m s^{-1}. Figures 8-2 and 8-3 shows the experimental set-up. Note, figure 8-2 depicts only half of the stored potatoes in the mud storehouse. The surface of the potato pile was divided into 32 subsections (grids) with surface area of 0.375 x 0.307 m for measurement of headspace air velocities. It is worth to mention that air velocity measurements at low velocities remain a tedious task and no ideal instrument has been developed for measurements of low velocities (Hoang et al., 2000). Therefore, a tapered channel (fig. 7-2) was used to accelerate the air (Román

et al., 2012; Hoffmann et al., 2007; Parker et al., 1992) in order for air velocities at the headspace of the potatoes to be measured. The large end of the tapered channel has cross section dimensions, similar to the potato pile grids to collect the air flowing through them, and its opposite side had dimensions 0.170 x 0.104 m. The gradual contraction of the tapered channel would increase air velocity and also bring a more uniform air distribution at the outlet section (Hoffmann et al., 2007), where a hot wire anemometer (PL-135HAN, Voltcraft, Germany) with resolution of 0.01 m s^{-1} was placed at the centre to measure air velocity. Two trials were conducted and for each trial, 10 measurements were taken for headspace air velocity in a given grid and averaged to represent a single point measurement of air velocity.

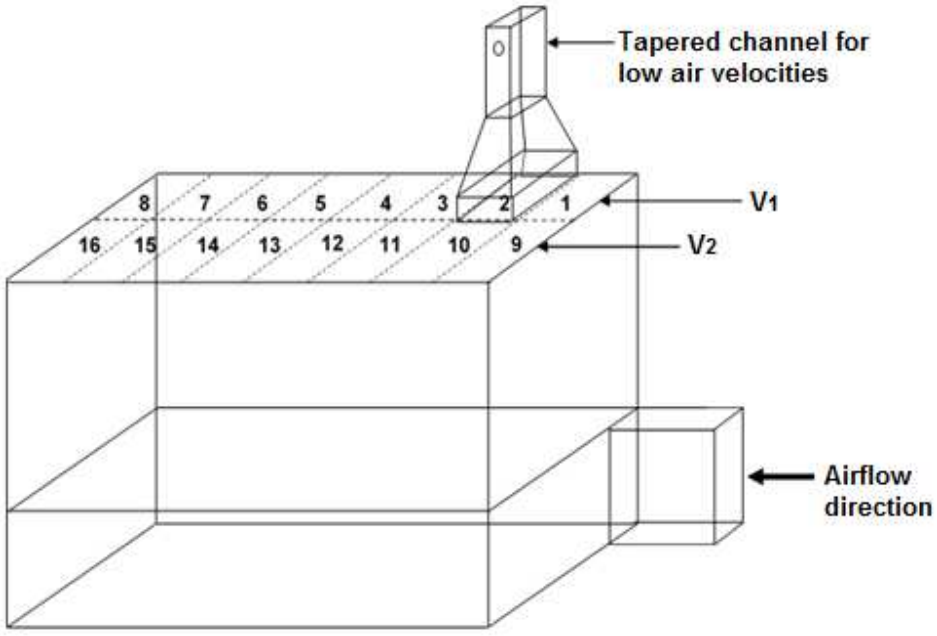

Figure 7-2 Measurement positions (grids) of bulk potatoes headspace air velocities (V_1 and V_2 represent inner and outer subsection rows of left half of the mud storehouse, respectively).

Figure 7-3 pictorial view of tapered channel used for measuring bulk potatoes headspace air velocities.

7.4 Simulated results

Figure 7-4a and b shows flow pathlines, their color representing air velocity magnitude for both empty and loaded potatoes inside the mud storehouse. In the empty mud storehouse, visualization of airflow is not conclusive. Higher airflows can be observed at the end of the plenum chamber, the upper part of the storage room and at the outlet. In contrast, simulation with loaded potatoes clearly shows uniform distribution of airflow through the bulk of potatoes as was expected for the selected design. This comparison demonstrates that by knowing some design parameters of the products to be stored (pressure drop and porosity), airflow visualization can be made simple thus facilitating the design of forced-air handling systems with improved airflow distribution. The use of large air inlet and air plenum in the selected design allowed the air within the plenum chamber to circulate adequately before flowing through the products. As the air outlet was somewhat small, high velocities can be observed. Various recommendations such as, (a) the introduction of guides in the plenum chamber to deflect air; (b) the use of several air inlets; (c) the use of an adequate transition duct at the entrance to the plenum chamber which slows down the air, and (d) the reduction of the cross-sectional area of the plenum chamber from the fan side to the opposite side, to improve airflow distribution in forced-air handling systems have been reported (Román et al., 2012; Janjai et al., 2006). Nevertheless, the inclusion of several air inlets will require additional fan or at least a complicated air duct system to

deliver air, while the use of air deflectors in plenum chamber seems difficult to transfer to other air handling systems of different geometries, sizes and aspect ratio (Román et al., 2012). In a ventilated enclosure such as that presented in this study, the use of large air inlet and air plenum chamber proved adequate to provide satisfactory airflow distribution for bulk products ventilation.

Figure 7-5a and b shows velocity contours at two different positions in the vertical direction of the loaded storage chamber for the selected design. With the given fixed inlet air velocity, the corresponding superficial air velocity was 0.06 m s^{-1}. As shown in the figure, uniform distribution of airflow can be observed through the various bulk height of the loaded potatoes. This further strengthens the applicability of the chosen design which is simple in terms of air duct assembly.

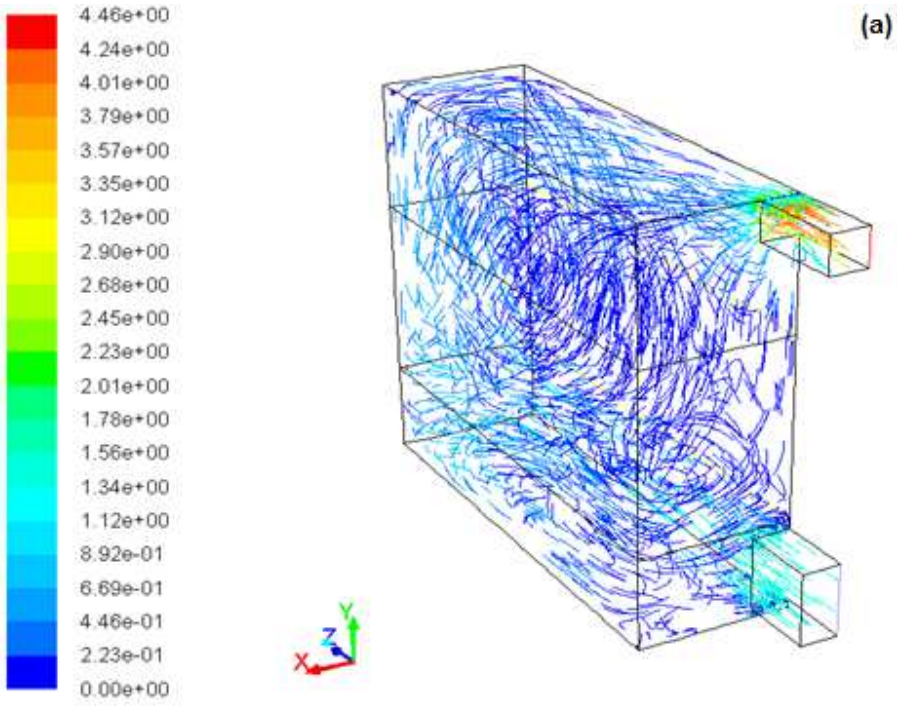

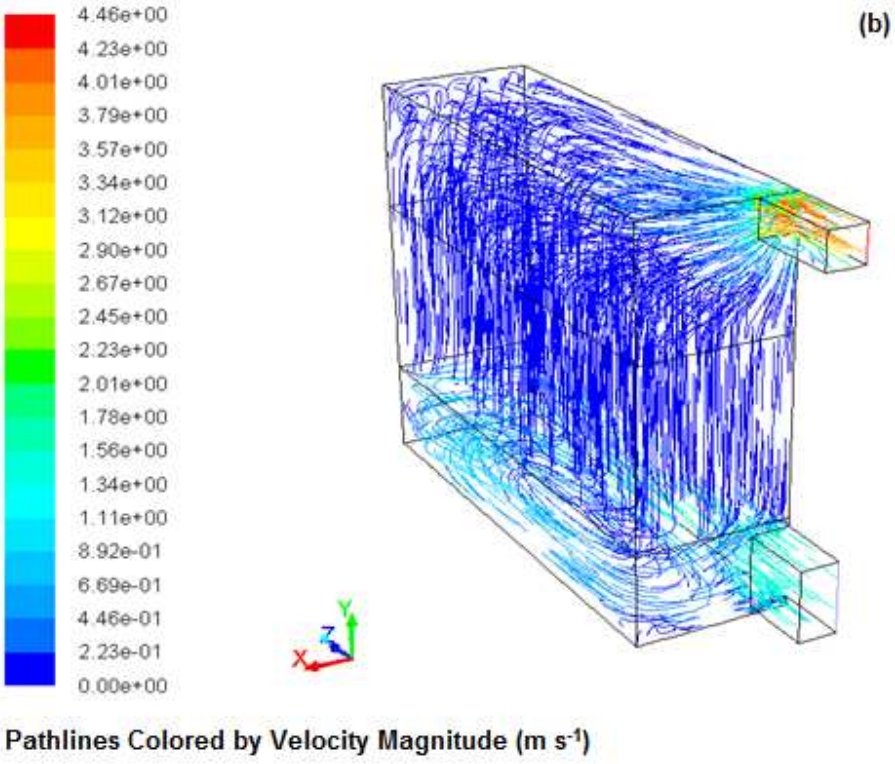

Figure 7-4 Simulated pathlines of air velocity for (a) an empty mud storehouse and (b) loaded potato mud storehouse.

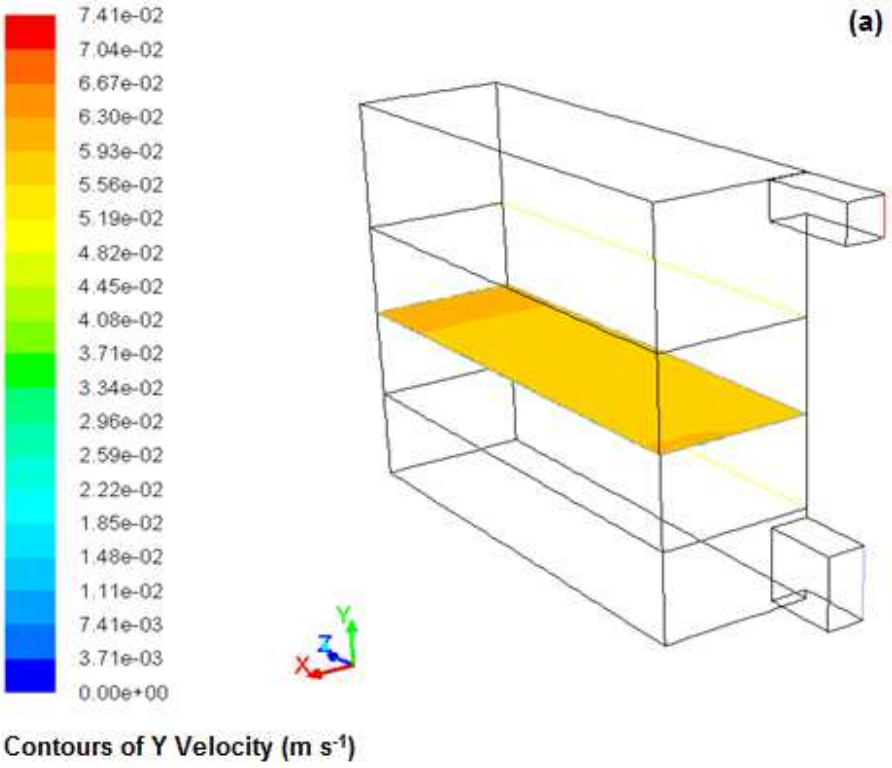

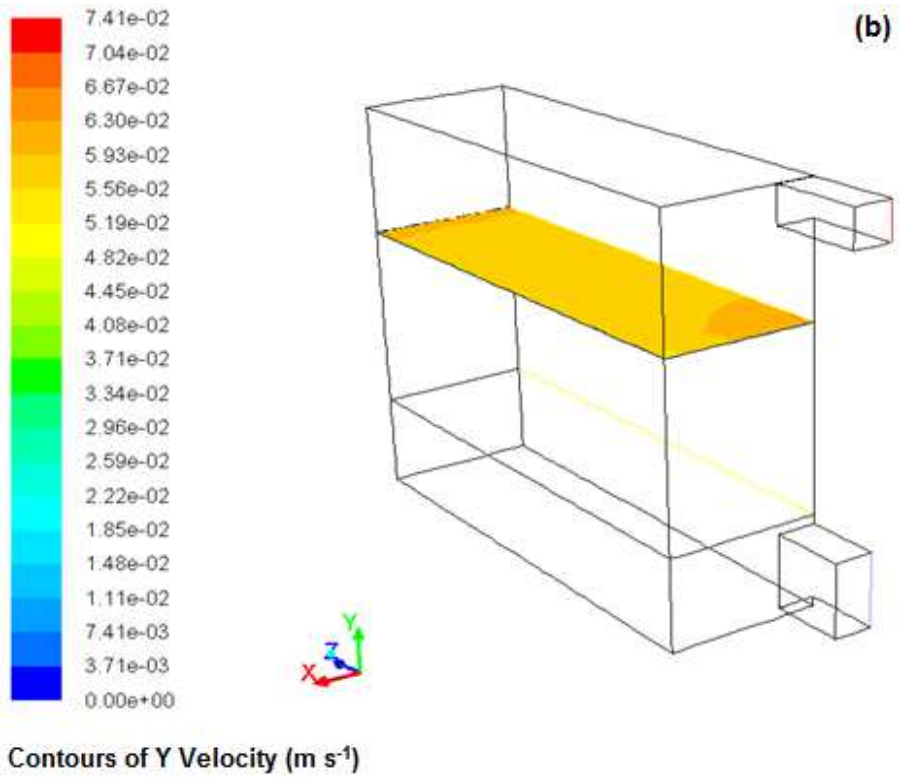

Figure 7-5 Simulated air velocity contours inside the mud storehouse loaded with bulk potatoes at y= 0.50 m (a) and y= 1.00 m (b).

7.5 Validation of simulated results

Through CFD simulations, the velocity profile at the headspace of bulk potatoes was investigated. The simulated headspace air velocities were compared to the measured air velocities. In the CFD solution, lines were drawn passing through each grid in longitudinal direction at three points (right, middle and left). This procedure is in accordance with the literature (Amjad et al., 2015). The results of the comparison are satisfactory and are illustrated in figure 7-6. A critical look at the figure revealed higher headspace velocities for trial 1 and 2 in fig. 7-6b as compared to fig. 7-6a, except for few cases in fig. 7-6a. The higher headspace velocities may be attributed to channeling effect (see fig. 7-2). The slight differences between the measured and the simulated headspace velocities can however be explained by the extent of lack of uniformity of the potatoes, since no grading was done prior to the experimental test. Relative error values between the measured and the simulation are shown in figure 7-7. Across the entire bulk surface, the average relative error value of the headspace air velocity was 10.4%.

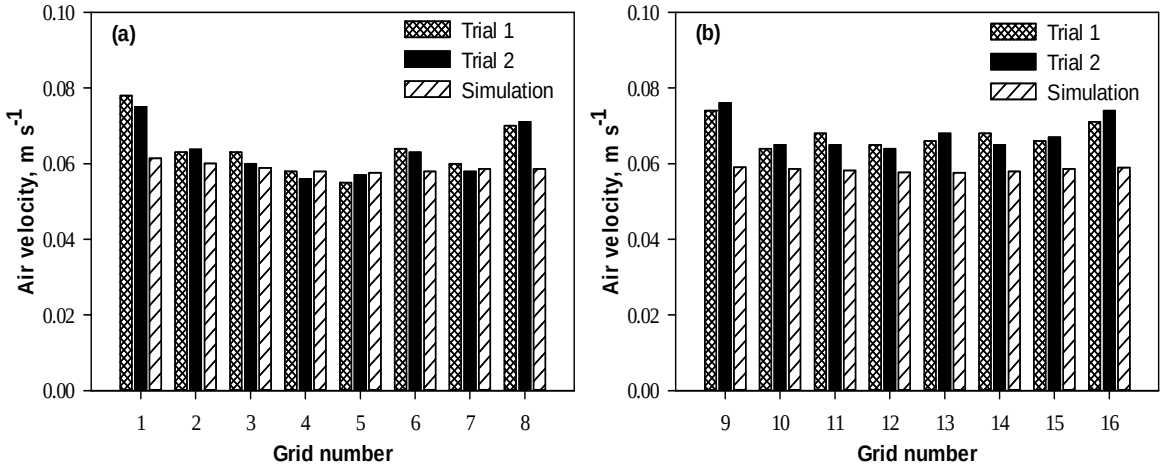

Figure 7-6 Comparison of measured and simulated average air velocity in the headspace of bulk potatoes; (a) V_1, inner grid row for trial 1 and 2; (b) V_2, outer grid row for trial 1 and 2.

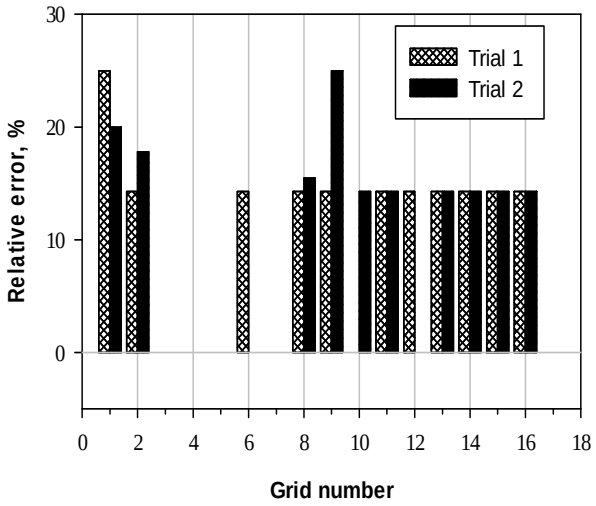

Figure 7-7 Relative error between measured and simulated average air velocity in the headspace of bulk potatoes as a function of grid position.

7.6 Conclusions

In the present study, CFD simulations were performed in order to identify the best geometric configuration for the construction of air handling system's in a newly built mud storage structure. Using potatoes as a test material, the design was modeled and analyzed using ANSYS-Fluent software. Comparison of the simulated and experimental data shows satisfactory distribution of airflow in the headspace of bulk potatoes. This results demonstrates that CFD technique is a powerful tool not only to catch the complexity of the 3D asymmetry, but also to design and simulate possible solutions for flow and to reduce design time and cost.

7.7 Acknowledgements

The authors wish to thank the German Academic Exchange Service (DAAD) and the German Federal Ministry of Education and Research (BMBF) for providing financial support.

7.8 References

Amjad, W., Munir, A., Esper, A., & Hensel, O. (2015). Spatial homogeneity of drying in a batch type food dryer with diagonal air flow design. Journal of Food Engineering, 144, 148-155.

ASABE Standards. (2011). D272.3: Resistance to airflow of grains, seeds, other agricultural products and perforated metal sheets. St. Joseph, MI: ASABE.

Amanlou, Y., & Zomorodian, A. (2010). Applying CFD for designing a new fruit cabinet dryer. Journal of Food Engineering, 101, 8-15.

ANSYS. (2009). ANSYS Fluent 12.0 User Guide. ANSYS.

Anderson, J. D. (1995). Computational Fluid Dynamics: The basics with applications. International editions, McGraw-Hill, New York.

Boyette, M. D. (2009). The investigation of negative horizontal ventilation for long-term storage of sweetpotatoes. Applied Engineering in Agriculture, 25(5), 701-708.

Hoffmann, T., Maly, P., & Fürll, Ch. (2007). Ventilation of potatoes in storage boxes. Agricultural Engineering International: CIGR Journal. Manuscript FP 06 014. Vol. IX.

Hoang, M.L., Verboven, P., De Baerdemaeker, J., & Nicolaï, B.M. (2000). Analysis of the airflow in a cold store by means of computational fluid dynamics. International Journal of Refrigeration, 23, 127-140.

Irvine, D. A., Jayas, D. S., & Mazza, G. (1993). Resistance to airflow through clean and soiled potatoes. Transactions of the ASAE, 36(5), 1405-1410.

Janjai, S., Intawee, P., Chaichoet, C., Mahayothee, B., Haewsungcharern, M., & Müller, J. (2006). Improvement of the air flow and temperature distribution in a convectional longan dryer. International Symposium towards Sustainable Livelihoods and Ecosystems in Mountainous Regions, Chiang Mai, Thailand. 7-9 March.

Mühle, J. (1972). Berechnung des trockenen Druckverlustes von Lochböden. Ingenieur Technik-CIT, 44(1-2), 72-79.

Parker, B.F., White, G.M., Lindley, M.R. Gates, R.S. Collins, M., Lowry, S., & Bridges, T.C. (1992). Forced-air drying of baled alfalfa hay. Transactions of the ASAE, 35(2),607-615.

Román, F., Strahl-Schäfer, V., & Hensel, O. (2012). Improvement of air distribution in a fixed

bed dryer using Computational Fluid Dynamics. Biosystems Engineering, 112, 359-369.

Teodorov, T., Scaar, H., Ziegler, T., & Mellmann, J. (2012). Homogenization of air flow in a fixed bed dryer for medicinal plants based on Computational Fluid Dynamics. In: Proceeding. International conference of Agricultural CIGR-Ageng 2012. Valencia, P. 1-6.

Tzempelikos, D.A., Vouros, A. P., Bardakas, A.V., Filios, A.E., Margaris, A.P. (2012). Analysis of air distribution in a laboratory batch-type tray air dryer by computational fluid dynamics. International Journal of mathematics and Computers in Simulation, 6(5), 413-421.

Yongson, O., Badruddin, I.A., Zainal, Z. A., & Narayana, P.A.A. (2007). Airflow analysis in an air conditioning room. Building and Environment, 42, 1531-1537.

8 Development and performance evaluation of an autonomous photovoltaic ventilated mud storehouse for storage of sweet potato roots under tropical conditions

Joseph Kudadam Korese[1, 2)], Franz Román[1)], Oliver Hensel[1)]

[1)] Department of Agricultural Engineering, University of Kassel, Nordbahnhofstr. 1a, 37213 Witzenhausen, Germany

[2)] Department of Agricultural Mechanisation and Irrigation Technology, University for Development Studies, Post Office Box 1882, Nyankpala Campus, Tamale, Ghana

8.1 Abstract

The lack of suitable storage systems among sweet potato farmers in tropical developing countries is an impediment to large-scale investment into its production and limits its food security prospects. This has prompted the quest for suitable storage alternatives that can be adapted by farmers in these regions. The present study was initiated to set-up an adequate storage system for fresh sweet potato roots handling under tropical climate conditions. This paper describes the development considerations followed by results of field experiments to evaluate the performance of the system. The system comprises of a 10.85 m^3 mud storehouse, a newly developed PV driven fan and a secondary evaporative cooling system. Test results using about 4.13 tons of potatoes as storage product showed that, the developed fan delivered airflow of about 1079 m^3 hr^{-1} at solar irradiance value of 878 W m^{-2}. The patterns of changes in airflow rate and total pressure was observed to follow the patterns in solar irradiance. As the fan has a relative low operating voltage threshhold, it operated continuously during the entire experimental duration. The utilization of mud as a construction material and the low-cost evaporative cooling system proved beneficial in reducing the ambient temperature and increasing the relative humidity, especially during the hottest hours of the day. Due to the utilization of PV panels for direct powering of the fan and the water pump, this PV ventilated storage system can be used in rural areas without grid connected electricity for storage of sweet potato roots. Further research on sweet potato roots storage performance is however necessary to ascertain the percentage loss of sweet potato roots as compared to the rudimentary storage practices in remote rural areas of developing countries.

Keywords. Mud storehouse, PV driven fan, Evaporative cooling system, Airflow, Temperature, Relative humidity.

8.2 Introduction

Storage of fresh sweet potato roots in tropical developing countries is a major challenge to farmers due to unfavorable climatic conditions. With the steadily growing necessity of more satisfactorily husbanding of sweet potato roots produced especially in remote areas, adequate storage systems are required (Mukhopadhyay et al., 2011). The use of specialized ventilated cool storage houses is universally recognized as the key to successful marketing of sweet potato roots in developed countries (Boyette, 2009; Woolfe, 1992). Undoubtedly, many small and marginal farmers in tropical developing countries cannot afford to build these special storage houses.

Fortunately, the traditional mud houses, which are common in rural Africa can further be developed as storage structures due to their good thermic and humidity balancing behaviour. Boyette (2009) has indicated that storage facilities for sweet potato roots require air movement through the pile roots to remove field heat immediately after harvest and to remove the products of respiration during the storage period. Continuous air circulation and adequate humidification reduce shrinkage and aid in maintaining the quality of sweet potato roots in storage (Boyette, 2009; Edmunds et al., 2007). The circulation of air through the bulk of sweet potato roots is usually provided by installing fans while fitted humidifiers provide the ideal humidity in storage facilities, both of which require electricity to operate. The electricity requirements to operate fans and humidifiers becomes a constraint for their application in remote areas without access to grid-connected power. The present study is based on the premise that the success of the concept of direct PV powered ventilated solar dryers (Esper, 1995), may be applied in mud constructed storehouses for ventilation of bulk sweet potato roots.

Generally, for PV powered systems that require continuous operation, such as offshore navigational light systems or radio repeaters, batteries are usually indispensable. But for applications such as ventilation of farm structures with fans – among other possibilities – batteries which are responsible for a significant portion of the capital cost can be eliminated by carefully choosing the components of the system (Roger, 1979). Such a direct coupling between the PV panel, a DC motor and fan impeller is of interest for applications in remote rural areas. While the commercial market offers a wide range of DC fans for different

applications in the agricultural and food sectors, most of these fans are mostly equipped with electronic circuits and require high current to start operating. This makes their use in off-grid PV systems unattractive. Davies et al. (2008) recommended that fan manufacturers expand their product range to include such solutions. According to Atlam and Kolhe (2013), PV powered permanent magnet (PM) DC motor – impeller system has a very good potential in aerodynamic applications. Therefore, a direct PV powered electro-mechanical system necessitates a complete study from the mechanical load to the PV array, but it leads to a very simple and reliable installations (Boutelhig et al., 2012; Badescu, 2003).

The scope of this work was therefore to develop a prototype, off-grid PV ventilated mud storehouse for storage of sweet potato roots in tropical climate conditions. In addition, the aim was to test its effectiveness in respect of the flow of air and pressure drop when loaded with products as well as to ascertain its reliability to maintain reasonable storage conditions (i.e. temperature and RH) for fresh sweet potato root storage. The design concept of such a storage system should allow farmers to easily build and install at the farm or homes with locally available materials like mud. In this way, farmers can plan their production and marketing and do not have to resort to distress sales of sweet potato roots in case of glut production. To achieve the overall objective, the study was planned in the following sequential manner.

- Construct an experimental storage structure from mud material.
- Develop a PV driven fan, and integrate it into the mud storage structure for ventilation purposes.
- Utilize a low-cost evaporative cooling system for forced-air evaporative cooling purposes.
- Evaluate the performance characteristics of the directly coupled PV ventilated system.

8.3 Materials and methods

8.3.1 Construction of the experimental storage structure

A 10.85 m^3 store structure with external dimensions, 3.14 x 2.42 x 2.20 m was built at the Experimental and Demonstration farm of the Department of Agricultural Engineering, University of Kassel, Witzenhausen, Germany. The store was built using mud material (here

referred to as mud storehouse) in order to simulate typical farmhouses in rural areas in SSA. The mud storehouse has a wall thickness of 0.25 m and is roofed with corrugated iron roofing. To prevent ponding of water during rainfall, a roof slope of 35° on both sides of the mud storehouse was chosen based on recommendations of Bengtsson and Whitaker (1988). The inner and outer sides of the walls were covered with about 0.01 m concrete plaster and 0.02 m clay plaster, respectively. An outlet window of dimension 0.4 x 0.2 m was installed in the Western side of the mud storehouse and covered with a wire mesh to prevent entry of birds and other animals. The floor consists of 0.10 m lightweight concrete installed over a well-compacted gravel, which can take the load of stored commodity. To reduce air infiltration, an airtight door was installed while the ceiling was covered with 0.016 m particleboard sections. The constructed mud storehouse is shown in the Appendix (fig.1-A).

At the heart of the mud storehouse is a storage bin with internal dimensions of 2.58 x 1.6 x 1 m and a storage capacity of about 4.13 tons. The bottom side of the bin is made of a rectangular perforated metal plate with opening area of 60% while the top side is opened for loading of products. A rectangular air plenum of 2.58 x 1.6 m was built beneath the storage bin. Additionally, an air inlet was designed in the Western part of the plenum and cut through the wall of the mud storehouse for fan connection.

8.3.2 Development of PV driven fan*

The main object of this section was to develop a prototype PV driven fan that can be integrated into sweet potato crop handling systems for ventilation purposes. Crucial is that such a directly coupled PV panel-motor-impeller system must start in the morning with no external intervention. Basic of the work described is the optimal energetic combination of all parts such as DC motor, impeller and PV panel and to fit it to the real needs of a storage structure as described in section 8.3.1 in respect of air flow and pressure drop. In order to enable for scale-up, a detailed procedure is described in section 8.3.2.1 and 8.3.2.2. Based on data presented in Chapter 4 and information on the mud storehouse size, an estimated airflow rate of 1060 $m^3\ hr^{-1}$ at a total pressure of 20 Pa is required, assuming the storage bin in the mud storehouse

* Mention of trade names and/or model names in the text is solely for the purpose of providing specific information and does not constitute endorsement by the authors over others of similar nature not considered.

is to be loaded with sweet potato roots to a bulk height of 1 m.

8.3.2.1 DC motor and impeller system

In order to optimally combine a DC motor and impeller system to obtain the estimated airflow and total pressure discussed in section 8.3.2, the following simplified mathematical relationships, which are exclusively for permanent magnet (PM) DC motors, are presented. The procedure can however be directly transferred to other types of motors. For a typical PM DC motor, the geometrical arrangement of the magnetic circuit and winding defines in detail how the motor converts electrical input power (current, voltage) into mechanical output power (speed, torque). Two characteristic values of this energy conversion are speed constant, K_n and the torque contant, K_m. To deduce the speed torque equation, it is important to look at the motor as an electrical circuit (fig. 8-1).

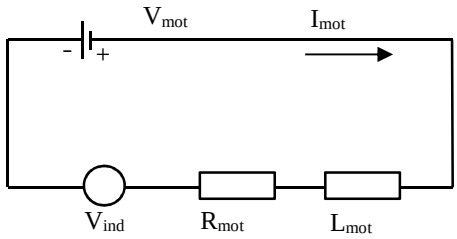

Figure 8-1 Permanent magnet DC motor as an electrical circuit.

If a fixed voltage, V_{mot} is applied to a motor, a steady-state current, I_{mot} will flow (fig.8-1) (Braun, 2012). The applied voltage has to overcome the voltage drop due to the motor inductance, L_{mot}, and due to the ohmic resistances, R_{mot}. Additionally, the applied voltage has to work against the induced voltage, V_{ind} (= emf). Hence for DC motors, the resulting equation is simplified as:

$$V_{mot} = R_{mot} I_{mot} + V_{ind} \tag{8-1}$$

Equation (8-1) can be rearranged as:

$$V_{ind} = V_{mot} - R_{mot} I_{mot} \tag{8-2}$$

Generally, the speed constant relates the speed (n) of the motor to the voltage induced in the winding, V_{ind} while the torque constant links the produced torque of the motor, M_{mot} with the electrical current. They are represented by the equations:

$$n = K_n V_{ind} \tag{8-3}$$

$$M_{mot} = K_m I_{mot} \tag{8-4}$$

Equations (8-2) to (8-4) are rearranged as:

$$\frac{n}{K_n} = V_{mot} - R_{mot}\frac{M_{mot}}{K_m} \tag{8-5a}$$

Now, rearranging equation (8-5a), we obtain the same equation between motor speed and torque. It is expressed as:

$$n = V_{mot}K_n - R_{mot}\frac{M_{mot}}{K_m}K_n \tag{8-5b}$$

The dependence between K_n and K_m is given as (Braun, 2012):

$$K_n K_m = \frac{30000}{\pi} \tag{8-6}$$

If K_n in equation (8-6) is replaced with the second term K_n in equation (8-5b), then the following expression can be derived:

$$n = K_n V_{mot} - \left(\frac{30000}{\pi}\frac{R_{mot}}{K_m^2}\right) M_{mot} \tag{8-7}$$

Using the well known speed-torque curve (fig. 8-2), the mechanical behaviour of the motor and an external load can be described at constant voltage (Braun, 2012). The symbols used in the figure are carefully defined within the text and in the Nomenclature. From this figure, the possible operating points (n, M_{mot}) of a motor at constant voltage can be deduced.

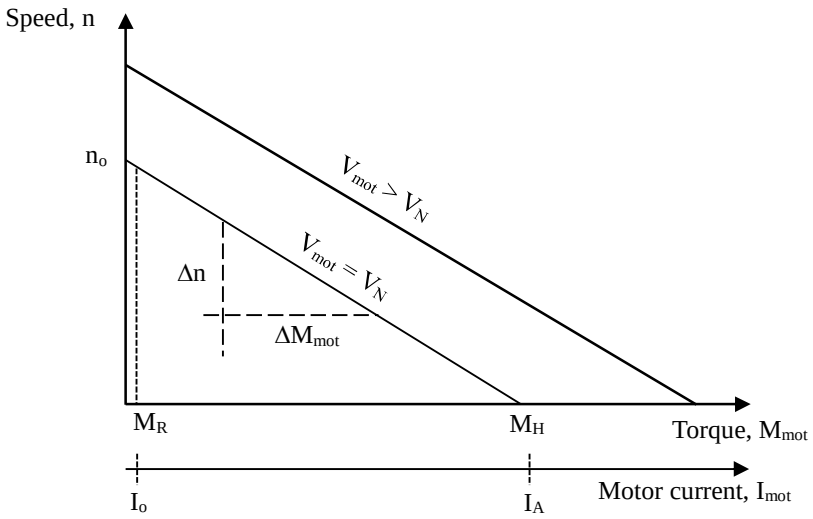

Figure 8-2 Typical speed-torque line for a DC motor.

Assuming an impeller is connected to the shaft of a motor, the torque that will be developed at the rotor is equal to the friction torque (M_R) of the motor plus the resisting torque (M_L) due to external mechanical load (impeller). This is represented as:

$$M_{mot} = M_R + M_L \tag{8-8}$$

The impeller used in this study was selected using Multi-Wing Optimizer 9.0.2.83 software of the company Multi-Wing. Table 8-1 shows the output data from the optimizer selection software which indicates the chosen impeller with its mechanical properties.

Table 8-1 General information of selected impeller.

Input data	
Impeller diameter	400 mm
Tip clearance	0.5 %
Motor speed	800 rpm
Impeller information	
Impeller type	400/3-6/25°C/PPG[(a)]
Torque (M_L)	0.0965 Nm
Airflow	1060 m^3 hr^{-1}
Total pressure	20.2 Pa
Efficiency	74 %
[(a)] Multi-Wing™	

According to Braun (2012), the speed-torque gradient ($\Delta n/\Delta M_{mot}$) indicated in figure 8-2 is one of the most informative pieces of data to consider when computing the working point of a motor-impeller system. It is represented as:

$$\frac{\Delta n}{\Delta M_{mot}} = \frac{30000}{\pi}\frac{R_{mot}}{K_m^2} \approx \frac{n_o}{M_H} \tag{8-9}$$

Substituting equation (8-9) into (8-7), we obtain the equation:

$$n = K_n V_{mot} - \left(\frac{\Delta n}{\Delta M_{mot}}\right) M_{mot} \tag{8-10}$$

The voltage required by the motor is therefore expressed as:

$$V_{mot} = \frac{n}{K_n} + \frac{\Delta n}{\Delta M_{mot}} M_{mot} \tag{8-10b}$$

From equation (8-4), the current of the motor can also be determined. It is represented by the expresion:

$$I_{mot} = \frac{M_{mot}}{K_m} \tag{8-11}$$

Based on the data presented in table 8-1, a PM DC motor with low nominal speed and current was selected for the fan development. The motor design data is shown in table 8-2.

Table 8-2 Motor design data.

Motor type		GNM 4125[(a)]
Nominal speed	rpm	1600
Nominal voltage	V	24
Nominal current	A	2.15
Nominal power	P	35
Mechanical data		
Friction torque, MR	Nm	0.025
Speed regulation constant	$N^{-1}cm^{-1}min^{-1}$	21
Electromechanical data		
Torque constant	$Nm\ A^{-1}$	0.11
Voltage constant	$V\ (1000\ rpm)^{-1}$	11.47

[(a)] ENGEL Elektromotoren GmbH

The efficiency of the motor for the defined current and voltage will then be calculated using the relation:

$$\eta_{mot} = \frac{M_L n}{V_{mot} I_{mot}} \tag{8-12}$$

Hence, the total design efficiency is given as:

$$\eta_T = \eta_{mot} \eta_{imp.} \tag{8-13}$$

where $\eta_{imp.}$ is impeller efficiency and is given in table 8-1.

Using equations (8-10b) and (8-11) and the data presented in tables 8-1 and 8-2, a DC fan for direct PV drive was developed. Figure 8-3 shows the basic components and the developed fan. The impeller of the fan is made of three airfoil-shaped blades made of Glass Reinforced Polypropylene (PPG) material. Retaining bolts are used to hold the root of the blades casting in position in a spherical pocket around a steel hub. It has a hub center boss which is made of cast iron and is straight bored thus allowing the DC motor shaft to be attached. The motor together with the impeller is then mounted within a circular metal duct that serves as the fan housing. The clearance between the impeller tips and the duct within which they turn is small, 0.002 m hence keeping energy losses to a minimum at the entrance and at the impeller tips where turbulence takes place. The fan is capable of delivering an airflow rate of 1060 m^3 hr at a total pressure of 20 Pa which corresponds to 13.31 W power requirement. The overall design efficiency of the fan is 45%.

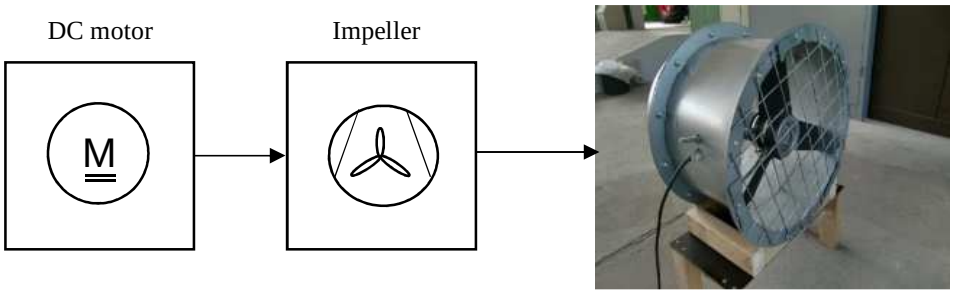

DC fan

Figure 8-3 PM DC motor, impeller and the fully assembly DC fan.

8.3.2.2 PV panel model formulation for DC load matching

The PV panel consists of a number of solar cells, which are connected in series and parallel to achieve the required voltage and current. To drive the DC fan described in section 8.3.2.1,

first we need to know the current (I)-voltage (V) characteristics of the PV panel. The general equation for the relation between current and voltage of a PV cell is (Yang et al., 2015; Masters, 2004):

$$I = I_{ph} - I_d - \frac{V_d}{R_p} = I_{ph} - I_r\left[\exp\left(\frac{q(V+IR_s)}{A_f k T_j}\right) - 1\right] - \left(\frac{V+IR_s}{R_p}\right) \quad (8\text{-}14)$$

where I is the PV cell output current (A), V is the PV output voltage, I_{ph} is the photo current, I_d is the diode current, I_r is the reverse saturation current, q is the charge of the electron (1.602 x 10^{-19} Coulomb), A_f is the ideality factor which takes value of between 1 and 2 (Green, 1992), k is the Bolzmann's constant (1.381 x 10^{-23}J K^{-1}) and T_j is the operating temperature of the PV cell (K).

According to Hussein et al. (1995), equation (8-14) can be simplified by neglecting parallel resistance R_p and series resistance R_s. If there are n_s number of cells in series connected in a panel and np number of panels connected in an array, then equation (8-14) can be written as;

$$I = n_p I_{ph} - n_p I_r\left[\exp\left(\frac{qV}{A_f k T_j n_s}\right) - 1\right] \quad (8\text{-}15)$$

By using equation (8-15), the current-voltage characteristics curves for varying solar irradiances and operating cell temperature can be generated by mathematical modeling on a spreadsheet. The photocurrent, I_{ph}, is directly proportional to the incident solar radiation and also depends on the cell temperature according to Hua et al. (1998). This is given by the expression:

$$I_{ph} = \frac{G_a}{G_{as}}\left[I_{sc(Ts)} + k_i\left(T_j - T_r\right)\right] \quad (8\text{-}16)$$

In equation (8-16), G_a is the solar irradiance and T_r is the reference temperature at standard test conditions (STC). The other terms are constant : $I_{sc(Ts)}$ is short circuit current on STC, G_{as} is standard irradiance (1000 W m^{-2}), k_i is the temperature coefficient on short circuit current. Cell operating temperature is approximately proportional to the incident solar irradiance (Hwang et al., 2009; Luque and Hegedus, 2003) and is given by:

$$T_j = T_a + \lambda G_a \quad (8\text{-}17)$$

where λ has a constant value:

$$\lambda = \frac{\mathrm{NOCT(^{\circ}C)-20}}{800\ \mathrm{W\,m^{-2}}} \tag{8-18}$$

NOCT is the normal operating cell temperature, which is generally given by the manufacturers. The reverse saturation current, I_r, (eq. (8-15)) of the solar array varies with temperature according to the following relationship (Qi and Ming, 2012; Chin et al., 2011):

$$I_r = I_{r(Ts)}\left(\frac{T_j}{T_r}\right)^{\frac{3}{A}} \exp\left(\frac{qE_g}{kA_f}\left[\frac{1}{T_r}-\frac{1}{T_j}\right]\right) \tag{8-19}$$

and

$$I_{r(Ts)} = I_{sc(Ts)}/\left(\exp\left(\frac{qV_{oc(Ts)}}{A_f k T_j n_s}\right)-1\right) \tag{8-20}$$

Using equation (8-15), the power output of the PV panel (P_{pv}) can be calculated as:

$$P_{PV} = VI = n_p I_{ph} V - n_p I_r V\left[\exp\left(\frac{qV}{AkT_j n_s}\right)-1\right] \tag{8-21}$$

Hence, the efficiency (η_{PV}) of the PV panel is evaluated by the equation:

$$\eta_{PV} = \frac{P_{PV}}{G_a A_{PV}} \tag{8-22}$$

where A_{pv} is the effective area of the PV panel.

8.3.3 Utilization of evaporative cooling system in a PV driven ventilated system

In order to provide adequate conditions for storage of fresh sweet potato roots under tropical conditions, an evaporative cooling concept, previously used and described in Chapter 6 was integrated into the PV driven ventilated system. Depending on the test being carried out, flow of water for forced-air evaporative cooling was provided by a DC pump connected to either a DC power source regulator or directly to a PV panel. The matching of a DC pump to a PV panel was based on the following observations made in Chapter 6: (1) at low air velocity, double and triple layers charcoal evaporative cooling pad configurations are effective. On the basis of this, double layers pad configuration was selected; (2) water flow rate of 2 to 5.2 l min^{-1} is adequate to maintain high relative humidity, as long as the water is uniformly sprayed on

the evaporative cooling pad. Since the water flow rate will vary with solar irradiance when fluid is circulated by a DC pump directly coupled to a PV panel (Bai et al., 2011), a maximum flow rate of 3.2 l min^{-1} was chosen. Based on this, a DC water pump (type SP20/20 Solarproject, UK) was selected. The commercially available pump has a characteristic of 12 V, 14 W, maximum head of 5 m and maximum flow rate of 30 l min^{-1}.

8.3.4 Experimental set-up and data acquisition

Optimal matching of direct coupling of DC fans and DC pumps to PV panels is well documented in the literature (Atlam and Kolhe, 2013; Esper, 1995; Appelbaum, 1986; Roger, 1979). The emphasis in this study is however on matching the DC loads to a closely rated PV panel to guarantee automatic start at low solar irradiance as well as to prevent fatigue or damage of motors due high current. Using a DC power regulator source, the input current and the output air velocity and water flow rate of the DC fan and the pump was measured after the loads were intalled to the mud storehouse. The minimum operating current and voltage of the fan and pump after startup are 0.1 A and 0.85 V and 0.3 A and 3.6 V, respectively. The maximum current and voltage that corresponds to airflow rate of 1060 m^3 hr^{-1} is 1.1 A and 12.1 V, respectively. In the case of the pump, the maximum current and voltage that correspond to 3.2 l min^{-1} is 0.40 A and 5 V, respectively. Graphical representation of the fan and pump I-V curves are discussed in section 8.4.1. Based on the above preliminary analysis, a 20 W_P rated PV panel was selected to power the fan while three 5 W_P rated PV panels were connected in parallel and coupled to the DC pump to provide the desire water flow rate. The operational parameters for the PV panels, given by the manufacturer are presented in table 8-3.

Table 8-3 Parameters of two types of polycrystalline PV panels*.

Parameters	20 W 3-01-001270	5 W 3-01-001555
	Value	Value
Peak power (P_{max})	20 W_P	5 W_P
Peak power voltage (V_{max})	17.8 V	17.6 V
Peak power current (I_{max})	1.13 A	0.28 A
Open circuit voltage (V_{sc})	22.3 V	21.9 V
Short circuit current (I_{sc})	1.22 A	0.31A
Temperature coefficient of open circuit voltage	-0.45%/°C	-0.45%/°C
Temperature coefficient of short circuit voltage	-0.45%/°C	-0.45%/°C
Nominal Operating Cell Temperature (NOCT)	45±2 °C	45±2 °C

*Measured at STC: 1000 W m^{-2}, 25 °C, AM 1.5

Performance evaluation of the direct PV drive ventilated system was carried out in two stages: (1) direct ventilation with ambient air conditions when the storage bin in the mud storehouse is loaded with products; (2) utilization of evaporative cooling system during direct ventilation without loaded products. The PV panels were mounted at a tilt angle of 51.3° (equal to the latitude of Witzenhausen) and oriented in the north-south direction. The experimental set-up is shown in figures 8-4 and 8-5. In figure 8-4, the 20 W_P rated PV panel is connected directly to the DC fan which is integrated into the mud storehouse. The fan was connected to the plenum chamber located inside of the store through a 0.4 m diameter round duct. In figure 8-5, charcoal used as an evaporative cooling media is that described in section 8.3.3. The arrangement of the water distribution system is similar to that presented in Chapter 6.

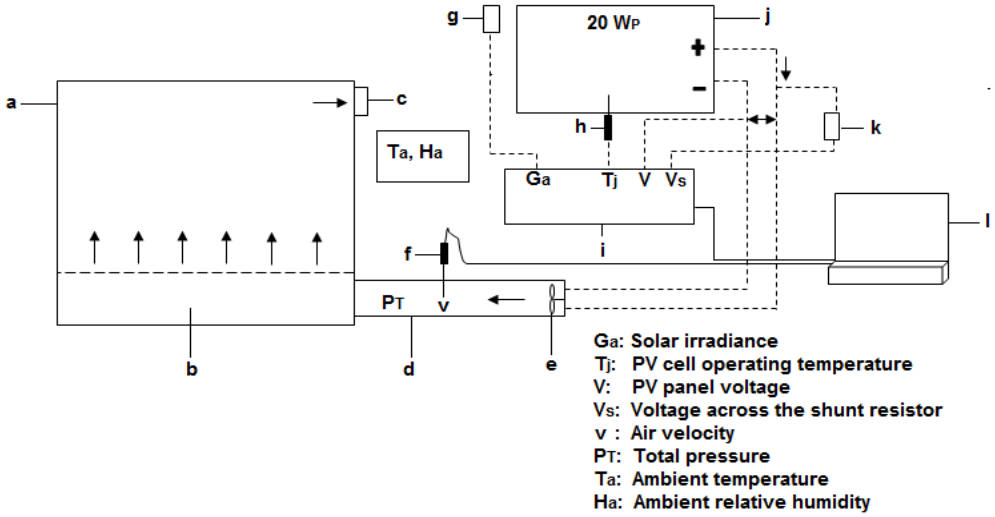

Figure 8-4 Schematic of the experimental set-up for direct ventilation with ambient air conditions (not drawn to scale). (a = mud storehouse, b = air plenum, c = air outlet, d = air duct, e = fan, f = hot wire anemometer, g = pyranometer, h = thermocouple, i = data logger , j = PV panel, k = shunt resistor, l = computer).

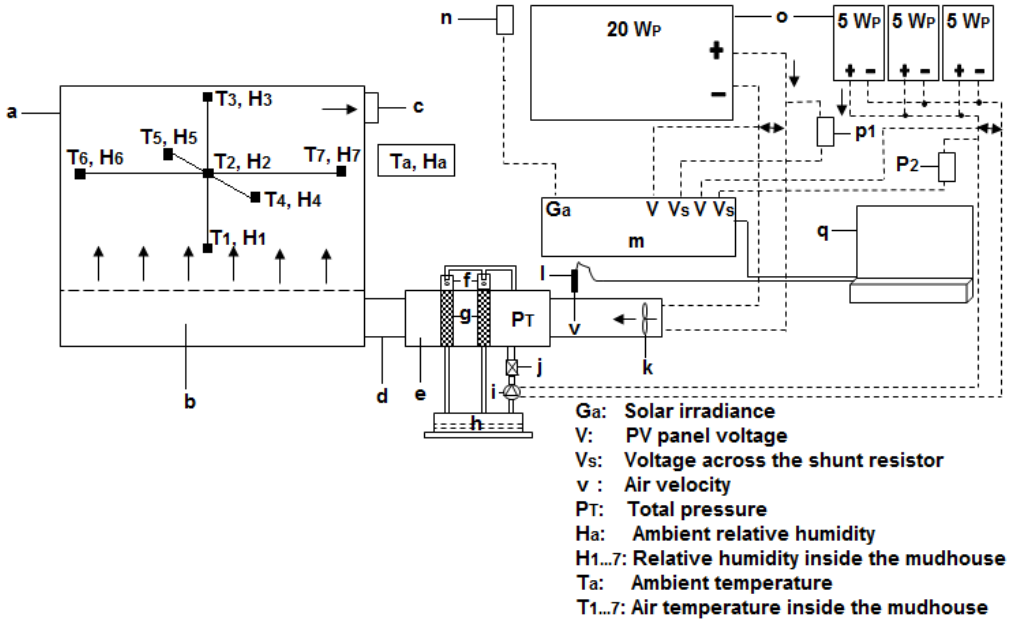

Figure 8-5 Schematic of the experimental set-up of PV ventilation with evaporative cooling system (not drawn to scale). (a = mud storehouse, b = air plenum, c = air outlet, d = air duct, e = evaporative cooling chamber, f = water distributor, g = wetted medium, h = water tank, i = water pump, j = flowmeter, k = fan, l = hot wire anemometer, m = data logger, n = pyranometer, o = PV panels, p_1&p_2 = shunt resistors, q = computer).

To investigate the effect of environmental and operating parameters on the performance of the system, various measuring devices were employed. A pyranometer (SP Lite: response time < 1 s) was placed at the same position with the PV panels to measure solar irradiance. The sensivity of the pyranometer is 73 µV $(W\ m^{-2})^{-1}$. Thermocouples (K type, acurancy ±1.5 K) were used to measure temperature of the PV panels and air temperature in the evaporative cooling system. For the PV panel's temperature, the thermocouples were firmly attached with epoxy adhesive at the rear side of the PV panels. The exact PV cell temperature can be found when a thermocouple is inserted into the junction of the PV cell, but in this case it not possible to reach the junction of the PV cell. The voltage of the panels was measured directly using a data acquisition unit/data logger (Fluke Hydra). The current characteristics of the PV panels was computed by measuring the voltage drop across the shunt resistors (BADER manganin, accuracy 10 mΩ ± 0.01%). A hot wire anemometer (Voltcraft PL-135HAN, accuracy ±1% full scale) was used to monitor the air velocity in the duct. The total pressure and water flow rate were measured using a digital differential pressure meter (Testo 510, accuracy ±1.5%) and flowmeter (GARDENA water smart flowmeter, accuracy ±5%), respectively. The temperature and RH of the ambient air and inside the mud storehouse were also continuously measured

using mini temperature and humidity data loggers (Testo 174H, accuracy ±0.2 °C and ±3% RH).

Voltage signals from the pyranometer, thermocouples, shunt resistors and the PV panels were recorded every 5 minutes by the data acquisition unit (Fluke Hydra) controlled by a computer. The air velocity in the duct, temperature and RH of the ambient air and inside the mud storehouse were also measured every 5 minutes. The devices used for these measurements were programmed via computer interface. The total pressure and water flow rate was manually recorded at 15 minute intervals.

8.4 Results and discussion

8.4.1 Characterization of DC fan, DC pump and the PV panels

By appying equations (8-15) to (8-20), I-V characteristic curves of a PV panel for varying solar irradiances and cell temperatures have been generated by mathematical modeling on an excel spreadsheet. Before matching the DC fan and the DC pump with the PV panels electrical characteristics, it is necessary to compare the simulated output characteristics of the PV panels with experimentally measured characteristics. For this purpose, only the 20 W_P rated PV panel is used. The experiments were conducted on 28th June, 2015. To simulate the I-V characteristic curves, the average values of solar irradiance and ambient temperature of all the experimental data points during the hours of 12.00 to 14.00 (clear and cloud-free hours in the day) were taken as inputs: specifically 918.7 W m^{-2} and 20.1 °C, respectively. Figure 8-6 shows experimental and simulated I-V characteristic curves of the PV panel used. It can be seen that the simulated results closely match the experimental data output, with a discrepancy of 4.5%. The model calculates the average PV panel temperature as 43.3 °C, using the experimentally-measured average solar irradiance and average ambient temperature value. This is very close to the experimentally-measured average value of the PV panel temperature of 42.2 °C using all the data points during the measurement period.This small difference is mainly due to the fact that the PV temperature is measured at the back of the PV panel, which is not exactly the PV junction temperature. Moreover, the difference could also be due in the part of neglecting series and parallel resistances in the equivalent circuit of the PV cells in order to simplify the model, as suggested by Xiao et al. (2004), Kuo et al. (2001) and Hussein et al. (1995). Since the study aim to understand the operating points of the DC loads for given

solar irradiances, the less detailed model of the PV panel itself has been adopted in the present work.

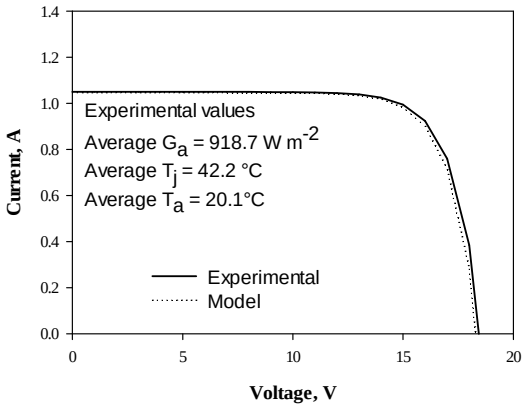

Figure 8-6 Experimental and simulated I-V characteristic curves of polycrystalline 20 W_P PV panel (Witzenhausen, 28th June, 2015, from 12.00 to 14.00 hours).

To understand the possible operating points, if the DC fan and DC pump were to be coupled directly to the PV panels, an analysis is carried using experimental I-V curves of the DC fan and the DC pump and the simulation data of the output curves of the PV panels under different solar irradiance (fig.8-7). It can be seen that the fan will start operating at a solar irradiance of nearly 100 W m^{-2} (fig.8-7A). At solar irradiance value of over 900 W m^{-2}, the voltage and current of the PV panel is slightly beyond the computed working point of the fan (1.1 A, 12.1 V). Hence, the fan will deliver more airflow at this point. The short circuit current of the PV panel used is 1.22 A (table 8-3), therefore fatigue or damage to fan motor can be ruled out. Grassie (2006) did not report any signal of fatigue or damage in a similar PV driven fan installation after long term testing at high voltages. In the case of the commercial DC pump (fig.8-7B), it can be observed that the pump will only start at solar irradiance of over 200 W m^{-2}. It will require more starting current and has higher armature resistance.

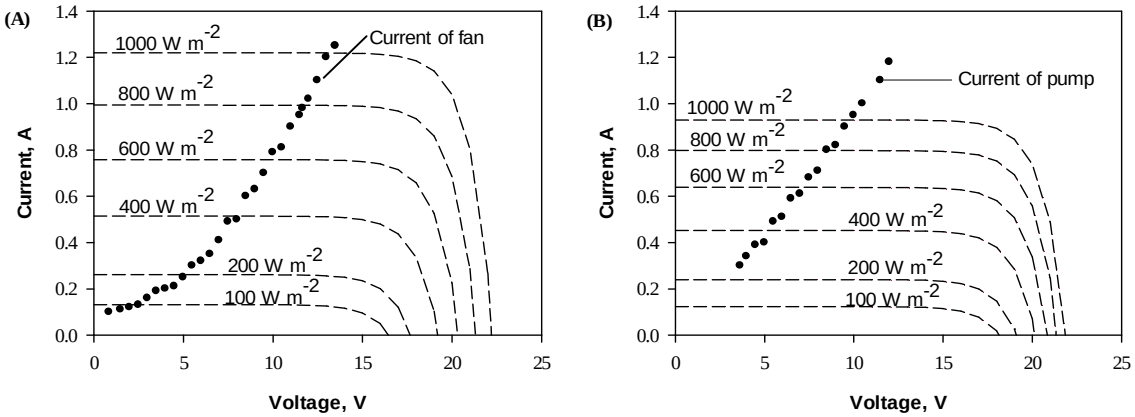

Figure 8-7 Simulated PV output curves and experimental I-V curves of (A) fan and (B) pump.

8.4.2 Performance of the system

Investigations were also carried out to determine the performance and reliability of the directly coupled PV ventilation system. The experiments were carried out in two phases as previously described in section 8.3.4 in respect of PV panel electrical characteristics and the resulting airflow rate and total pressure. In addition, pattern of temperature and RH in both the inside of the mud storehouse and ambient conditions were investigated. Depending on the measurements being made, the mud storehouse was either loaded with product or without product.

8.4.2.1 Direct PV powered ventilation with ambient air conditions

For this testing phase, the aim was to evaluate the system performance in respect of PV panel electrical characteristics and the resulting airflow rate and total pressure under actual weather conditions when loaded with products. Therefore, potatoes (*Solanum tuberosum* (L.)) were procured directly from a nearby farm in Witzenhausen (Germany) for loading into the mud storehouse due to the unvailability of sweet potato roots in large quantity. The variety of the potatoes and the growing conditions under which they were produced are unknown. According to ASABE standard D272.3 (ASAE, 2011), the resistance of sweet potato roots to airflow is slightly lower than that of potatoes. Therefore, it is expected that test results using potatoes will not differ greatly if actual sweet potato roots were to be used. To this end, the storage bin in the mud storehouse was loaded with about 4.13 tons of potatoes with an average diameter of 0.065 m. Typical results during operation in the month of July are shown in figures 8-8 and

8-9. Figure 8-8 shows the variations of solar irradiance and the PV panel current and voltage during a typical experimental test. It can be seen that solar irradiance increased sharply from 8 am till noon but was considerably decreased after 14.00 hours. Generally, there were random fluctuations in solar irradiance due to clouds. Nevertheless, the overall patterns in solar irradiance were sinusoidal with a sharp peak at noon. At 8 am, the average minimum value of solar irradiance was 326 W m^{-2} which corresponds to current and voltage of 0.22 A and 4.37 V, respectively. At noon, the maximum average solar irradiance recorded was 878 W m^{-2} with a corresponding current and voltage of 1.23 A and 14.08 V, respectively.

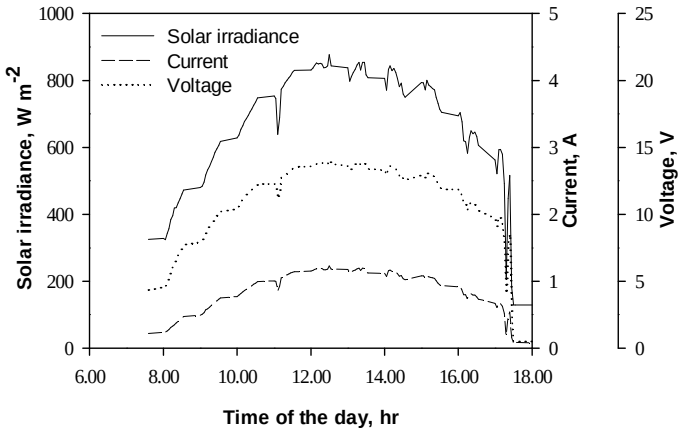

Figure 8-8 Variations of solar irradiance, current and voltage with time of the day for a typical experimental run during ventilation with loaded potatoes (Witzenhausen, 4th July, 2015).

Figure 8-9 shows variations in the solar irradiance, airflow rate and total pressure of a typical experimental run during potatoes ventilation. The airflow rate increased in the early part of the day, then becomes fairly constant and then drops suddenly in the afternoon. The pattern of changes in airflow rate follows the pattern of the changes in solar irradiance. This is due to the fact that airflow was provided by the DC fan operated by the PV panel and the output power of the PV panel depended strongly on solar irradiance. Similar observation have being reported by Janjai et al. (2009) and Esper (1995). Interestingly, maximum airflow of 1079 m^3 hr^{-1} was recorded at the highest solar irradiance level. Table 8-4 further shows the variation of average efficiency of the PV panel and airflow rate under hourly solar irradiance conditions. It is seen from the table that the PV panel efficiency is varied from 1.9% to11.8%. The fan started operating at solar irradiance value of 87.5 W m^{-2}. As this threshold is relatively low, the fan operated continuously during the entire experimental duration. Experimentally, a clear

dependence of the total pressure values on the solar irradiance is also observed (fig.8-9). This is in accordance with the literature (Esper, 1995).

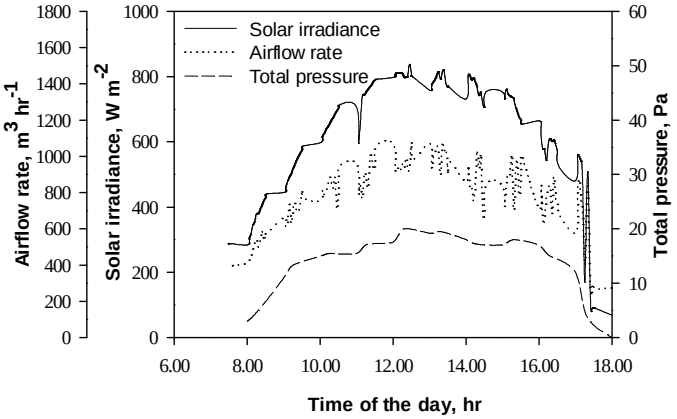

Figure 8-9 Variations of solar irradiance, airflow rate and total pressure with time of the day for a typical experimental run during direct ventilation with loaded potatoes (Witzenhausen, 4th July, 2015).

Table 8-4 Hourly average efficiency of the PV panel and airflow rates (Witzenhausen, 4th July, 2015).

PV panel	Time, hr										
(20 W)	8.00	9.00	10.00	11.00	12.00	13.00	14.00	15.00	16.00	17.00	18.00
η_{PV}, %	1.9	3.5	6.8	9.3	10.8	11.4	11.8	11.2	10.5	8.4	3.9
V_a, m^3 hr^{-1}	405	542	730	847	930	968	982	867	860	743	548

8.4.2.2 Need of evaporative cooling during direct PV powered ventilation

The direct PV powered ventilation system worked effectively during sunny hours and is therefore suitable for use in remote rural areas in tropical countries. The degree of reliability desired of the directly coupled PV ventilation system to lower temperature and increase/or maintain relative humidity can be achieved by a combination of an evaporative cooling system as described in section 8.3.3. For this purpose, experiments were conducted to ascertain its functionality under actual weather conditions. The tests have been carried out without load (products). It is to be noted that the charcoal pads used as evaporative cooling media will offer resistance to airflow as indicated in Chapter 6. Nevertheless, this resistance to airflow is expected to be marginal under the estimated airflow requirements for sweet potato roots ventilation. Figures 8-10 and 8-11 presents measured parameters under unload conditions.

The trend in solar irradiance, current, voltage, airflow rate and total pressure is similar to that previously discussed in section 8.4.2.1.

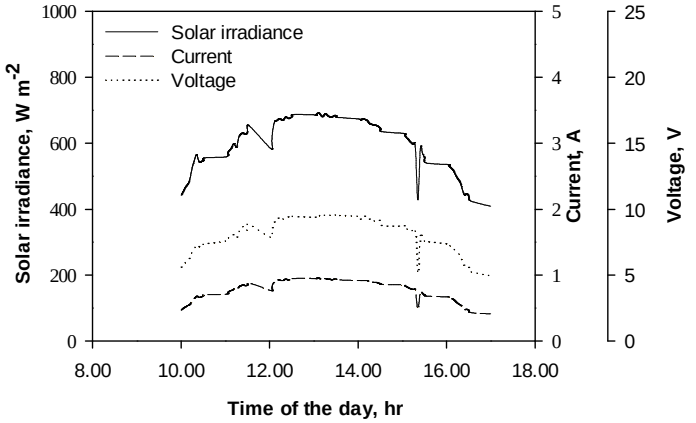

Figure 8-10 Variations of solar irradiance, current and voltage with time of the day for a typical experimental run during ventilation without products (Witzenhausen, 31st August, 2015).

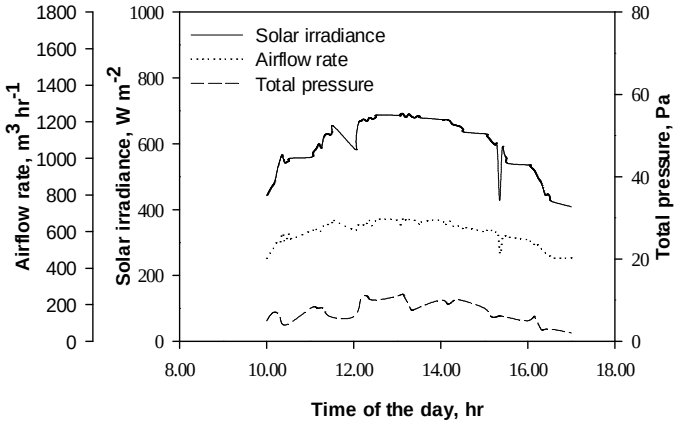

Figure 8-11 Variations of solar irradiance, airflow rate and total pressure with time of the day for a typical experimental run during ventilation without products (Witzenhausen, 31st August, 2015).

Figure 8-12 shows comparison of air temperatures and RH at seven different locations inside the mud storehouse (fig. 8-5) for a typical experimental run with the evaporative cooling system. First, a DC power source regulator was used to provide constant water flow (3.2 l min^{-1}). In figure 8-12A, the patterns of the temperature changes in the different positions were comparable for all locations. Air temperatures in different positions at these seven locations vary within a narrow band, with a marginal increase during the day time. However, ambient air temperature continuously increased during 10.00 hours to 13.00 hours and thereafter starts to decrease after 17.00 hours onwards. Similar trends have been reported by Tilahun (2010).

Temperature reduction was highest during the hottest time of the day (13.00 to 16.00 hours). Using air temperature measurement at position one (T1) as an example, a temperature drop of 3.2 to 9.4 °C from ambient condition was observed. It is worth mentioning that, while optimum temperatures of 13 to 15 °C, for sweet potato roots storage can be achieved by refrigerators (Boyette, 2009; Woolfe, 1992; Picha, 1986), the theoretical minimum temperature that can be reached by evaporative coolers is the wet-bulb temperature of the location where the system is used (El-Refaie and Kaseb, 2009).

The data presented in figure 8-12B shows RH at seven different locations inside the mud storehouse. The patterns of RH changes in the different positions were as well comparable for all locations.The evaporative cooling system maintained high RH inside the mud storehouse compared with the ambient RH that decreased continuously during the experiments.The maintenance of a fairly constant air temperature and high RH inside the mud storehouse is explained by the unique properties (thermic and humidity balancing behaviour) of mud material. As solar radiation is one of the major sources of heat gain, constructing the mud storehouse under shade would help in further reducing possible heat accumulation especially under tropical climates.

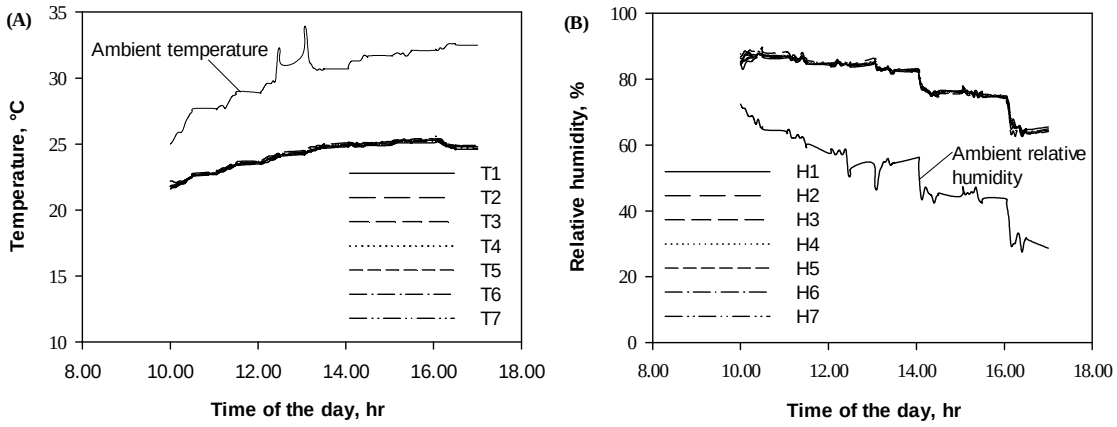

Figure 8-12 Comparison of (A) air temperatures, (B) relative humidity at various positions inside the mud storehouse and the ambient temperature and relative humidity for a typical experimental test with evaporative cooling system integrated during PV ventilation (Witzenhausen, 31st August, 2015).

Tests were also performed when the DC water pump was directly coupled to a PV panel. Figure 8-13 depicts variations of the solar irradiance, current and voltage of 20 W_P (for fan) and 15 W_P (for pump) PV panels used. The results for the entire measurement period are characterised by sporadic fluctuations in solar irradiance, caused by scattered clouds. Nevertheless, this test presents essentially a situation which is naturally unavoidable under field conditions. The variation of solar irradiance, airflow rate and total pressure with time of the day for experimental run with the evaporative cooling system is shown in figure 8-14. The total pressure follows the pattern of the solar irradiance. Similarly, the performance of the DC pump follows the pattern of the solar irradiance (fig. 8-15). According to data presented in Chapter 6, air stream passing through wetted charcoal evaporative cooling pads is reported to cause an emergence of water entrainment off the medium at water flows of 7.2 l min^{-1}. This was taken into account in the present study in matching the 15 W_P PV panels to the DC pump. The maximum short circuit current that can be delivered by the 15 W_P PV panels is 0.93 A (table 8-3) which corresponds to water flow rate of about 5.5 l min^{-1}. The field experiments, however, could not establish these trends clearly due to unfavorable climatic conditions. Even though the flow of water was fluctuating (fig. 8-15), the trend in air temperature and RH variation inside the mud storehouse (data not shown) was similar to that reported in figure 8-12.

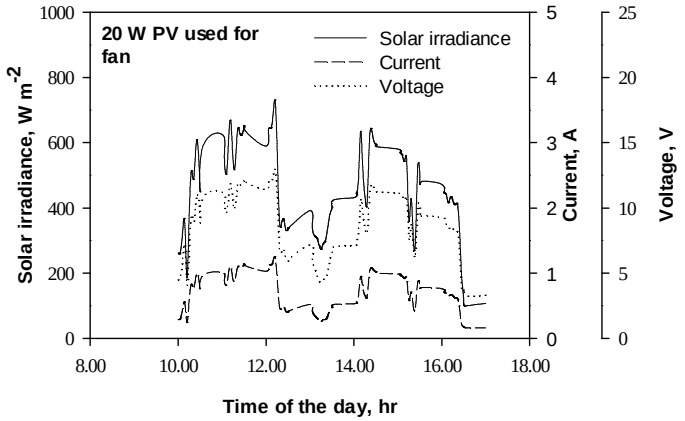

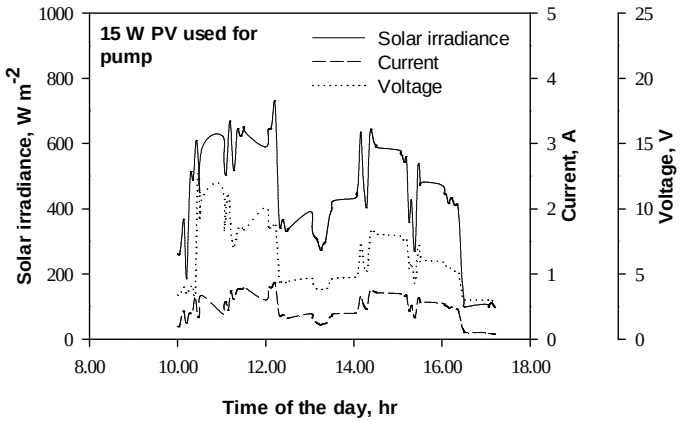

Figure 8-13 Variations of solar irradiance, current and voltage of 20 W_P and 15 W_P PV panels with time of the day for a typical experimental run with evaporative cooling system (Witzenhausen, 12th September, 2015).

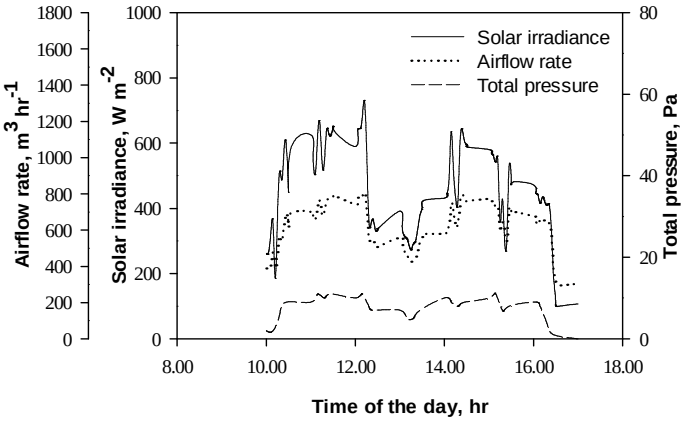

Figure 8-14 Variations of solar irradiance, airflow rate and total pressure with time of the day for an unloaded experimental run with evaporative cooling system (Witzenhausen, 12th September, 2015).

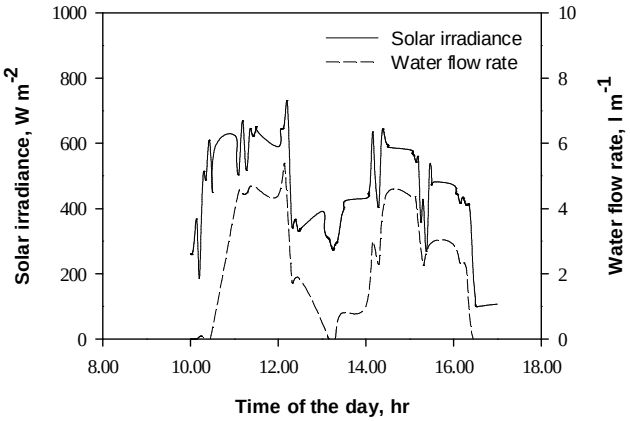

Figure 8-15 Variations of solar irradiance and water flow rate with time of the day for a typical experimental run with evaporative cooling system (Witzenhausen, 12th September, 2015).

8.5 Conclusions

An autonomous PV ventilated storage system was successfully developed and tested under field conditions of Witzenhausen (Germany). The experimental results during the test showed that solar irradiance varies almost sinusoidally around the peak at noon. The patterns of changes in airflow rate and total pressure were observed to follow the patterns in solar irradiance. Test results showed that under solar irradiance of around 800 W m^{-2}, the developed PV driven fan can provide airflow required for ventilating bulk sweet potato roots. As the fan has a relative low operating voltage threshhold, it operated continuously during the entire experimental duration, even under low solar irradiance (85 W m^{-2}). The utilization of an evaporative cooling system in the PV ventilated mud storehouse was found capable of reducing the ambient temperature and increasing the RH, especially during the hottest hours of the day. Consequently, the integration of evaporative cooling system into directly coupled PV ventilated systems is recommended for use under tropical climates. Due to the utilization of PV panels for direct powering of the fan and the water pump, the developed system can be used in rural areas without electricity for storage of sweet potato roots. Further research is however recommended to ascertain the percentage loss of sweet potato roots during storage as compared to the rudimentary storage practices in remote areas of tropical developing countries.

8.6 Acknowledgements

The first author, Joseph Kudadam Korese would wish to acknowledge financial support from the German Academic Exchange Service (DAAD) for his research stay in Germany. This study is part of Global Food Supply (GlobE) project RELOAD (FKZ 031A247 A), funded by the German Federal Ministry of Education and Research (BMBF). We gratefully acknowledge their financial contributions.

8.7 References

Atlam, O., & Kolhe, M. (2013). Performance evaluation of directly photovoltaic powered DC PM (direct current permanent magnet) motor-propeller thrust system. Energy, 57, 692-698.

ASABE Standards. (2011). D272.3: Resistance to airflow of grains, seeds, other agricultural products and perforated metal sheets. St. Joseph, MI: ASABE.

Appelbaum, J. (1985). Performance characteristics of a permanent magnet DC motor powered by solar cells. Solar Cells, 17, 346-362.

Boutelhig, V., Bakelli, Y., Hadj Mahammed, I., & Hadj Arab, A. (2012). Performance study of different PV powered DC pump configurations for an optimum energy rating at different heads under the outdoor conditions of a desert area. Energy, 39(1), 33-39.

Braun, J. (2012). Maxon formulae handbook. Maxon Academy, pp. 1-56.

Bai, Y., Fraisse, G., Wurtz, F., Foggia, A., Deless, Y., & Domain, F. (2011). Experimental and numerical study of a directly PV-assisted domestic hot water system. Solar Energy, 85, 1979-1991.

Boyette, M. D. (2009). The investigation of negative horizontal ventilation for long-term storage of sweetpotatoes. Applied Engineering in Agriculture, 25(5), 701-708.

Badescu, V. (2003). Dynamic model of a complex system including PV cells, electric battery, electrical motor and water pump. Energy, 28(12), 1165-1181.

Bengtsson, L.P., & Whitaker, J.H. (1988). Farm structures in tropical climates. Rome, Italy: United Nations FAO, SIDA Rural Structures Program.

Chin, C.S., Babu, A., & McBride, W. (2011). Design, modeling and testing of a standalone single axis active solar tracker using MATLAB/Simulink. Renewable Energy, 36, 3075-3090.

Davies, P.A., Hossain, A.K., Lychnos, G., & Paton, C. (2008). Energy saving and solar electricity in fan-ventilated greenhouses. Acta Horticulturae, 797, 95-101.

El-Refaie, M.F., & Kaseb, S. (2009). Speculation in the feasibility of evaporative cooling. Building and Environment, 44,826-838.

Edmunds, B.A., Boyette, M.D., Clark, C.A., Ferrin, D.M., Smith, T. P., & Holmes, G.J. (2007). Postharvest handling of sweetpotatoes – AG 413-10-B. N.C. Cooperative Extension Service. Raleigh, N.C.

Esper, A. (1995). Solarer Tunneltrockner mit photovoltaischen Antriebssystem. Forschungsbericht Agrartechnik 264 des Arbeitskreises Forschung und Lehre der Max-Eyth Gesellschaft Agrartechnik. VDI (VDI-MEG).

Grassie, T. (2006). Performance and modeling of a PV driven transpired solar air heater. EuroSun 2006, Glasgow.

Green, M.A. (1992). Solar cells – Operating principles, technology and system application. University of NSW, Kensington, Australia.

Hwang, J.J., Lai, L.K., Wu, W., & Chang, W. R. (2009). Dynamic modeling of a photovoltaic

hydrogen fuel cell hybrid system. International Journal of Hydrogen Energy, 34, 9531-9542.

Hua, C., Lin, J., & Shen, C. (1998). Implementation of a DSP-controlled photovoltaic system with peak tracking. IEEE, Transactions on Industrial Electronics, 45(1), 99-107.

Hussein, K.H., Muta, I., Hoshino, T., & Osakada, M. (1995). Maximum photovoltaic power tracking: An algorithm for rapidly changing atmospheric conditions. IEE Proceedings – Generations, Transmission and Distribution, 142(1), 59-64.

Janjai, S., Lamlert, N., Intawee, P., Mahayothee, B., Bala, B. K., Nagle, M., & Müller, J. (2009) Experimental and simulated performance of a PV-ventilated solar greenhouse dryer for drying of peeled longan and banana. Solar Energy, 83, 1550-1565.

Kuo, Y-C., Liang, T-J., & Chen, J-F. (2001). Novel maximum-power-point-tracking controller for photovoltaic energy conversion system. IEEE Transactions on Industrial Electronics, 48(3), 594-601.

Luque, A., & Hegedus, S. (2003). Handbook of photovoltaic science and engineering. West Sussex: Wiley.

Mukhopadhyay, S.K., Chattopadhyay, A., Chakraborty, I., & Bhattacharya, I. (2011). Crops that feed the world 5. Sweetpotatoes. Sweetpotatoes for income and food security. Food Security, 3, 283-305.

Masters, G. M. (2004). Renewable energy and efficient electric power systems. New Jersey: Wiley.

Picha, D.H. (1986). Weight loss in sweet potatoes during curing and storage. Contribution of transpiration and respirations. Journal of the American Society for Horticultural Science, 111 (6), 889-892.

Qi, C., & Ming, Z. (2012). Photovoltaic module Simulink model for a stand-alone PV system. Physics Procedia, 24, 94-100.

Roger, J. A. (1979). Theory of the direct coupling between DC motors and photovoltaic solar arrays. Solar Energy, 23, 193-198.

Tilahun, S. W. (2010). Feasibility and economic evaluation of low-cost evaporative cooling system in fruits and vegetables storage. African Journal of Food, Agriculture, Nutrition and Development, 10(8), 2984-2997.

Woolfe, J. A. (1992). Sweet potato: An untapped food resource. Cambridge, UK: Cambridge University Press.

Xiao, W., Dunford, W.G., & Capel, A. (2004). A novel modeling method for photovoltaic cells. 35th IEEE Power Electronics Specialists Conference, Aachen, Germany, 3, 1950-1956.

Yang, Z., Zhang, G., & Lin, B. (2015). Performance evaluation and optimum analysis of a photovoltaic-driven electrolyzer system for hydrogen production. International Journal of Hydrogen Energy, 40, 3170-3179.

9 General discussion

This thesis focuses on improving scientific knowledge on sweet potato postharvest handling, in order to support decision-making in the design and optimization of sweet potato post-harvest storage and preservation systems and the development of new processes. In addition, the thesis seeks to demonstrate how this scientific knowledge can be useful in the development of low-cost forced convection storage systems, focusing on decentralized applications for storage of sweet potato roots under tropical climates. The results are presented in two parts and six chapters which were accomplished through laboratory and field research, supported by modeling/simulation exercises. For each of the chapters, the methodological limitations, assumptions, and results were already discussed. For brevity, the majority of this information will not be repeated here. In this part of the thesis, the key findings will be put into a more practical perspective, and the main directions for future research will be presented.

9.1 Airflow resistance of sweet potato components

Previous works reported in the literature (in Chapter 3 and 4) have acknowledged the importance of airflow resistance data of crops for the design of forced-air handling systems. As a result, the ASABE standard D272.3 (ASABE Standards, 2011) have documented the pressure drop data for more common products like grains and seeds, as well as other agricultural products. The investigations presented in Chapter 3 is apparently the first of its kind to be conducted. In the study, critical factors such as airflow rate, moisture content and bulk depth at various levels were defined and the relationship between bulk depth and bulk density established. The research results revealed that airflow rate, moisture content and bulk depth of all the aerial vine components of sweet potato investigated have significant effect on airflow resistance. Consistently, the pressure drop curves were found to decrease as the moisture content of a particular media tested reduces for a fixed bulk depth. Furthermore, pressure drop was also observed to increase linearly with increasing airflow rate for all the conditions examined. Bulk density, which is considered an important part in the design of the dryers was found to be significantly affected by moisture content. Since the investigated factors (airflow rate, moisture content and bulk depth) were observed to affect the pressure drop, an empirical ‘‘derating’’ modification was developed to improve the Hukill and Ives (1955)

model adopted by the ASABE standard D272.3 and related studies. The developed models accurately described airflow resistance through sweet potato leaves and chopped sweet potato aerial vines and can be broadly used in practical applications. It is worth mentioning that with the exception of airflow rate, the model adopted in the ASABE standard does not have the ability to incorporate other variables deemed to influence airflow resistance of agricultural crops. Accordingly, this part of the study provided a set of useful data as a starting database for future design of hot air dryers, especially for fan selection. Future work should focus on the use of these data in the design and development of forced-air dryers such as decentralized solar dryers, batch-type dryers etc. in order to make the anticipated gains from sweet potato aerial vine components.

In the next study, the focus was on airflow resistance through bulk unwashed and clean sweet potato roots. Some attempts have been made in the past to characterize airflow resistance through clean hand graded sweet potato roots (Abrams and Fish, 1982). Nevertheless, the results presented in Chapter 4 differed from that of the earlier study by Abrams and Fish (1982). Importantly, the present research examined the effect of process parameters such as shape factor, roughness factor, orientation to airflow and the presence of soil fractions on airflow resistance of sweet potato roots, which is limited in the literature. The physical properties of the fluid (air) and the sweet potato roots were explicitly incorporated into a physically meaningful model. The model adequately reproduced the experimental data on pressure drop of all the batches investigated as compared with an empirical model. Through the use of this physical model, the pressure drop differences that resulted from the various influencing factors was better explained by the contribution of particle drag and surface friction. The analysis presented in chapter 4 therefore allows interpretation of the experimental results from a physical point of view, which will be instrumental in the design of bulks for improved cooling of sweet potato roots. Critical analysis of the results also showed that airflow resistance was more pronounced in the unwashed sweet potato roots than in the clean roots for all the batches studied. In particular, the presence of soil fraction on the sweet potato roots was observed to obstruct airflow, hence increases the pressure drop in all the batches investigated. The presence of soil fraction in roots should be taken into account when choosing a fan for ventilation of sweet potato roots pile, for it will affect the pressure drop as well as uniformity of airflow. Parts of the results in this study was applied in the development

of a ventilated storage system which is presented in Chapter 8.

9.2 Heat transfer during forced-air cooling and heating of whole sweet potato roots

The systematic analysis of the influencing factors on cooling and heating of whole sweet potato roots (Chapter 5) is desirable to help in the design and optimization of effective treatment protocols of sweet potato roots. The research results have shown that heat conduction in sweet potato roots depends largely on the root size, air velocity and the medium air temperature. As roots of different sizes in bulk may either cool or heat at different times, sorting is very important to help achieve uniform cooling or heating among sweet potato roots especially when operating under forced convection conditions. Transient simulation process was very useful in estimating the cooling and heating times of whole sweet potato root under forced convection. This study is the first to describe the use of a transient simulation model for estimating cooling and heating times of whole sweet potato roots. The simulation scheme outline in the study is convenient because the key input is the mass of sweet potato roots and is also presented in standard spread-sheeting tools to give an immediate output for a wide range of users. The simulation work presented here however did not consider the effect of sweet potato root water loss during the various treatments processes. Some of the assumptions made to simplify the model during simulations could be further investigated to improve the accuracy of the results. Additionally, the model could further be generalized to include microbial reaction and insect mortality for further evaluating the quality of sweet potato roots under forced convection cooling and heating treatments. However, a trade-off need to be made between increasing the complexity of the simulation method through incorporating these, and any practical benefits in the resulting estimate that could be demonstrated.

9.3 Performance of charcoal evaporative cooling pad configurations

In this study, the performance of charcoal cooling pad configurations was investigated experimentally using a wind tunnel test rig (Chapter 6). The study has found that the effectiveness of charcoal pads used as an evaporative cooling media is compound and many parameters are involved in the process, including: inlet air (air velocity, temperature and relative humidity), charcoal pad configurations and water flow rate. Strong links were identified between pressure drop, cooling efficiency and specific water consumption rate. Pressure drop data for the various charcoal pad configurations obtained in this research can be used to select

fans for use in forced-air evaporative cooling systems. Moreover, the information on the effect of water flow on cooling is of great importance, since potential users can practically reduce water flow supplied to a given pad configuration by providing flow rates that will completely wet the media while the cooling performance remain unchanged. This will also make it possible for engineers to reduce the designing power of a water pump for wetting media, consequently resulting in less water usage. The findings in this study are a foundation for recommending suitable charcoal pad configuration for use in the development of low-cost forced-air evaporative cooling systems, especially in resource-constrained regions in tropical developing countries. Furthermore, the findings also contribute to the knowledge base of charcoal as a media for evaporative cooling purposes, which currently have very limited documentation. Practical application of the test results from the research is demonstrated in Chapter 8.

9.4 Airflow distribution in a forced convection mud storehouse

The design of air distribution is one of the most important factors to consider when designing forced convection systems for handling perishable agricultural products. In view of this, CFD technique in the ANSYS Fluent software was used in the study to simulate airflow distribution in a low-cost mud storehouse. The study formed part of the initial design procedures for the mud storehouse presented in Chapter 8. By theoretically investigating different geometries of air handling configurations (air inlet, plenum chamber and air outlet), an acceptable geometry with uniform airflow distribution was selected and constructed. A series of experimental measurements were conducted to validate the CFD results. Comparison between average headspace air velocities extracted from the simulation and the measured headspace air velocities revealed a reasonable agreement. Across the entire bulk surface, the average relative error value between the simulated and measured headspace air velocity was 10.4%. In the global perspective, the results from this study clearly shows that CFD technique can be utilized to design simple post-harvest handling systems which do not require complicated duct and air plenum design.

9.5 Performance of autonomous PV ventilated mud storehouse for storage of sweet potato roots

The development and experimental results of a low-cost PV ventilated storage system which

apply the principle of evaporative cooling for storing sweet potato roots under tropical climate conditions is presented and discussed in Chapter 8. In this research, the construction of the mud storehouse was made possible, using literature recommendations and as well as CFD simulation results presented in Chapter 7. Aside, the results of the laboratory studies presented in Chapter 4 proved instrumental in the development of a PV driven fan, which is a key component for the development of ventilated storage systems. Additionally, the performance data on the charcoal pad configuration (Chapter 6) were crucial in selecting a water pump with low power requirements as well as decisive in determining which pad configuration offers a compromising performance in terms of pressure drop and cooling efficiency. Under field conditions, several experiments were carried out to evaluate the performance of the system. Results revealed that the developed fan can be operated under low solar irradiance. Within maximum solar irradiance of 878 W m^{-2}, which corresponded to current and voltage of 1.23 A and 14.08 V, the fan was observed to deliver airflow rates which were within the range required for sweet potato roots ventilation. The option of integrating a low-cost evaporative cooling system into the mud storage structure for use under tropical climates was also investigated. The results showed a reduction of ambient temperature inside the mud storehouse while relative humidity was enhanced. It is important to mention that the traditional storage technologies used by farmers in most tropical countries (Hall and Devereau, 2000) can hardly create the ideal environmental conditions required for storage of fresh sweet potato roots. The ability of the developed storage system to provide and maintain airflow, temperature and relative humidity which are the key parameters for shelf-life extension of sweet potato roots highlight its ability to reduce post-harvest losses at the farmer level, particularly under tropical climate conditions. Further investigations on sweet potato roots performance under tropical conditions is however highly recommended in order to further optimize the storage system. Future investigations should also focus on the thermal behaviour of mud storehouses, particularly under tropical conditions. The design concept employed in the research makes it possible for the construction of the various components of the storage system in an ordinary workshop. With the continual reduction in the prices of PV panels worldwide (IRENA, 2016), there is a huge potential for adoption of the system in tropical developing countries. The performance evaluation revealed satisfactory results, thus emphasizing the importance of basic engineering design data for the design of appropriate forced convection post-harvest crop handling systems.

9.6 Implications of the research findings to food security

Post-harvest losses of sweet potato components is a threat to food security of many households particularly in developing countries. As sweet potato plays a dual role in food security strategies as a staple food grown and consumed by poor people and as a cash crop sold in high-value markets, experts have agreed that any effort that contributes to extending the shelf-life of this valuable crop will ultimately improve household food security and livelihoods of many rural poor. Generally, appropriate post-harvest storage and preservation technologies for sweet potato roots and aerial vine components, respectively can contribute to food security in multiple ways. For example, extending the shelf-life of fresh sweet potato roots will increase the amount of food available for consumption by farmers and poor rural and urban consumers. Additionally, this will allow farmers to plan their production and marketing and do not have to resort to distress sales of sweet potato roots in case of glut production. For poor farmers with no access to commercial animal feed or feed supplements, preservation of the aerial vines will be important in their livelihoods, since this will ultimately reduce the financial burden associated with the purchase of commercial feed/feed supplements. The current research thus, clearly complements other efforts to enhance food security, particularly in developing countries.

9.7 Reflections on the research approach

The goal of this section is to reflect upon the research approaches employed in the study. Generally, the overall research approach has a dual essence. It come from the fact that the research aim was not only to examine the different process parameters experimentally, but also to apply parts of the results to a practical case in order to support immediate learning and consequences of the decisions taken. Reflecting over these, it is fair to say that the study approach has profited from the use of both laboratory experiments, modeling/CFD simulation and actual field work which complemented one another. The laboratory experiments aided in better understanding the importance of the various process parameters which are critical for the design, optimization and development of forced convection storage and preservation systems. Strictly, the laboratory experiments supported decision making for subsequent work packages in the research. Additionally, the physical experiments also enabled the development of mathematical models that will allow broader application of the findings from

this study. Nevertheless, these experimental measurements were labor-intensive, time-consuming and costly to say the least. The combination of theoretical reasoning and practical implementation of the laboratory studies resulted in the development of a PV ventilated mud storehouse. Since sweet potato property values are now known as well as the key design parameters, CFD simulation which has been applied in the present study can be used in future for design optimization of forced convection storage and preservation systems for sweet potato handling. With the later approach, the repetitive process of modelling and iteration for solution using different solver models and boundary conditions to obtain suitable and logical results not only will save research time but it is economical as well (see Section 2.5). Nevertheless, experimental assessment of an envisaged system in its real geometrical form is essential for proper functionality, since CFD uses many approximate models as well as few assumptions.

9.8 References

ASABE Standards. (2011). D272.3: Resistance to airflow of grains, seeds, other agricultural products and perforated metal sheets. St. Joseph, MI: ASABE.

Abrams Jr., C. F., & Fish Jr., J. D. (1982). Air flow resistance characteristics of bulk piled sweet potatoes. Transactions of the ASAE, 25(4), 1103-1106.

Hall, A. J., & Devereau, A. D. (2000). Low-cost storage of fresh sweet potatoes in Uganda: lessons from participatory and on-station approaches to technology choice and adaptive testing. Outlook on Agriculture, 29(4), 275-282.

International Renewable Energy Agency (IRENA) (2016). The power to change: solar and wind cost reduction potential to 2025.

10 Summary

Sweet potato (*Ipomoea batatas* (L.) Lam) is an important strategic agricultural crop grown in many countries around the world. The roots and aerial vine components of the crop are used for both human consumption and, to some extent as a cheap source of animal feed. In spite of its economic value and growing contribution to health and nutrition, harvested roots and aerial vine components has limited shelf-life and is easily susceptible to post-harvest losses, especially in many parts of tropical developing countries. Various storage and preservation techniques have been employed to extend the shelf-life of harvested components of sweet potato, but with varying success. In developed countries for instance, low temperature storage (13-15 °C, 85-95% RH) has been demonstrated to be capable of insuring year round availability of sweet potato roots in the fresh form. While these conditions are attainable in developed countries, farmers in tropical developing countries are restrained by lack of temperature and relative humidity controlled infrastructure. Storage of roots in rudimentary storage systems often results in high post-harvest losses, which vary between 15% to 70% due to decay, sprouting, alongside pests and insect attack. Unlike the roots, sweet potato aerial vine components under ambient conditions easily decay within two to three days after harvest due to their high moisture content. Experts have agreed that any effort to extend the shelf-life of sweet potato roots and aerial vine components, particularly in tropical developing countries, would make marketing over a longer period of time feasible, thus improving food security and farmers' incomes.

Although post-harvest losses of both sweet potato roots and aerial vine components is significant, there is no information available that will support the design and development of appropriate storage and preservation systems. The lack of suitable post-harvest storage and preservation systems among sweet potato farmers, especially in developing countries is a disincentive to large-scale investment into its production and limits its food security prospects. In this context, the present study was initiated to improve scientific knowledge about sweet potato post-harvest handling, through experimental and modeling studies of design parameters in order to support decision-making in the design and optimization of sweet potato storage and preservation systems and the development of new processes. Additionally, the study also seeks to utilize locally available material such as mud to construct a simple storage

structure, explore the possibility for integrating evaporative cooling media as well as renewable energy sources, such as photovoltaic panels as energy sources in order to establish adequate environmental conditions (temperature, relative humidity and airflow) for storage of sweet potato under tropical conditions.

In the first study, airflow resistance of sweet potato aerial vine components was investigated. The influence of different operating parameters such as airflow rate, moisture content and bulk depth at different levels on airflow resistance was analyzed. All the operating parameters were observed to have significant ($P < 0.01$) effect on airflow resistance of the investigated components of sweet potato. Prediction models that has the ability to incorporate these influencing operating parameters were developed. The developed models provided a good fit to the experimental pressure drop data obtained in the range of airflows, moisture contents, and bulk depth considered. Bulk density of sweet potato leaves and chopped aerial vine components was significantly affected by moisture content. In the second study, the resistance of airflow through unwashed and clean sweet potato roots was investigated. An attempt was made to examine the effect of sweet potato roots shape factor, surface roughness, orientation to airflow, and presence of soil fraction on airflow resistance. The physical properties of the roots were explicitly incorporated into a physically meaningful modified Ergun model and compared with a modified Shedd's model. The modified Ergun model was able to account for the different structural parameter values of the sweet potato roots and hence provided the best fit to the experimental data when compared with the modified Shedd's model. The differences in the pressure drop between sweet potato roots arranged differently to airflow and with or without soil fraction on the surfaces of the roots were further explained by the contribution of particle drag and surface friction. The pressure drop through unwashed and clean sweet potato roots was observed to increase with higher airflow, bed depth, root grade composition, and presence of soil fraction. The findings on the effect of soil fraction stress the importance of cleaning sweet potato roots before storage.

Next, the effect of sweet potato root size (medium and large), different air velocity and temperature on the cooling/or heating rate and time of individual sweet potato roots were investigated experimentally. Also, a simulation model which is based on the fundamental solution of the transient equations was proposed for estimating the cooling and heating time

at the centre of sweet potato roots. The simulation model was adapted to receive input parameters such as thermo-physical properties of whole sweet potato roots as well as the surrounding air properties, and was verified with experimental transient temperature data. The experimental results showed that increasing air velocity during cooling and heating influences the cooling and heating rates, thus significantly ($P < 0.05$) affects the cooling and heating times. Furthermore, the cooling and heating times were significantly different ($P < 0.05$) among medium and large size sweet potato roots, thus pointing to the importance of sorting of sweet potato roots before forced-air cooling or heating treatment. Comparison of the simulation results with experimental data confirmed that the transient simulation model can be used to accurately estimate the cooling and heating times of whole sweet potato roots under forced convection cooling and heating.

Due to the need for low-cost cooling technologies in tropical rural areas, an experimental study was undertaken to investigate the performance of charcoal evaporative cooling pad configurations for integration into sweet potato roots storage systems. The experiments were carried out at different levels of air velocity, water flow rates, and three pad configurations: single layer pad (SLP), double layers pad (DLP) and triple layers pad (TLP) made out of small and large size charcoal particles. The results showed that higher air velocity has tremendous effect on pressure drop. Increasing the water flow rate above the range tested had no practical benefits in terms of cooling. It was observed that DLP and TLD configurations with larger wet surface area for both types of pads provided high cooling efficiencies and higher pressure, though it evidently lead to increase in water consumption. SLP configuration showed the lowest cooling efficiency, pressure drop and specific water consumption. DLP and TLP configurations at low air velocity is therefore recommended for practical applications.

Airflow distribution is one of the most important factor to consider when designing forced convection systems for handling perishable agricultural products. Therefore, CFD technique in the ANSYS Fluent software was used to simulate airflow distribution in the low-cost mud storehouse. The study formed part of the initial design procedures of the ventilated mud storehouse presented in Chapter 8. By theoretically investigating different geometries of air inlet, plenum chamber, and outlet as well as its placement using ANSYS Fluent software, an acceptable geometry with uniform air distribution was selected and constructed. A series of

experimental measurements were conducted to assess the design using potato as a stored product. Comparison between average air velocities extracted from the CFD simulation and the experimental measurements of headspace air velocities revealed good agreement. Across the entire bulk surface, the average relative error value between the simulated and measured headspace air velocity was 10.4%. The validation procedure used further strengthen the selected design and thus shows that CFD technique can be used to design post-harvest handling systems which do not require complicated duct and air plenum design.

Field research was conducted to demonstrate the applicability of some of the data from the laboratory studies in the development of a PV ventilated system for storage of sweet potato roots under tropical climates. The developed system comprised of a 10.85 m^3 mud storehouse, a newly developed PV driven fan and a secondary evaporative cooling system. Test results showed that under solar irradiance of around 800 W m^{-2}, the developed PV driven fan can provide airflow required for ventilating bulk sweet potato roots. As the developed fan has a relative low operating voltage threshhold, it operated continuously during the entire experimental duration. The option of integrating a low-cost evaporative cooling system into the mud storage structure for use under tropical climates was also investigated. The results showed a reduction of ambient temperature inside the mud storehouse while relative humidity was enhanced. The ability of the developed storage system to provide and maintain airflow, temperature and relative humidity which are the key parameters for shelf-life extension of sweet potato roots highlight its ability to reduce post-harvest losses at the farmer level, particularly under tropical climate conditions. Due to the utilization of PV panels for direct powering of the fan and the water pump, this PV ventilated storage system can be used in rural areas without grid connected electricity for storage of sweet potato roots.

Zusammenfassung

Die Süßkartoffel (*Ipomoea batatas* (L.) Lam) ist in vielen Ländern der Welt ein strategisch wichtiges landwirtschftliches Erzeugnis. Die Knollen und oberirdischen Ranken werden als Lebensmittel für die menschliche Ernährung sowie zu einem gewissen Grad als preiswerte Futtermittelquelle verwendet. Trotz ihrer wirtschaftlichen Bedeutung und ihres wachsenden Beitrags zur Gesundheit und Ernährung, weisen sich die geernteten Süßkartoffeln und Ranken durch eine sehr eingeschränkte Lagerfähigkeit aus und unterliegen signifikanten Nachernteverlusten. Dies trifft besonders auf viele tropische Entwicklungsländer zu. Eine Vielzahl von Lager- und Verarbeitungsmethoden zur Verlängerung der Lagerfähigkeit sind bereits angewandt worden, jedoch mit sehr unterschiedlichen Ergebnissen. In Industrieländern beispielsweise hat sich die Niedertemperaturlagerung (13-15 °C, 85-95 % RH) zur ganzjährigen Versorgung mit frischen Süßkartoffeln etabliert. Während diese Lagerbedingungen in Industrieländern bereitgestellt werden können, ist sie Landwirten in Entwicklungsländern durch den fehlenden Zugang zur benötigten Infrastruktur vorenthalten. Die Lagerung der Süßkartoffeln in sehr einfachen Lagerungssystemen resultiert oft in hohen Nachernteverlusten (15%...70%) welche durch Zerfall, Keimung, sowie Schädlinge und Insekten verursacht werden. Anders als die Knollen verderben die Ranken aufgrund ihres hohen Feuchtegehaltes bei Umgebungsbedingungen innerhalb von 1-2 Tagen. Experten sind sich einig, dass besonders in tropischen Entwicklungsländern eine Erhöhung der Haltbarkeit von Knolle und Ranke die Vermarktung über einen längeren Zeitraum ermöglichen und somit die Ernährungssicherung und den Einkommensstatus von Bauern verbessern würde.

Obwohl die Nachernteverluste sowohl der Knollen als auch der Ranken sehr hoch sind sind keine Informationen darüber erhältlich, die den Entwurf und die Entwicklung von geeigneten Lagerungs- und Verarbeitungseinrichtungen unterstützen könnten. Der fehlende Zugang zu geeigneten Konservierungsverfahren und Lagermöglichkeiten besonders von Süßkartoffelanbauern in Entwicklungsländern behindert Investitionen in die Süßkartoffelproduktion im großen Stil und limitiert somit deren Beitrag zur Ernährungssicherung. Die vorliegende Arbeit wurde daher initiiert, um den wissenstand über die Nacherntebehandlung von Süßkartoffeln durch experimentelle und modellbasierte Studien zu erweitern, die die Entscheidungsfindung in der Entwicklung und Optimierung von

Süßkartoffellager- und Verarbeitungssystemen unterstützen. Zusätzlich strebt die Studie an, lokal erhältliche Materialien (z.B. Lehm) zum Bau einfacher Lagerstrukturen zu nutzen, und die Möglichkeiten der Integration der Verdunstungskühlung sowie erneuerbarer Energiequellen (Photovoltaik) zur Bereitstellung adäquater Umweltbedingungen (Temperatur, relative Feuchte und Luftströmung) in der Lagerung von Süßkartoffeln unter tropischen Bedingungen zu untersuchen.

Im ersten Teil der Arbeit wurde der Strömungswiderstand der Süßkartoffelranken untersucht. Der Einfluss verschiedener Prozessparameter wie Luftvolumenstrom, Feuchtegrad und Schütthöhe auf den Strömungswiderstand wurde auf unterschiedlichen Ebenen untersucht. Alle Prozessparameter zeigten einen signifikanten Effekt ($P < 0,01$) auf den Luftströmungswiderstand der untersuchten Komponenten der Süßkartoffel. Voraussagemodelle wurden entwickelt, in welche alle relevanten Prozessparameter einbezogen werden können. Die entwickelten Modelle lieferten eine gute Übereinstimmung mit den experimentell bestimmten Druckverlustdaten für die untersuchten Luftmengen, Feuchtegrade und Schütthöhen. Die Schüttdichte von Süßkartoffelblätter und der zerkleinerten Ranken wurde dabei maßgeblich vom Feuchtegrad beeinflusst.

In einer zweiten Studie wurde der Strömungswiderstand bei ungewaschenen und saubere Knollen untersucht. Es wurde angestrebt, den Einfluss des Formfaktors, der Oberflächenrauhigkeit, der Orientierung zum Luftstrom und des Erdanhanges auf den Strömungswiderstand zu ermitteln. Die physikalischen Eigenschaften der Knollen wurden in ein modifiziertes Ergun Modell eingebunden und mit einem modifizierten Shedds Modell verglichen. Mithilfe des modifizierten Ergun Modells war es möglich, alle strukturellen Parameterwerte zu berücksichtigen und eine bessere Übereinstimmung zu erzielen, als mit dem modifizierten Shedd Modell. Die Unterschiede im Druckverlust zwischen den in Bezug auf die Strömungsrichtung der Luft unterschiedlich angeordneten Knollen und mit/ohne Bodenfraktion konnte durch den Beitrag der Oberflächenreibung bzw. der Partikelbewegung erklärt werden. Der Druckverlust durch ungewaschene und saubere Knollen erhöhte sich mit steigendem Luftdurchsatz, größerer Schütthöhe, Knollenklassenzusammensetzung und des Erdanhanges. Die Ergebnisse in Bezug auf die verschmutzung zeigen, dass die Reinigung der Knollen vor der Einlagerung von außerordentlicher Wichtigkeit ist.

Anschließend wurde der Effekt der Knollengröße (mittelgroß und groß), unterschiedlicher Luftgeschwindigkeiten und der Temperatur auf die Kühl- bzw. Erwärmungsrate und –zeit der einzelnen Knollen experimentell untersucht. Weiterhin wurde ein Simulationsmodell, welches auf der fundamentale Lösung transienter Gleichungen beruht, vorgeschlagen, mit dessen Hilfe die Kühl- bzw. Heizdauer im Kern einer individuellen Süßkartoffel vorausgesagt werden kann. Das Simulationsmodell wurde so angepasst, dass Eingangsgrößen wie thermo-physikalische Eigenschaften der Knollen, sowie der umgebenden Luft eingegeben werden konnten. Das Modell wurde anschließend experimentell mit transienten Temperaturdaten verifiziert. Die experimentellen Ergebnisse zeigten, dass eine Erhöhung der Luftgeschwindigkeit während des Kühlens und Erhitzens die Kühl- bzw. Erwärmungsraten beeinflusst und somit die Abkühlungs- und Erwärmungszeiten signifikant beeinflusst ($P < 0,05$). Weiterhin waren diese zwischen den untersuchten Knollengrößen signifikant unterschiedlich ($P < 0,05$). Dies lässt den Schluss zu, dass die Sortierung nach Größe vor der Einlagerung von großer Wichtigkeit ist. Der Vergleich zwischen den experimentell bestimmten und simulierten Werten bestätigte, dass das transiente Simulationsmodell zur akkuraten Bestimmung der Abkühlungs- und Erwärmungszeiten ganzer Knollen unter erzwungener Konvektion anwendbar ist.

Eine experimentelle Studie zur Untersuchung des Verhaltens einer Verdunstungskühlung in unterschiedlichen Konfigurationen zur Integration in ein Süßkartoffelknollenlager wurde durchgeführt, da in ländlichen Gegenden von tropischen Ländern ein sehr hoher Bedarf an preiswerter Kühltechnologie besteht. Die Experimente wurde mit unterschiedlichen Luftgeschwindigkeiten, Wasserfließraten und drei unterschiedlichen Mattenkonfigurationen durchgeführt: einlagig (SLP), zweilagig (DLP) und dreilagig (TLP), welche aus kleinen und großen Partikeln bestanden. Die Ergebnisse zeigen, dass eine höhere Luftgeschwindigkeit einen imdeutlichen Einfluss auf den Druckabfall hat. Die Erhöhung der Wasserflussrate über die obere festgelegte Grenze hinaus brachte keine praktische Verbesserung der Kühlleistung. Es konnte beobachtet werden, dass die DLP und TLP Konfigurationen mit einer vergrößerten nassen Oberfläche in beiden Fällen eine höhere Kühlkapazität lieferten und einen höheren Druck verursachten, und dies zu einem höheren Wasserverbrauch führte. Die SLP Anordnung wies sich durch die niedrigste Kühlleistung, den geringstem Druckverlust und den geringen Wasserverbrauch aus. Daher werden die DLP und TLP Anordnungen mit niedrigen

Luftgeschwindigkeiten für die praktische Anwendung empfohlen.

Die Strömungsverteilung der Luft ist einer der wichtigsten zu berücksichtigenden Faktoren bei der Entwicklung von auf erzwungener Konvektion beruhenden Systemen zur Lagerung verderblicher landwirtschaftlicher Güter. Daher wurde die Strömungsverteilung der Luft in einem einfachen auf Lehmbauweise basierenden Lagerhaus unter Zuhilfenahme der computer gestützten Strömungssimulation (CFD) mit dem ANSYS Fluent Paket simuliert. Diese Untersuchung bildete einen Teil der ersten Entwurfsvorschriften zur Entwicklung des in Kapitel 8 präsentierten Lehmhauses. Ein funktionierendes Design wurde entwickelt, indem eine theoretische Untersuchung unterschiedlicher Geometrien für den Lufteinlass, die Leiteinrichtungen und den Auslass sowie deren Positionierung in ANSYS Fluent durchgeführt wurde. Es wurde eine Reihe von experimentellen Untersuchungen mit Süßkartoffeln gemacht, um das Design zu validieren. Ein Vergleich der durchschnittlichen Luftgeschwindigkeiten aus Experimenten, welche über der Schüttung gemessen wurden, und Simulation zeigten eine gute Übereinstimmung. Der relative Fehler zwischen Experiment und Simulation über den gesamten Oberflächenquerschnitt betrug 10,4%. Das verwendete Validierungsverfahren verbesserte das gewählte Design weiter. Es konnte gezeigt werden, dass CFD Simulationen zur Entwicklung von Lagerhausern, die keine komplizierten Geometrien für die Ein- und Auslässe sowie die Vergleichmäßigungseinrichtungen benötigen, geeignet ist.

Zur Demonstration der Anwendbarkeit/Funktionalität der erhobenen Labordaten und in Zusammenhang mit der Entwicklung eines photovoltaisch (PV) angetriebenen Ventilators zur Nutzung in Lagersystemen für Süßkartoffeln unter tropischen Bedingungen wurde ein Prototyp gebaut. Das entwickelte System bestand aus einem Lehmlagerhaus mit einer Grundfläche von 10,85 m², einem neu entwickelten PV betriebenen Ventilator und einem folgenden Verdunstungskühlsystem. Die Ergebnisse der Versuche zeigten, dass der entwickelte Ventilator bei einer Solaren Einstrahlung von ca. 800 W/m² die benötigte Luftströmung zur Belüftung der Süßkartoffelknollenschüttung bereitstellen kann. Da der entwickelte Ventilator eine sehr niedrige Anlaufspannung benötigt konnte er durchgängig während der gesamten Versuchszeit betrieben werden. Weiterhin wurde die Einbindung des Verdungstungskühlsystems in die Lehmlagerstruktur untersucht. Die Ergebnisse zeigten eine Reduzierung der Umgebungslufttemperatur bei gleichzeitiger Erhöhung der relativen

Luftfeuchte. Das entwickelte System kann einen angemessenen Luftstrom bereitstellen, sowie die Lufttemperatur und –feuchtigkeit halten. Alle drei beschriebenen Stellgrößen sind Schlüsselaspekte in der Verbesserung der Lagerfähigkeit von Süßkartoffelknollen. Folglich konnte gezeigt werden, dass mit Hilfe des entwickelten Systems die Nachernteverluste auf dem landwirtschaftlichen Betrieb, besonders unter tropischen Bedingungen, reduziert werden können. Durch die Nutzung von PV Panels zum direkten Antrieb des Ventilators und der Wasserpumpe ist dieses System sehr gut zur Nutzung in ländlichen Gegenden ohne Netzanbindung geeignet.

10 Appendix

Figure 1-A Constructed mud storehouse.

ISSN 0931-6264